POLITECNICO DI TORINO

FACOLTÀ DI INGEGNERIA

Master degree course in Aerospace Engineering

Master Degree Thesis

Hybrid-Electric Propulsion System

Design and Simulation Study of a Hybrid-Electric Propulsion System for a VTOL Tilt-Rotor UAV

Supervisors
prof. Dario Pastrone
prof. Afzal Suleman

Laureando
Daniele Obertino
Student ID: s269706

Internship Tutor
Centre for Aerospace Research
ing. Jay Matlock

December 2021

Acknowledgements

I would like to start by expressing my gratitude to professor Suleman for the incredible opportunity he gave me. Being selected for such an exciting and challenging Master Thesis project was the beginning of a terrific adventure, for me as a human being as well as for my academic career.

This project would not have been possible without all the people who make the University of Victoria Center for Aerospace Research, UVIC CFAR, what it is: a beautiful environment built on support and collaboration, which helped me to grow new teamwork skills and to develop practical knowledge. A special mention goes to the Eusphyra team and their leader Sean Bazzocchi, whom brilliant talent and invaluable patience guided me through every obstacle I encounter along the way.

I keep a special debt of gratitude to Jay Matlock for his constant support and the many hours he spent discussing with me about hybrid. His wide knowledge, deep passion and experienced advices were of utmost importance to overcome all the problems I faced throughout the development of my thesis. I am confident that the hybrid project will soon leave the ground and take flight thanks to his impressive experimental work and constant positive attitude.

I would like to thank the Politecnico di Torino and Instituto Superior Tecnico for the education they provided me with during these years. From the many classmates and professors I encountered along my way I was able to learn and develop a steadfast work ethic and problem-solving skills that I will always carry with me during my future professional career.

A warm thank goes to my amazing P&F friends, who made this journey a pleasant and fun one. You accompanied me as my first-row supporters and I am honored to have shared so many great moments, full laughs, eased more stressful times and for being bros in work and adventure.

More than just a few lines should be dedicated to Mariana T., Beatriz, Diogo, Hugo F., Mariana S., Pedro and Hugo C.. All together we created a weird and funny group which I hope will last over the years. For all the trips we shared and especially for that last miracle night I will always be grateful to you.

Finally, to you, my beloved family. Thank you for supporting my choices and keeping me going when the enthusiasm seemed to lack. To my sister Miriam, for setting an example of hard work, perseverance and ambition. To my brother Marco, who has been with me every step of my undergraduate and graduate degree, cheering me up and giving me the confidence needed to succeed. To my grandfathers, for introducing me to the engineering field, making you proud has always been the greatest challenge, which inspired me to try

and improve myself day after day. Lastly, I am very grateful to my parents, for teaching me values that were instrumental in achieving my life goals and for their ever-lasting love, emotional encouragement and financial support that allowed me to get here.
This is for you.

Summary

In recent years, the development of Unmanned Aerial Vehicles (UAV) combined with Hybrid-Electric Propulsion Systems (HEPS) have emerged as a promising area of research in the aviation field mainly due to the increasing concerns about environmental issues and to the need for more efficient propulsion systems to integrate onboard of novel aircraft concepts, such as Vertical Take-Off and Landing (VTOL) architectures. The increase in mission complexity of both military and civil applications has led to a widespread of these configurations. In this context, hybrid-electric propulsion systems emerge as a solution to the power-matching problem that comes up with these configurations: the power needed for take-off is much greater than the power demand for cruise.
The main focus of this thesis is the design of a hybrid-electric propulsion system for a tilt tri-rotor VTOL UAV. A power-based conceptual sizing approach is adopted to evaluate the propulsion and energy mass of four different architectures (electric, gasoline, hybrid parallel and series) over a reference mission. The results demonstrated that the hybrid solution with a Degree of Hybridization (DoH) of 70% outperforms the other architectures in terms of endurance and range improvements. The series configuration was preferred and thus taken as a reference for the selection of off-the-shelf components. The serial hybrid configuration is critically assessed against the other three considered propulsion concepts. This was conducted maintaining a common mission profile in a simulation environment designed for hybrid VTOL UAVs configurations. The results suggest that the series hybrid-electric solution represents a viable trade-off for this class of UAVs.

Keywords: Hybrid Electric Propulsion, Series and Parallel architectures; Unmanned Aerial Vehicles, Vertical Take-Off and Landing;

Contents

List of Tables

List of Figures

To you,
who believed in me before anyone else.

Chapter 1

Introduction

1.1 Motivation

For many decades the mobility in all its means, from ground to sea and up to the sky, has been based on fossil fuels and on the assumption that their supply would last forever. But nowadays it is becoming clearer day after day that this assumption is false. Moreover, environmental concerns are spreading among society, which is increasing the pressure on the authority of each sector to develop new laws and regulations in order to reduce the carbon footprint of mankind.
Particularly, this new awareness of the threats represented by greenhouse gases is affecting mostly the aviation sector, due to the fast and constant growth of the air-traffic demand, which is predicted to continue with a trend of almost 5% per annum over the next 20 years, [1, 2], and thus raising even more the consumption of fossil sources, as displayed in figure 1.1.

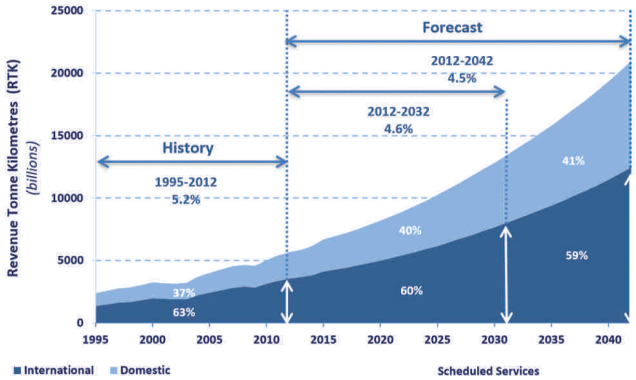

Figure 1.1. Growth rate prediction of passengers for the aviation sector.[1]

In view of this, tight emission regulations have been imposed to aircraft manufactures and the pressure from legislation to improve the modern means of powering the aircraft

will further increase in the near future. In Europe, the guidelines defined in Vision 2020 project, set by the European Commission in association with the Advisory Council of Aviation Research (ACARE), have already been renewed through "Flightpath 2050" and the corresponding Strategic Research and Innovation Agenda (SRIA). These aggressive technological objectives aim to reduce the CO_2 emissions per passenger kilometer by a factor of up to 75%, to decrease the NO_X emissions by 90% and to reduce the noise emissions of aircraft, perceived by nearby industrial and residential areas, by 65% for the middle of this century, when compared to the technology level at the beginning of the millennium.
In the wake of that, AGAPE 2020 and NASA Environmentally Responsible Aviation N+ series programs put forward similar ambitious goals.[3] The N+2, N+3, and N+4 projects define the recommended guidelines for the next four aircraft generations with respect to the early 2000s technologies.
Many technology improvements are being explored to optimize the airframe and structural designs, and to increase the efficiency of the propulsion systems to achieve the espoused readiness level. However, despite the sector has yet to achieve its full growth potential and market reach, the prospective of efficiency improvements made from evolutionary development of conventional technology alone has already reached a stall point .[4]
Therefore, novel ideas and designs for the mobility of tomorrow are being explored. Especially More Electric Aircraft (MEA) concepts are expected to unleash big potential, not only by making the operation more energy-efficient, less polluting, and quieter, but also for increased design flexibility. [5]. However, the conversion of propulsion systems towards the use of more electric power is still constrained by the technology level of battery which make them impractical. [6]
An intermediate step in this process is represented by the implementation of hybrid-electric propulsion systems. This approach should not affect significantly the aircraft's current performance in terms of payload weight capacity, range, and endurance, and at the same time more electrified forms of propulsion would be integrated on board. The growing interest in hybrid technology has created new engineering challenges for the aviation industry. Next-generation aircraft must aim to leverage hybrid electric powertrain technology in order to decrease fuel consumption and associated emissions.
A usual approach to validate new technologies and designs, is to demonstrate their feasibility at a smaller scale and then transfer the results to larger aircraft through a scaling-up process. In the same way, this research aims to assess the feasibility of hybrid-electric propulsion systems on small-scale Unmanned Aerial Vehicles (UAVs) so as to demonstrate the potential of these novel architectures. The working principle for a HEPS in a UAV is to take advantage of the power from an electric motor and internal combustion engine in such a way to optimize the efficiency of the overall system, extend endurance, or increase the output power. The combination of two different components allows the system to operate in various regimes or modes in order to meet the requirements coming from the mission performed by the UAV. In this way, the hybrid solutions feature many challenges but also advantages, especially for Vertical Take-Off and Landing (VTOL) configurations, in which the high gap in required power between take-off and cruise makes extremely difficult to define a single propulsion system that is efficient in both phases. Instead, thanks to the synergic operation of both electric motors and internal combustion engines, hybrid-electric propulsion systems appear to be a well-suited solution to this power-matching problem. Specifically, for distributed propulsion configurations the series hybrid solution can lead to

higher freedom in the design, together with aerodynamic advantages. However, many aspects need to be taken into consideration unlike the conventional systems. For an optimal design and correct sizing of the hybrid configuration, not only the UAV features play an important role, but also the mission performed and the strategy adopted to maximize the performance of interest, all together lead to the best component integration on the aircraft. Therefore, sophisticated tools and methods are needed to determine the optimal aircraft design configuration. A simulation tool capable of evaluating the propulsion system performance independently from the aircraft configuration was built up in the *MATLAB®* environment. The idea is to allow for comparison between different propulsion system architectures, in order to optimize the integration of the system into an airframe. With this framework, aircraft design engineers or researchers should be able to make decisions for improved UAV concepts.

1.2 State of the Art

The study of hybrid-electric aircraft has been the subject of discussion between researchers and engineers at universities and in the aeronautics industry over the last years. This section overviews the projects around the world in small-scale UAVs powered by hybrid-electric propulsion systems and the availability for purchasing on the market.

1.2.1 Hybrid-Electric UAVs

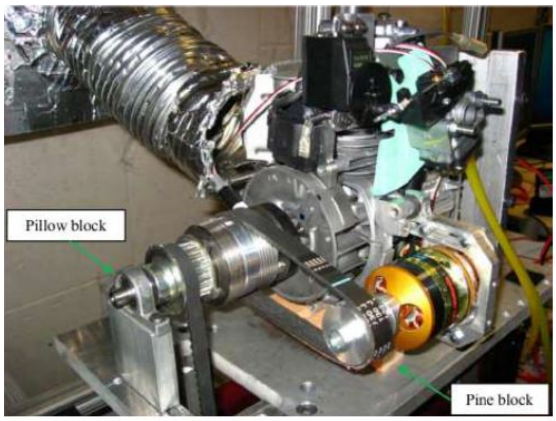

Figure 1.2. AFIT parallel HEPS on dynamometer.[7]

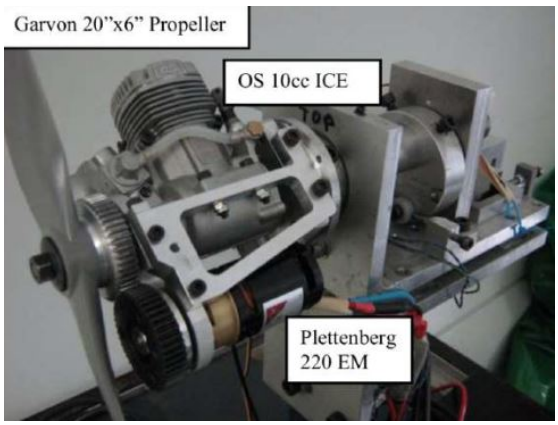

Figure 1.3. QUT parallel HEPS test bench prototype.[8]

In general, the main target of academic studies on hybrid UAV at a small-scale level is to assess the feasibility and explore the potential of HEPS.
The first milestone in the investigations of small hybrid unmanned aircraft for Intelligence, Surveillance, and Reconnaissance (ISR) application was set by Harmon et al. [9] in a research project at University of California-Davis. The main accomplishment was to develop a conceptual design method capable of sizing the aircraft structure and the hybrid propulsion system components at the same time. Its validation yielded a 13.6kg hybrid UAV. In

order to optimize the onboard energy distribution, a neural network controller was simulated, achieving 54% fuel savings compared to a gasoline UAV.[10]
This study was followed by another research group from the Air Force Institute of Technology (AFIT). The first step was to evaluate the best battery discharging strategy in relation to the application. The conclusion led to a clutch-start parallel configuration with the battery charge-sustaining strategy as optimal in order to minimize the empty weight. [11] The design was then actually built and integrated into a UAV as part of the 'Project Condor'. [7, 12] The main components of the parallel system were a Honda GX35 engine (969W) and a Fuji motor (1.2kW). A partial validation was performed on a ground test bench but no flight campaign has ever been completed.
Another research team from the Queensland University of Technology (QUT) developed a test rig for the parallel HEPS that combined a 10cc ICE and a 600W BLDC. [8] The results obtained through a dynamometer setup suggested an increase of 17% in efficiency when compared to a conventional powerplant.
A 20kg hybrid UAV was designed by Friedrich and Robertson [13] through a scale-down process from a manned aircraft 10 times heavier. The optimal ICE for the UAV was identified in a unit with a power output of 900W, coupled in a parallel connection with a 400W EM. The results demonstrated up to 47% fuel savings with respect to the original gasoline configuration.

Figure 1.4. Quaternium HYBRIDX 2.1 quadcopter.[14]

Figure 1.5. Top Flight Technologies Airborg.[15]

Recently, multirotor UAVs have been gaining popularity in many sectors. One of the first products on the market, presented in figure 1.4, was introduced by Quaternium with its HYBRIX 2.1 [14]. This fuel-electric drone implements a series-hybrid configuration that allows achieving almost 2h of flight while carrying a 6kg payload.
Another series-hybrid multicopter, named Airborg [15], was presented by Top Flight Tech. This quad-arm 8-rotor UAV platform has a Maximum-Take-Off-Mass (MTOM) of 40kg and can stay in flight for over 1h with 10kg of payload.
Finally, Yeair! is the only concept that managed to integrate a parallel hybrid configuration into a multicopter [16]. It implements four rotors, each powered by a 600W electric motor and 1kW two-stroke combustion engine. The combination of the systems allows up to 6.4kW of total power enabling around 1h of time in flight with 5kg payload.
New advanced configurations featuring both the capabilities of the systems discussed above,

meaning vertical take-off and landing (VTOL) and forward fixed-wing (FW) flight, have recently widespread in civil and military aviation. Usually, these configurations either install EM for the axial motion and then turn on an ICE to power the cruise segment, or use a tilting mechanism (wings or rotors) to perform both phases in the most efficient way. First prototypes have been developed by the US Army Combat Capabilities Development Command (CCDC) Army Research Laboratory for package delivery applications. [17] Two models with the same quadrotor biplane tail sitter architecture, but with a difference of weight in a 1 to 10 scale, named CRC-20 and CRC-3, have been used to explore the possibility of both series and parallel HEPS and are presented in the figures 1.7 below.

Figure 1.6. Yeair! parallel hybrid quad-copter.[16]

Figure 1.7. CRC-20 and CRC-3 quadrotor biplane tail sitter UAVs from Army Research Lab.[17]

Recently, Ranasinghe and Don Lakitha Gunawardana [18] developed a gasoline-electric hybrid propulsion VTOL UAV for surveillance and reconnaissance purposes with a MTOM of 27kg, shown in figure 1.8. It implements a FW-VTOL architecture, with four EM used to take off vertically and an ICE for the forward pusher propeller. A generator is attached to the engine in order to recharge the battery during cruise, creating a sort of serial hybrid concept, but without actually linking the two power sources.
Finally, in the market is increasing the availability for purchasing such technologies; an example is given by PRT XV concept from Plymouth Rock Technologies [19]. The UAV presents fixed-wing with the added capability of VTOL and with the possibility to carry onboard up to 25kg of payload. In this way, its operational range is extended for up to 7 hours of flight time, thanks to the ICE in the back. Again, this concept simplifies the serial hybrid architecture neglecting any synergetic operation of the two propulsion systems; therefore the definition of hybrid is a bit tight. One of its available multiple models is presented in figure 1.9.

1.3 Project Overview

The University of Victoria Center for Aerospace Research (UVIC CfAR) has long-term plans to research and develop hybrid-electric propulsion technologies for use in a variety of UAV applications. As part of this effort, the exploration of the viability of a hybrid-electric propulsion system (HEPS) for an unmanned aerial vehicle, featuring vertical take-off and

Figure 1.8. Gasoline-Electric Hybrid VTOL UAV.[18]

Figure 1.9. PRT XV VTOL fixed-wing UAS platform.[19]

landing capabilities, is assessed in this thesis work. The application scenario of this concept, developed in partnership with Defence and Research Department Canada (DRDC), is to conduct Magnetic Anomaly Detection (MAD) operations along the Canadian coast, in order to detect and track eventual intruding submarines through their magnetic signature. Its unusual canard-wing architecture was driven by magnetic interference studies performed during the first conceptual design phase by [20], in order to correctly allocate the payload, represented by the CAE Inc MAD-XR sensor [21], in the nose part. Recently, scaled-down prototypes have been developed as a proof of concept of the airworthiness of the system [22].
During these design studies, the implementation of a tri-rotor 80-20 configuration has been strongly suggested, where the '80-20' refers to the rotors disposition with respect to the center of gravity (CG) and to the consequent thrust distribution between front and rear rotors. This concept features a tilting rear rotor mechanism which allows to reduce the power installed on board, to optimize the usage of the components, and thus reduce the overall weight, as well as increasing the aerodynamic performance and the maximum forward speed.
Therefore, the unique characteristics of this vectored-thrust setup were given as requirements for the design and comparison of the performance of the hybrid-electric propulsion system against other conventional systems. The end goal must be to state the most efficient propulsion design capable of handling the complexity and the requirements of this concept. This clearly can only be achieved through a simulation analysis to allow for unbiased and parametric study of the different UAV systems and to explore the design space. Hence, a theoretical model developed to form baseline results and explore predicted efficiency of the UAV with purely electric, purely combustion engine, parallel and series hybrid configurations is given to the project.

1.4 Objectives

The main goal of this research is to define and size the correct propulsion system for the VTOL tilt-rotor UAV concept discussed before. The aim of the study is to evaluate if a hybrid-electric propulsion system can be proven as a feasible solution for small unmanned

aerial vehicles implementing vertical take-off and landing capabilities.
The advantages of these novel efficient propulsion technologies are assessed by means of a *MATLAB®* simulation framework able to run comparisons and trade-off analysis against conventional systems.
The potential of this tool is combined with a power-based sizing approach in order to quantitative assess the conceptual design of a propulsion system, for the specific aircraft under analysis, in terms of components dimensions, power output capabilities, propulsive mass, fuel and energy consumption.
The results allow a first insight into hybrid-electric propulsion system design trends. This enables the aircraft designer to identify for which mission and which requirements hybrid-electric aircraft should be considered as a design alternative. Despite possibly providing results that do not favour hybrid electric systems, the tool ensures transparency on which propulsion technology is the correct choice for the application. These impartial and quantitative results can be then translated into engineering design decisions for the selection of correct hybrid-electric propulsion system components to integrate into the UAV.
Showing that hybrid-electric propulsion systems are viable for VTOL UAVs, and have prospective performance and operations advantages is critical for the future of this project and of similar studies in the aviation field.

1.5 Thesis Outline

Chapter 1 - Introduction

The motivations behind the need for a greener aviation, which justify the pursuing of hybrid-electric propulsion system technologies for UAVs are here introduced. In the state-of-the-art section a review of the available solution on the market and of the many projects around the world that are working towards the same final goal for a more energy-efficient propulsion is presented. A description of the project and of the configuration of interest for the application of the hybrid solution is covered. Finally, the objectives section states the tasks and goals outlined for the scope of this research.

Chapter 2 - Theoretical Overview

A theoretical overview of the hybrid-electric propulsion system concepts is presented. The most common hybrid architectures for UAVs applications are discussed and compared. The working principle and the way of modelling the main components in a HEPS are introduced. Lastly, several control scheme models are proposed to be later introduced into the simulation framework.

Chapter 3 - HEPS Simulation Framework

The HEPS simulation framework developed is here presented, with the numerical models implemented for each component of the hybrid systems then assembled in the aircraft model. The working strategy of the tool is explained together with the main results that can be obtained from it in order to evaluate and compare the systems' performance. In addition, component-level bench tests and flight campaigns data are used to update and to validate these first-order models and the whole *MATLAB®* framework.

Chapter 4 - HEPS Sizing Analysis

This chapter contains a complete presentation of the design procedure followed to size the propulsion system of the given VTOL UAV. First, a full description and explanation of the configuration, its baseline mission and the rationale used throughout the power-based sizing approach is provided. Afterwards, through the developed tool, the components and energy sources mass are modelled and estimated for four propulsion system configurations, leading to a preference for the series hybrid-electric solution. The results obtained for the propulsion system under analysis are then translated into COTS chosen after market research. Finally, the components of the HEPS are integrated onboard and the sizing results are validated.

Chapter 5 - Mission Performance Evaluation

The hybrid propulsion system designed in the previous chapter is here assessed in more detail through the *MATLAB®* simulation framework. First, a validation of the results obtained from the sizing process over the same mission profile is provided, together with addition of features and tuning of the rotors model into the tool. After, trade studies over the mass distribution of the sources onboard are analysed in order to obtain the best performances and to compare the different propulsion concepts. Lastly, a study of how the single mission segments affect the configuration is discussed, with a final focus on the payload available to carry on board.

Chapter 6 - Conclusions

In this chapter, the achievements of this project are reviewed, as well as a critical recapitulation of the results obtained. In addition, recommendations for future work regarding potential improvements to the hybrid-electric propulsion system and the next steps that should be taken are discussed.

Chapter 2

Theoretical Overview

This chapter presents an overview of the theoretical information required for the analysis of a HEPS, including descriptions of the operational concepts and their main components. The new potential brought by the advancements in these technologies must be fully explored in order to reach the desired gain in performance for novel UAV designs, such as VTOL and transitioning configurations. Together with the practical description of the working principles of the units, a first introduction to the numerical models, formulated afterwards in the *MathWorks MATLAB®* simulation tool, is given. These models are necessary to describe the components at a computational level, and also to evaluate and compare their performance according to the level of detail required. The topics covered in this section should give sufficient information to form a complete understanding of the work performed in the next chapters and explain part of the reasons behind the sizing and components selection of the HEPS.

2.1 Hybrid-Electric Systems Architectures

The concept of operation for a HEPS in a UAV is to combine the power from an electric motor and another propulsion type in such a way to optimize the efficiency of the overall system and to increase the performance of the vehicle. Depending on the requirements of the mission, the hybrid system can enter into different operating modes in order to meet the goals. Usually, for small UAVs the hybrid propulsion systems consist of a conventional internal combustion engine coupled with an electric motor to power the aircraft. However, the same approach can be extended for future technologies such as distributed propulsion configurations, where more than two components drive the power output. There are two main hybrid propulsion system architectures: series and parallel, together with the power-split or 'series-parallel' configuration which is more advanced since it combines the two architectures but, although it has been emerging for some specific applications, it is usually not considered for UAV due to the additional mass of the planetary gearbox and generator. Although many of the components are similar in these configurations, their architecture and performance are quite different. More detailed functional schemes of these concepts are presented.

2.1.1 Series Hybrid System

The power flow of the series or serial hybrid architecture is presented in figure 2.1. For this configuration it can be easily seen that the ICE is completely decoupled from the EM and it does not directly power the propeller. Instead, a separate generator is attached to the internal combustion engine in order to generate the onboard electrical power. Therefore, in this case, the chemical energy stored in the hydrocarbon fuel goes through three conversions: it is first converted into mechanical energy inside the ICE; secondly, through the generator it becomes electric energy, which can be used to charge the battery or, lastly, to directly power the EM connected to the propeller by means of one last conversion again into mechanical torque. Therefore, on one hand the main disadvantage of a series configuration are its inherent losses due to the many energy conversion steps along the powertrain, which strongly decrease the overall efficiency compared to a parallel configuration. The only recovery can be found in the lower electrical transmission losses compared to mechanical shafts. On the other hand, a series architecture can mechanically decouple the ICE from the EM and thus the propeller, meaning that it can be operated independently. This condition allows a full control on the operational point of the ICE, which can be programmed to operate at the most ideal operating point or optimal operating point (OOP) where it fulfills the power request with the least amount of fuel consumption. Moreover, if a more complex power electronic is mounted on board, such as a power management unit (PMU), the control logic can be not as simple as for the case where the hybridization considerations are only between the energy sources. In fact, especially for more complex architectures implementing distributed propulsion systems, considerations about the combination of the electric energy coming from the generator and from the battery can be made. In this way, with a correct selection of the battery capacity onboard, the ICE-generator system can be sized for cruise conditions and use the support of the battery in case of a boost in power request appears. Still, this power electronic unit usually is heavy and the EM needs to be sized according to the maximum power demand. Due to this mass penalty, the series configuration is not suitable for micro-UAVs [23]. Whereas, it has been largely applied in bugger configurations where the impact of extra components only slightly reduces the benefits due to its ease in control, lower mechanical complexity and eventual aerodynamic advantages brought by the possibility to allocate the components in the most suitable location. Some applications are listed in [4].

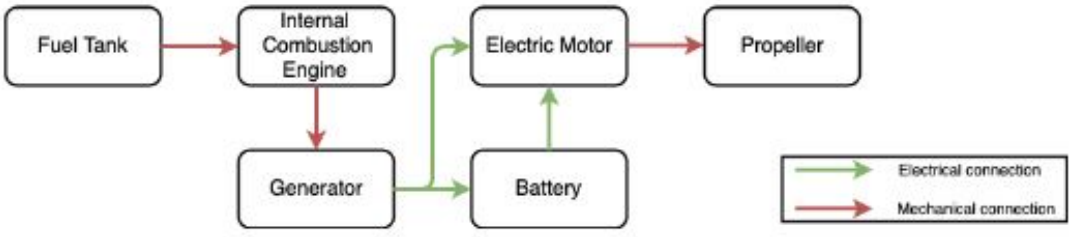

Figure 2.1. Series hybrid power flow diagram

2.1.2 Parallel Hybrid System

The flow diagram of power for the parallel hybrid propulsion scheme is presented in figure 2.2. In a parallel configuration, two power sources are mechanically combined through some form of a mechanical coupling that often consists of a simple clutch, which does not allow to operate the ICE at its most efficient point, or in a more complex continuous variable transmission (CVT) to directly drive the propeller. The need for a mechanical coupling device clearly adds a level of complexity to the control of the system compared to the series case and it represents the main disadvantage, especially for distributed propulsion systems or tilting applications where different shafts should be rotated and coupled at the same time. However, in standard concepts, thanks to this coupling mechanism, the parallel architecture allows to share the power request between the two sources and to operate the system with a combination of the two. This means that each power source can be sized below the total power requirement while it is not possible in a series configuration. Harmon et al. [10] demonstrated that for a small UAV the parallel concepts could lead to a 8% of mass advantage compared to the serial counterpart, due to the bigger size of the components, other than the extra additional generator. Despite these mass savings, the individual power sources then may not be able to provide sufficient power for the entire operating envelope and in case of more complex architectures, such as VTOL UAVs, this redundancy requirement must always be fulfilled in order to safely perform an emergency landing in the case of a power source failure. Therefore, the advantage of sizing the components for cruise requirements drops [24]. Nevertheless, the parallel system can still bring benefits to the aircraft thanks to its intrinsic several complex operational modes. It makes possible to control how power request is split between ICE or EM , allowing to isolate or combine the power sources. For example, the coupling system could combine the two power sources by adding the torque coming from each one. Furthermore, if the operating flying conditions allow it, the clutch can be engaged and the EM can be used as a generator for regenerative brake mode in which the EM draws power from the ICE into the onboard battery.

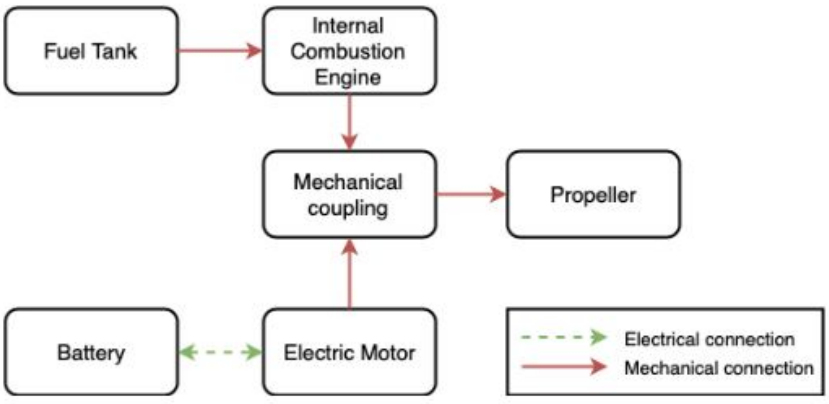

Figure 2.2. Parallel hybrid power flow diagram

2.1.3 Power-Split Hybrid System

The power-split, also known as series-parallel Hybrid configuration, is a combination of the two configurations described above. As shown in 2.3, propeller, internal combustion engine, electric motor and generator are connected to a planetary gear, through which the power is transferred according to the operating mode. Therefore, the load distribution is more flexible and it allows the ICE to operate at its ideal operating point since no direct connection between the power plants and the mechanical drivetrain exists. The planetary gear enables the configuration to save more fuel because it more efficiently combines the various power sources. A further advantage of the series-parallel configuration is the possibility to disable the combustion engine without mechanically disconnecting it from the powertrain. However, the use of the planetary gear makes this configuration the most complex to control and design. Moreover, the planetary gear and additional generator make the series-parallel architecture the heaviest one and therefore it is rarely implemented in UAV, but it has interesting application in the automotive field.[25]

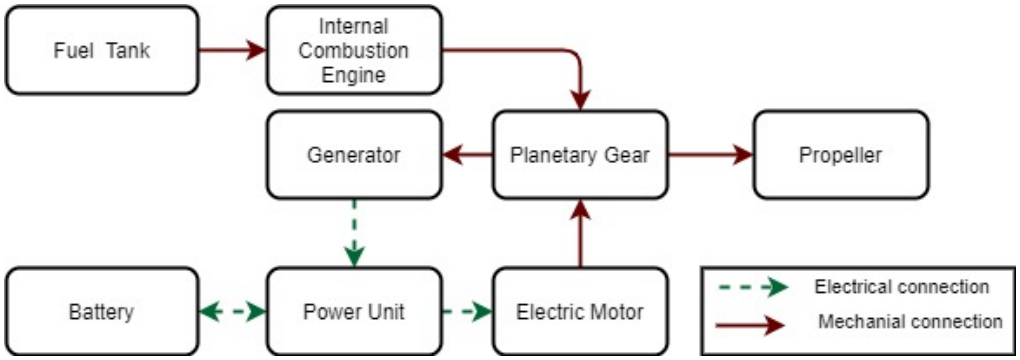

Figure 2.3. Power-Split hybrid power flow diagram.

2.1.4 Degree of Hybridization

The Degree of Hybridization (DoH) expresses the percentage of the total power required by the aircraft that comes from the electric system [26]. However, in literature it is more commonly used the Hybridization Factor for energy (HF_E) and power (HF_P). These parameters give an idea of how the power and energy sources are allocated onboard. The HF_P is the ratio of the installed propulsion power of all EMs to the total installed propulsion power at the propeller shaft; whereas HF_E is specified as the ratio of the required transport energy delivered by batteries (non-consumable) to the total required transport energy. Finger [27] gave a specific definition of these coefficients for the parallel and series configuration, respectively.
The level of hybridization of power for parallel-hybrid and series-hybrid aircraft is defined according to:

$$HF_{P,ph} = \frac{P_{EM,max}}{P_{max}} \qquad (2.1) \qquad\qquad HF_{P,sh} = \frac{P_{EM,max}}{P_{ICE,max}} \qquad (2.2)$$

where $P_{EM,max}$ is the maximum power of the electric motors, P_{max} is the overall power demand and $P_{ICE,max}$ is the maximum power of the ICE. The definitions make sure that parallel-hybrid powertrains are identified by a hybridization level smaller than 1, while serial-hybrid powertrains are identified by a hybridization level larger than 1. This avoids unnecessary ambiguity when talking about levels of hybridization.
The other critical parameter is the level of hybridization of energy. It is defined for every flight phase of a mission and determines the power demand from EM and ICE in each phase.

$$HF_{E,i} = \frac{\Delta E_i}{\Delta E} \tag{2.3}$$

For initial sizing, the different values of HF_E for every flight phase are determined by the ratio between the power requirement of the EM and the power demand.
These parameters need to be used together in order to understand how the sources are actually employed, since a configuration could show a really high hybridization factor of power due to an extremely powerful EM which, however, it is only used for a really short time of the mission; therefore the battery energy onboard is extremely low and so is the hybridization factor of energy. Thus, HF_E indicates how much of the propulsion system's electric part is used.

2.2 Components of Hybrid-Electric Propulsion Systems

This section presents the several components which, combined according to the schemes previously mentioned, form the core of a hybrid-electric propulsion system. A brief description of the main typologies of combustion engines, electric motors, batteries, mechanical couplings and propellers is given, together with an overview of the available models used to predict their behaviour. In the process of commercial-off-the-shelf (COTS) components selection and their integration design, this knowledge of their fundamental working principles and about the criteria behind the best operating synergy was of utmost importance.

2.2.1 Internal Combustion Engine

Figure 2.4 presents an overview of the many concepts of internal combustion engines (ICE) available for the aerospace field. For small and mid-scale UAVs, the most common types are the 4-stroke and 2-stroke spark-ignited (SI) and compression-ignited (CI) engines. ICEs are usually the main drivers of the hybrid electric powerchain. Its principle of operations is based on the conversion of the chemical energy into mechanical power through fluid expansion by combusting a hydrocarbon fuel with an oxidizer, usually air mixtures. However, the conversion process is highly inefficient due to friction and heat losses [29]. At the moment, the value of energy efficiency for an engine is under 35%, but an enormous research effort is being made in order to improve the overall performance and reduce pollution emissions.[30] Recently, LiquidPiston® has developed and tested a new non-Wankel rotary engine concept, implementing a novel patented High Efficiency Hybrid Cycle (HEHC), displayed in figure 2.5(a), which combines the advantages of Diesel, Otto and Atkinson thermodynamic cycles and claims to reach overall up to a 30% better efficiency.[31] The X-Mini engine,

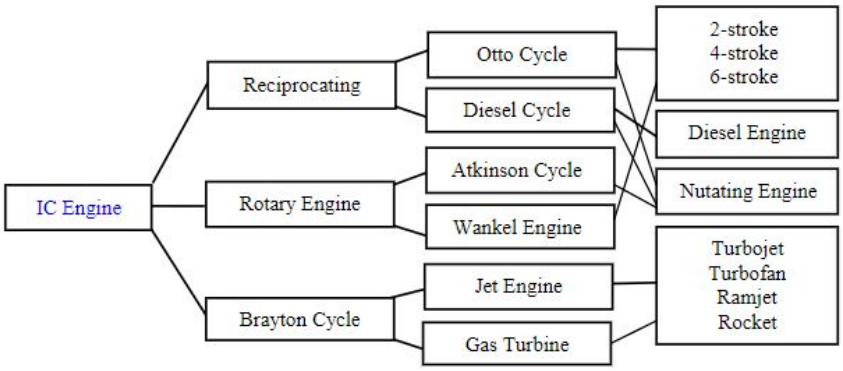

Figure 2.4. Engines technologies available in the aviation field. [28]

shown in figure 2.5(b), which implements a spark-ignition version of the cycle, states to be up to 30% and 80% smaller and lighter compared to spark-ignition gasoline engines and compression-ignition piston diesel ones. With an efficiency benefit leading to 50% and 30% decrease in fuel consumption compared to SI gasoline and CI diesel engines, it would represent a huge breakthrough for the combustion technology advancement. Moreover, it warrants lower vibrations and noise, and scalability between $0.7 - 700\ kW$, which makes it a suitable solution for a wide range of aircraft sizes.

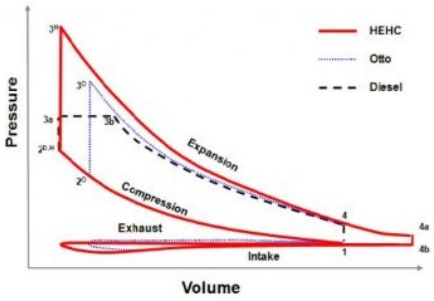

(a) LiquidPiston's HEHC patented thermodynamic cycle

(b) LiquidPiston X Mini 70cc proptotype (right) next to a 49cc Honda Metropolitan engine

Figure 2.5. LiquidPiston engine

As stated before, at the state of the art, the most common solutions for small UAV applications are the 2- and 4-stroke reciprocating engines, which convert fluid pressure on a piston into rotating mechanical power on a driveshaft. A two-stroke gasoline engine is typically preferred due to the weight-saving coming from the higher power density and improved simplicity, together with slightly lower noise and vibrations.[32] For this category, torque (τ) and Brake Specific Fuel Consumption (BSFC), which gives a measure of how efficiently an engine uses fuel to produce work, are frequently used to describe the engine

performance, according to their definition in equations 2.4 and 2.5. In the formulation P states for the engine power output in $[kW]$, $\dot{m}_f$ is the fuel flow rate in $[gr/hr]$ and rpm is the engine's speed in revolutions per minute.

$$\tau = \frac{P}{2\pi \cdot rpm} \cdot 60 \qquad (2.4) \qquad\qquad BSFC = \frac{\dot{m}_f}{P} \qquad (2.5)$$

Their behaviour as a function of the operational rpm is usually mapped by the manufacturers using a dynamometer connected to the output shaft which applies varying braking torque. The data collected in these maps are recorded at steady-state and thus they do not represent the engine dynamics. Anyway, these performance maps should give insights to the user on how to operate the engine effectively: by running it close to its minimum BSFC in order to optimize fuel efficiency, since the fuel consumption is interchangeable with the engine efficiency map in the sense of describing engine losses. An example of constant fuel consumption contour lines for a reference engine is shown in 2.6.

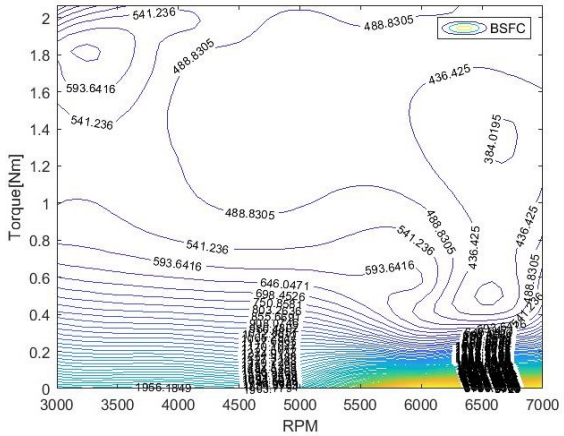

Figure 2.6. Performance map of a Corvid-29 extrapolated from [33].

However, despite efficiency maps are widely available for automotive engines, for smaller ICEs suitable for UAV applications these experimental data are very seldom published and extremely hard to find. Since the design of a hybrid-electric configuration can be strongly affected even by small variation of the engine performance, due to its influence on the hybridization factor, it is clear the necessity of an automated and scalable modelling method capable of constructing engine maps in order to explore the whole design space and support the components selection.
The focus of this work lies in the realization of a whole hybrid propulsion simulation tool rather than single highly detailed units. Therefore between the many numerical models available in the literature such as [34, 35], which offer a high precision, or even more accurate computational fluid dynamics (CFD) simulators like [36], which describes the chemical reactions of the combustion process, a different approach to model 2-stroke engines is pursued. The priority is given to simpler and low computational cost solutions, but still capable to evaluate the engine performance parameters on a large scale of alternatives.

Willans Line Method for Internal Combustion Engines

The Willans line modelling formulation from [37] is a widely applied and verified quasi-static method which allows to predict performance of unknown scaled engines. This parametric approach has been largely used in the automotive field, [38] and it was recently implemented in hybrid electric aircraft simulation and sizing tools. [39] [40]
The key assumption of this unique representation is that for each speed is possible to define an affine relation linking the available power in input, associated with the chemical energy of the fuel, to the power that is actually produced at the output axis of the energy converter, as shown in figure 2.7.

In the resulting approximately linear equation 2.6, the conversion efficiency e is defined

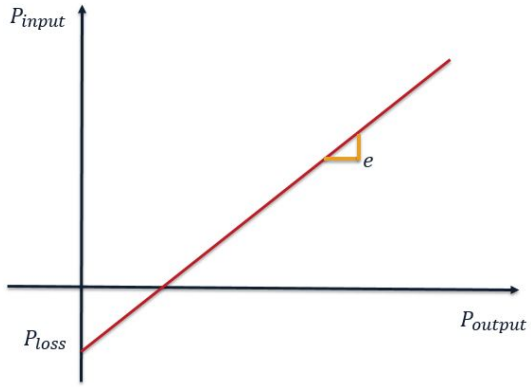

Figure 2.7. Linear relation between P_{out} and P_{in} extrapolated from [37].

by the slope of the function and accounts for the thermodynamic η_t and combustion η_b efficiencies, while P_{loss}, identified by the interception with the vertical axis, represents the losses due to friction and other auxiliary components.

$$P_{out} = e \cdot P_{in} - P_{loss} \tag{2.6}$$

The equation can be expressed in terms of torque 2.7, by substituting equation 2.4 inside it:

$$\tau_{out} = e \cdot H_{LHV} \frac{\dot{m}_f}{\omega} - \tau_{loss} = e \cdot \tau_a - \tau_{loss} \tag{2.7}$$

with τ_a available torque, H_{LHV} as the fuel lower heating value in $[MJ/kg]$, ω angular speed in $[rad/s]$ and τ_{loss} loss torque due to friction phenomena.

The basic idea, in order to eliminate sizing effects, is to express the engine parameters in a non-dimensional form to obtain a linear relation between the substituted normalized variables. Therefore, based on known steady-state efficiency data of a reference engine, normalized equations and coefficients can be determined and applied to estimate the efficiency of a new scaled engine of the same class. In this way, the impact of shrinking or enlarging the engine size can be accurately evaluated. The main advantages of adopting such a formulation to describe the ICE in any propulsion architecture are the possibility to make the model independent from the power output or size, thus permitting elastic

scaling, plus it requires only a few parameters in input. The previously mentioned aspect makes this model well-suited for immediate and approximate assessment of new design configurations and new engineering solutions for which usually few or not enough data are available. However, several aspects of the ICE such as its geometry, the fuel injection technique, thermal exchanges, emissions and other dynamics of the engine are not taken into account.

2.2.2 Electric Motor

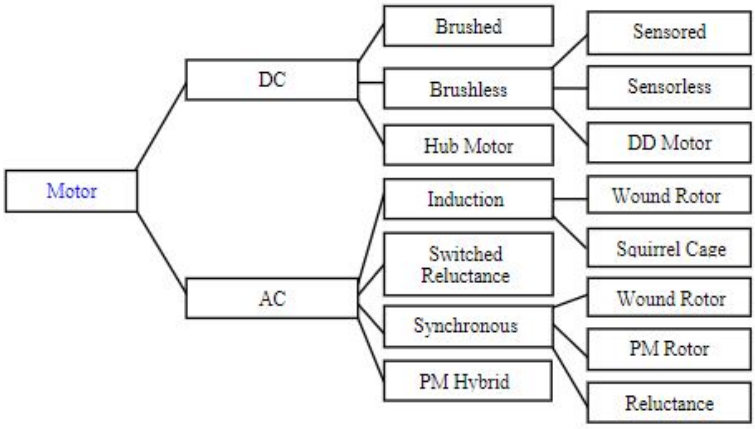

Figure 2.8. Electric Motor technologies available in the aviation field [28].

Figure 2.8 shows how electric power supplies are mainly divided into two classes: DC motors and AC motors. In the few applications where AC EM are used for hybrid-propulsion solutions, they are usually found in the form of induction and switched reluctance motors. However, DC motors are widely spread in the aviation field and especially in the UAV market because of their control simplicity and technological maturity, which makes them well suited for applications requiring variable speed, frequent start/stop, reversing and braking. The main two categories of DC motors are brushed (commutator) and brushless (commutatorless). The brushless DC (BLDC) motors are more commonly used in hybrid-electric propulsion systems since it offers high reliability and longevity compared to the brushed counterpart. BLDC motors are created by inverting the stator and rotor of brushed DC motors. A brushed DC motor tends to wear out substantially more quickly than a brushless DC motor since the brushes required for commutation degrade over time. Moreover, for parallel hybrid applications the BLDC can be used as both a motor and a generator depending on the required operating mode of the system. The concept of a brushless direct-current electric motor is based on the electronic phase commutation: permanent magnets are placed on the rotor, electromagnetic coils on the stator and the firsts are excited by the seconds to attract and repel the poles of the motor. There are two main types of BLDC motors distinguished by their rotor location. In an outrunner arrangement, the rotor runs around the stator, whereas in an inrunner arrangement it runs within the stator. Their performance characteristics are slightly different. The outrunner,

thanks to the bigger diameter of the rotor, allows to provide high torque capabilities at high rotational velocities, but its higher inertia limits the maximum speed of the EM. Whereas inrunner BLDC provides high-torque at low rotational velocities but it offers a lower torque at high rotational velocities [41]. As a consequence of the high rotational velocity, inrunner motors usually need the implementation of gearboxes. Therefore, in the majority of small UAV applications an outrunner BLDC is integrated since it requires lower energy magnets, it has larger rotor inertia and lower production costs.
It is important to mention that the brushless DC motor alone is not a DC motor, as it has three phases. To correctly operate a BLDC motor, an electronic speed controller (ESC) is mandatory. The electronic speed controller is a switching power circuit which converts the direct-current input into an approximated sinusoidal three-phase current using transistors, more often in the form of metal–oxide–semiconductor field-effect transistor (MOSFET) where the voltage determines the conductivity of the device. The main disadvantage of a BLDC motor of requiring a controller is largely outbalanced by its advantages, which include a higher efficiency thanks to the elimination of the brushes that brings to a decrease in friction and heat dissipation. This means that BLDC motors can achieve higher efficiency. Moreover, thanks to the lower heat problem, the motor can withstand higher current before reaching its critical temperature; consequently it has a higher specific power than the brushed motor.
The prediction of BLDC performances is way less empirical than for ICE. In fact, the Willans line method, previously explained, could also be applied to describe EM and generators efficiency maps [42]. However, the need of a detailed database with efficiency curves and its high computational cost does not justify its implementation, since fairly accurate results can be obtained by simple equivalent circuits based on fundamental electricity equations with a handful of motor specific constants.[43]

2.2.3 Battery

A battery is an electrochemical device that provides electrical voltage and it may be used to store electric energy onboard. It is made by a system of one or several cells connected in parallel or series. Each cell stores energy in chemical form and then uses a chemical reaction to convert it to electric energy. In the UAV field, especially for hybrid applications only rechargeable types are implemented. The many different types of batteries available on the market are represented as a function of their main properties in figure 2.9, where E^* is the energy density in Wh/kg and P^* is the power density in W/kg. It is easy to understand, by looking at it, that Lithium-based battery has a very high specific energy compared to the values of Lead-Acid, Nickel-Cadmium (Ni-Cd) and Nickel-Metal hydride (Ni-Mh) ones. Therefore, Li-based batteries are the most common solution in aeronautic applications since the main requirement is to reduce the weight on board. Specifically, Lithium-Polymer (Li-Po) batteries are the most interesting type since they offer the advantages of high specific energy and power as well as the high number of possible charge and discharge cycles [6]. Li-Po batteries are available in a wide range of capacities and in packs with a varying number of cells in series. The main disadvantage of Li-Po batteries is related to its safety constraints. LiPo cells have a nominal voltage of 3.7V per cell, and should not be discharged below 3.0V per cell, or charge above 4.2V per cell; which means keeping the charge level between 15% and 90%. Excess recharge or exceeding the maximum operating temperatures

leads to the decomposition of the anode and cathode which results in the releasing of gases which may overexpand the casing and fire it up once the lithium is exposed to oxygen causing an explosion. In the same way, an excess in the depth of discharge may lead to irreversible damages. In order to increase the lifespan of this type of battery, extreme care has to be taken in their use and storage. The application of Li-Po batteries shows achievable energy densities between 145 - 240 Wh/kg [44]. The value of 200 Wh/kg for current Lithium-ion batteries is not valid for every application. Therefore, a state-of-the-art value of 179 Wh/kg was derived from a database of TATTU Lithium-polymer batteries. It is important to mention that research activity in the field of advanced battery technology is very strong due to the demand across various industries. [45]

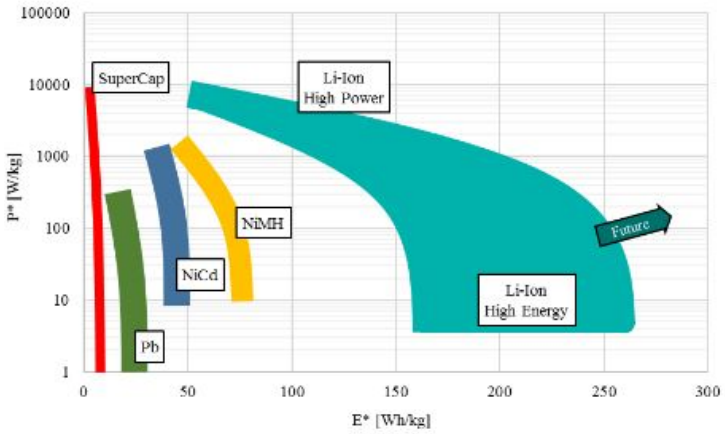

Figure 2.9. Properties of rechargeable batteries. [27]

2.2.4 Propeller

When designing a hybrid-electric propulsion system, the propeller connected at the end of the drivechain must be properly sized in order to achieve the thrust requested by the UAV and in the meantime maximize the operational performance of the propulsion architecture. The propeller is in charge to convert the rotational mechanical energy coming from the crankshaft in form of torque into translational mechanical energy for the aircraft, which is expressed in the generated thrust that causes the vehicle to move at a certain speed. The design point of the propeller should be for cruise condition, such as to have an efficiency as high as possible at this flight condition. But there are many restrictions when it comes to propellers that have to operate efficiently in more than one phase, such as tilting rotors. The main restriction is the tip Mach number. A propeller presents the maximum relative velocity at its tip. There, a Mach number above 0.85, which is the usual critical value adopted, should never be exceeded at any condition in order to avoid significant drops in efficiency and increasing noise. An important trade-off solution can be given by the use of fixed-pitch and variable-pitch propellers. Using a variable-pitch propeller allows to reach higher efficiency values and therefore the performance of the aircraft can be increased thanks to the less power request for the same flight condition. However, the added mass,

complexity due to extra parts and risk in failure of the system make it unfeasible for small UAV applications.
Figure **??** shows curves of propeller efficiency for different propeller pitches versus the advance ratio J, defined in equation 2.8, where V is the velocity of the incoming flow, and ω and D are the angular velocity and diameter of the propeller.
In the range of propeller sizes suitable for small unmanned aircraft, commercial components made of carbon fiber reinforced plastics (CFRP) are widely available. They are more lightweight and more rigid than wooden and plastic propellers counterparts.

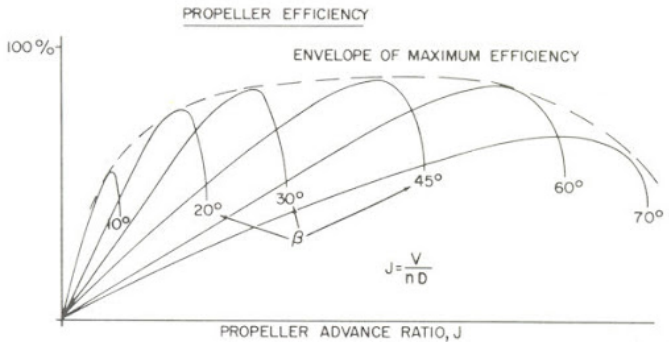

$$J = \frac{V}{\omega \cdot D} \tag{2.8}$$

Figure 2.10. Propeller efficiency curves.

From an aerodynamic point of view, the propeller blade may be characterized as a rotating wing. During their motion through the air, the blades generate lift, which, based on the angle of attack and the blade pitch angle, is decomposed in a thrust contribution. The other component, generated by the drag, defines the torque required to activate the propeller. The contribution of lift and drag along the propeller is not constant since usually the propeller has a varying distribution of chord and twist over its radius or even different aerofoils may be used for each blade sections. Therefore, in order to correctly predict the performance of the propeller, expressed usually through its efficiency, advance ratio, thrust and torque coefficients (defined below and in the next chapters), many models have been developed in the literature. A commonly used method is the Blade Element Momentum theory (BEMT) [46]. This model is capable of evaluating the performance of a propeller based on its mechanical and geometric parameters as well as the characteristics of incoming streamflow. It results from the combination of two theories: the Blade Element Theory and the Propeller Momentum Theory.
The former relies on a division into n sections of the blade, the blade elements, which are approximated by a planar model. According to it, the coefficients of lift and drag are computed for each section and are then integrated along the blade to obtain the global forces [47]. The Propeller momentum theory, also known as disk actuator theory or axial momentum theory [48], is a global theory that adopts a macroscopic point of view to model the behavior of an assumed inviscid and incompressible column of fluid passing through a propeller.
Another commonly used method to predict propeller performance is the vortex theory. The vortex theory implies the use of the blade-element theory previously described and it is based on the enhanced formulation given by Goldstein and Prandtl [49] on the minimum

energy condition. The theory for screw propellers assumes there is circulation around the blade, that vanishes at root and tip, and it can be replaced by a bound vortex system of strength.

2.3 Hybrid Powertrain Control Methods

Powertrain control systems are mainly used to regulate the power flow inside the hybrid electric system in order to achieve the highest possible efficiency of the overall system. In order to maximize the performances of each component these control strategies must be critically studied and adapted to the case of application. In fact, especially for small hybrid UAVs implementing this new combined type of propulsion, the control strategy is strongly linked to the features of the aircraft and its mission profile, therefore it should be carefully selected in order to optimize the working synergy between the units and thus to minimize the fuel consumption. As presented in figure 2.11, many control methods have been implemented on the automotive hybrid powertrains field and are slowly being adopted also in the aviation sector.

The simplest of the control strategies for hybrid propulsion systems are the so called 'more deterministic schemes'. In these a functional mapping is used to monitor the state of charge of the energy systems and thus the hybrid powertrain is operated in an 'on/off' mode. Once a specific percentage of charge is reached, depending on the charge sustaining or charge depleting logic selected, the controller switches modes according to the architecture. [50] Other deterministic control logics can be more complex and focused on energy management or optimization strategies to maximize efficiency. These rule-based controllers are still simple to implement and provide reliable control by increasing fuel economy, such as in [8] , where an Ideal Operating Line (IOL) control approach for a parallel hybrid powertrain configuration was employed. The goal of this method is to provide a simple deterministic approach to operate the engine in an efficient manner that does not rely on non-linear forms of control. These deterministic methods clearly must rely on some prior knowledge of the system.

In contrast, non-deterministic forms of control are more probabilistic and do not always behave in the same way even in response of the same input. At different points and conditions in time their logic can give different control results. Model predictive control strategies use their ability to forecast future information to influence the current state. This is perfectly suited for powertrain operation in which fuel economy needs to be optimized. [51] The state of the art in hybrid system controllers for the aviation field is represented by the cerebellar model arithmetic computer (CMAC) approach. This control, while being extremely more complex than the deterministic one, can achieve incredible performance as proved by Harmon et al. [10]. The neural network implemented in their parallel hybrid system represented a breakthrough for the control strategies. This control scheme is focused on optimizing the engine torque control surface, in order to develop a more efficient battery charge-sustaining or charge-depletion control; it can achieve between 30% and 60% saving in energy depending on the mission under analysis. Moreover, compared to the performance of a rule-based control strategy, this CMAC control was able to reduce fuel usage by 6.3%. However, if the priority of the application is not just to control efficiently the system in transient operation or to find the optimal point at each flight state, developing online

optimization control strategies such as neural networks may be not needed while still achieving good savings. In fact, if more accurate information about the components and about the flight mission is available to the developer, a deterministic control strategy can be equally capable of providing efficient operation. Fuzzy-logic controllers are one example of a deterministic controller that allows for more degrees of freedom and also for a number of variables to affect the control output. Fuzzy-logic controllers are based on the same principles as rule-based controllers, but instead of binary variables 0 and 1, they use any value between 0 and 1. However, the fuzzy-logic controller is not suited for high-input systems since it is susceptible to "exponential rule expansion" on non-linear problems. [8] A recent research suggests that a fuzzy-logic controller on a UAV can save up to 11% fuel for certain flight missions. [52]

To conclude, the two most important operating strategies for hybrid architectures must be mentioned: charge sustaining (CS) and charge depleting (CD). [51] The first strategy has the goal of keeping the state of charge (SOC) of the battery at a preselected value and it takes more advantage of the brake regenerative mode to fulfill this requirement. In other words, 'stealth operations', for which the EM is the only power supplier, are usually not allowed or prioritized. The second strategy, instead, allows to operate in EM only or in a hybrid mode and thus depleting the battery SOC along the mission. This solution is better suited for operational cases where the mission is known and the UAV can have the possibility to recharge along the flight or once on the ground. However, the CD strategy must always be coupled with a recharge mode or a well defined mission profile where the exact amount of energy needed from the batteries is known. Otherwise the aircraft might be incapable of fulfilling sudden variances in power requirements until even an emergency landing is needed. This is extremely true for hybrid VTOL applications where for most of the time no conventional landing system is mounted onboard in order to save weight and thus, if the battery goes under the necessary level to land, it might lead to a crash of the aircraft. In view of this, for these configurations, registering large power fluctuations during the mission, it is important to adapt the operating strategy to accommodate the mission requirements and design goals for endurance or fuel consumption. In order to provide a robust strategy, both CD and CS concepts should be implemented. Thus, it is clear that a supervisory controller is required in making decisions about the energy management on a HEPS.

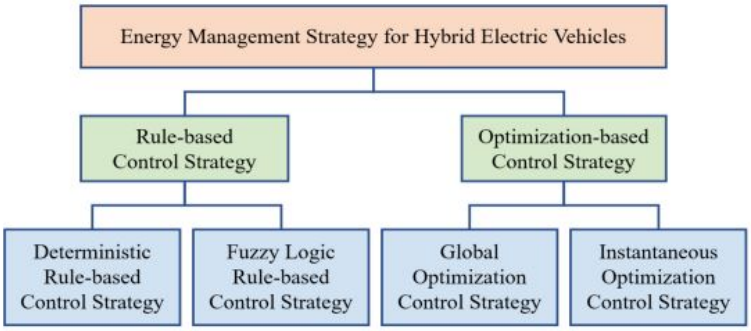

Figure 2.11. Control strategies for hybrid electric vehicles. [53]

Chapter 3

HEPS Simulation Framework

This chapter describes the numerical and surrogate modelling techniques developed in *MathWorks MATLAB®* to simulate the behaviour of the propulsion components and their synergy within the hybrid system. The framework has been explored in the past by David Pfurtscheller [54]; his thesis work was mainly oriented toward a performance matching problem between the simulation environment and the experimental data recorded from the parallel hybrid test bench, built at CFAR by Leonardo Machado and Jay Matlock [55] [56]. Therefore, the models were specialized in view of the configuration under testing.

The main effort of this work is to extend the capabilities of the framework in order to meet the requirements of different architectures and aircraft sizes. A multivariable approach is applied to allow for more complex distributed propulsion systems rather than single propeller ones. The scalability of the components is also a driving factor in order to allow the user to cover all the available combinations inside the design space of the hybrid propulsion system.

In order to increase the accuracy and validate the models, experimental measurements coming from both test bench demonstrations and flight campaigns of an eVTOL UAV configuration, named Mini-E, are taken as reference and integrated with the purpose of tuning the tool. In figure 3.1 the electric quadcopter architecture is displayed and in table 3.2 a brief description of the propulsion system is given. More details can be found in [22].

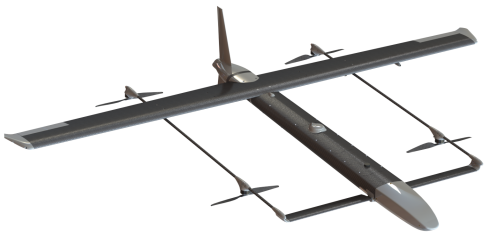

Figure 3.1. CAD rendering of the Mini-E.

Component	Type	n
Front/Rear Rotor EM	MN4012 KV480	4
Front/Rear Rotors	T-Motor P14x4.8	4
Front/Rear Rotor ESCs	Air40	4
Pusher Propeller EM	KDE4012 KV400	1
Pusher Propeller	APC 15x13N	1
Pusher Propeller ESC	KDE-UAS55	1

Figure 3.2. Components list of Mini-E.

3.1 Simulation Platform Architecture

The fundamental purpose of the framework, as introduced in chapter 1, is to evaluate the performance of conventional and novel hybrid FW-VTOL UAV configurations. Thus, in order to allow the user to sweep mission parameters, features of the components and to test different control strategies, the platform is structured in a modular chain, keeping each model independent and separated from the others, so that single parts can be exchanged or updated to meet the top-level-aircraft-requirements (TLARs) in the most effective way. This is achieved by employing an object oriented-approach.

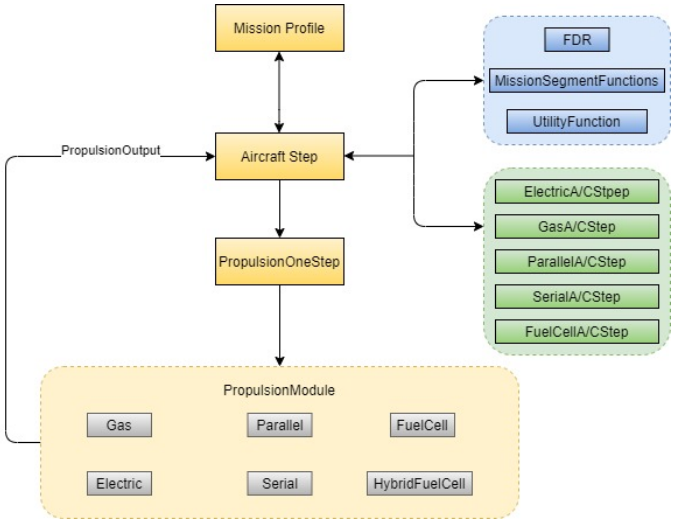

Figure 3.3. Flowchart of the information between the various modules of the simulation platform.

The flowchart displayed in figure 3.3, shows the iterative backward-looking architecture of the framework that was inherited from previous versions.[54]
In the iterative backward approach, the mission profile is the starting point of the simulation, from which at every time-step the performance of the powertrain are then evaluated in the lower levels of the code. This module is the one interfacing with the user, where the features of the aircraft under analysis, together with the mission parameters, are specified and given in input to the tool. The framework allows the user to select from a variety of flight conditions, such as vertical operations, hover, transition and forward motion, which can be combined in the most creative way in order to explore the behaviour of the concept being tested. Moreover, at this level it is enable to customize the profile through a control over the operational parameters, like vertical climb speed, hover time, climb angle and dash speeds. Finally, the user can set the time step of each segment to increase or reduce the resolution of the simulation; clearly for legs in which the aircraft is nearly in steady-state conditions the value should be higher to minimize the computational time and obtain fairly accurate results; while for more dynamics segments, it should be reduced to precisely evaluate the aircraft behaviour.
The operational data specified by the user are sent to the first level embedded in the

tool. The aircraft class loads the aerodynamic characteristics and structural properties of the system, such as polar curves, area of the main surfaces, empty weight and Maximum Take-Off Weight (MTOW). Utility and mission functions are linked to define boundary conditions such as current altitude, density, stall speed and the evolution of the aircraft mass in time which are fundamental in the computation of the forces acting on the aircraft. Finally, a Flight Data Recording (FDR) system saves the variables of interest for final interpolations and plotting purposes.
Depending on the propulsion system selected, the aircraft module receives components data and properties for the electric, gasoline, parallel, series or fuel cell architecture and accordingly, it activates the right propulsion module. This function generates the specific output to that subclass and then sends back the information to the aircraft module. The process iterates at each time-step until the end of the mission.

3.2 Aircraft Mechanics

The first step of the backwards energy state model implemented is to determine the thrust requirements for the specific flight condition according to the aircraft mechanics, which are then translated into power requirements inside the components modules. A variety of mission segments is available in the tool and for the majority of them the UAV is assumed to be in a trimmed steady-state and as a 2-Dimensional point mass on which vertical and horizontal forces act to achieve the equilibrium of the system. Since the overall performance rather than transient behaviour modelling of the UAV are the main focus, the previous assumption is deemed acceptable and the study maintains its legitimacy.

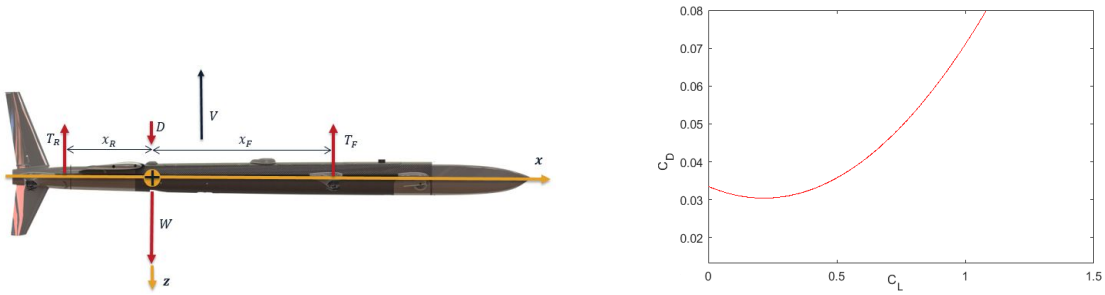

(a) Aircraft model.

(b) Mini-E drag/lift polar curve.

Figure 3.4. UAV scheme and aerodynamic characteristic.

3.2.1 Mission Segments

Vertical Flight

During axial operations, the aircraft must respect the vertical and momentum equilibrium equations presented in 3.1, which are written for multicopters mounting the rotors in a symmetric disposition or lying on the axis of symmetry. In the equations the vertical speed V_c is considered greater than zero during climb and lower than zero in descent.

$$\begin{cases} n_F \cdot T_F + n_R \cdot T_R - TWR \cdot W - D = 0 & \text{if } V_c > 0 \\ n_F \cdot T_F + n_R \cdot T_R - TWR \cdot W + D = 0 & \text{if } V_c < 0. \\ n_F \cdot x_F \cdot T_F - n_R \cdot x_R \cdot T_R = 0 \end{cases} \tag{3.1}$$

As displayed in 3.4(a), T_R and T_F are the thrust produced by the rear and front motors, respectively; x_R and x_F are the relative distances of the rotors to the centre of gravity, W is the weight of the aircraft, ρ is the air density for the prescribed altitude, D is the drag force. This parameter is defined according to 3.2, where the contribution coming from lifting surfaces and fuselage is modelled by mean of the theoretical coefficients defined for a flat plate and a cylinder perpendicular to the flow. [57] The TWR is the Thrust-over-Weight-Ratio required to guarantee the control and maneuverability of the UAV.

$$D = \frac{1}{2} \cdot \rho \cdot V^2 (A_{wing} \cdot 1.28 + A_{fuselage} \cdot 0.8425) \tag{3.2}$$

Hover

For the hover segment, the equations are kept as in 3.1, but in this case the vertical speed is set to zero and thus the contribution of the drag disappear.

Transition

The transition phase consists of a level transition flight, in which the altitude is assumed constant. During this mode, the UAV must respect the equilibrium equations along the vertical and horizontal axes, together with the pitch moment equilibrium, 3.3. At each time-step the forward speed increases and the aerodynamic forces are updated accordingly to the loaded polar curve, as shown in 3.4(b). From the system of equations the required vertical thrust to maintain the equilibrium is computed along with the thrust T_p of the defined number n_p of pusher propellers, with the additional boundary condition that the contribution of the VTOL rotors should only be set to zero if the stall speed of the aircraft is overpassed.

$$\begin{cases} L_w + n_F \cdot T_F + n_R \cdot T_R - W = 0 \\ n_p \cdot T_p - D = 0 \\ M_{aero} - n_F \cdot x_F \cdot T_F - n_R \cdot x_R \cdot T_R = 0 \end{cases} \tag{3.3}$$

Since the time required to transition in case of light UAVs results in the order of seconds, a high level of resolution must be kept in order to correctly simulate the evolution of forces during this mode.
The equations hold for both forward and backward transitions and also for the case of tilting rotors, since, instead of using the angle of rotation to define the contributions of the mechanism in the 2D plane, the thrust can be decomposed into the horizontal and vertical components which are then trigonometrically summed together to have the total request at the propeller.

Forward Flight

For the fixed-wing motion the loiter, cruise, dash or climb segments can be activated based on the input variable commanded, such as flight speed, flight time or climb angle. The equilibrium equations presented in 3.4 compute once again the thrust required to maintain the trimmed conditions, based on the aerodynamic characteristics of the aircraft.

$$\begin{cases} n_p \cdot T_p \sin\theta - D\sin\theta + L\cos\theta - W = 0 \\ n_p \cdot T_p \cos\theta - D\cos\theta - L\sin\theta = 0 \end{cases} \tag{3.4}$$

Where θ is the climb angle, defined between the horizontal earth axis and the velocity vector, which in case of small angles of attack, may be assumed overlapping with the longitudinal axis x of the aircraft.

3.3 Modelling of the HEPS Components

In order to reach a fair level of accuracy in the evaluation of the aircraft state and, particularly, of the propulsion system performance, the simulation must rely on proper modelling schemes for each component of the powertrain. Although the models formulation is based on a low fidelity approach, since most of them rely on manufacturer databases and simplified analytical equations, in this section their validity is reviewed, by comparing the results with experimental data recorded during test sessions.

3.3.1 Battery Model

The selection of Lithium-Polymer (Li-Po) battery for the framework model is due to its common use in the aerospace field as onboard energy harvesting system, especially for UAVs, and because of the deep knowledge CFAR has with this technology, since it has been largely applied in many projects, [22] [56], and a wide dataset could be used to validate the results.

The modelling and characterization of Li-Po has been explored in the past by a research group at University of Victoria [58]. The charging and discharging curves of LiPo were developed according to equations 3.5 and 3.6, proposed by *MathWorks MATLAB®* for the Simulink environment.[59]

- Charging ($I_n < 0$)

$$V(I_t, I_n) = V_0 - \frac{K \cdot Q \cdot I_n}{I_t + 0.1Q} - \frac{K \cdot Q \cdot I_t}{Q - I_t} + A \cdot \exp(-\beta \cdot I_t) \tag{3.5}$$

- Discharging ($I_n > 0$)

$$V(I_t, I_n) = V_0 - \frac{K \cdot Q \cdot I_n}{Q - I_t} - \frac{K \cdot Q \cdot I_t}{Q - I_t} + A \cdot \exp(-\beta \cdot I_t) \tag{3.6}$$

Thanks to constant rate battery discharging tests, the exponential voltage coefficient A, the exponential capacity coefficient β and the polarity voltage K required by the model to describe the exponential zones of the voltage output drop were assessed and uploaded. The

internal properties of the batteries, such as the nominal voltage V_0, the internal resistance and the capacity Q, were normalized with respect to the number of cells to ensure the scalability of the model. Thus, the nominal current I_n (A), the current request and the time-step, which defines the extracted capacity I_t (Ah), and the battery size (number of cell in series), are required as input to compute the output voltage V.
Based on the sign of the current in input, the charge mode or discharge mode is activated and thus the state of charge (SOC) of the battery can be evaluated using equation 3.7.

$$SOC = 100\left(1 - \frac{\int_0^t I_t}{Q}\right) \tag{3.7}$$

A mass model is also embedded, where a conservative value of 179 Wh/kg is assumed, [44], but it can easily be updated if more detailed information on the battery selected is available.
Finally, even though electric energy is seen as a zero emissions solution for the future greener aviation, at the state of the art its generation still relies on fossil resources and not only on renewable ones. Thus, an emission index of $7.09 \cdot 10^{-4}$ $metricTonCO_2/kWh$ is defined to take into account the indirect emission of CO_2, according to the standard set by ETA (United States Environmental Protection Agency) [60] in their greenhouse gases equivalences calculator website.

3.3.2 Propeller Model

Through the propeller model, the thrust requirements determined in the aircraft dynamic model are translated into torque, rpm and thus power demand at the propeller shaft. These parameters are then passed to the selected propulsion branch, in which a matching loop is used to find the operational point capable to fulfill the inputs. Thus, the accuracy of this starting point is of extreme relevance for the correct evaluation of the performance of the components. In order to achieve this result, a selection between three different methods is given to the user.

Blade Element Momentum Theory

In case the analysis is still at a conceptual design phase, in which many details on the components are missing, an in-house blade-element code is proposed to simulate the performances of two-blades propeller. The Blade-Element-Momentum-Theory (BEMT), as explained in [61], divides the propeller geometry into n sections along the radius and predicts the lift and drag properties of each section allowing to evaluate the thrust and torque generated by the propeller. The model is generated parametrically thanks to a APC propeller database collected by [58]. Using the information coming from this database the model can be morphed for any desired geometry and propeller sizes, allowing to compute the efficiency, thrust and power coefficients at any input velocity given along the mission. However, its accuracy drops when propeller designs extremely dissimilar to the APC brand are used and when the speed reaches static conditions.

Vortex Model

In case a full knowledge of the propeller geometry is available to the user, a MATLAB®script developed by Dr. Jose Vale, based on the Goldstein formulation of the Vortex theory, can be called.[47] [49] The model requires the number of blades, pitch, diameter, chord distribution along the radius and hub size in order to extrapolate the propeller's performance characteristics. The model has the advantage of closely matching thrust, power or rpm requirements even at zero stream velocity working conditions and it has been successfully tested by [22].

Experimental and Manufacturer Data

The last option available to the user is to upload in a dedicated folder the data coming from test bench experiments or manufacturer datasheets. The code elaborates the thrust, torque, rpm and power in input and creates the thrust and power coefficient curves necessary for the computational logic of the model, as explained in the next section. This simplified approach has been used in the past by [54] to match the performances of the parallel hybrid test bench.

Thrust Matching Problem

Regardless of the method selected, the simulation logic of the propeller model relies on the non-dimensional terms C_T and C_P, which are the thrust and power coefficient, respectively. These terms describe the main performance characteristics of the propeller, in terms of shaft power P and produced thrust T, as shown in equations 3.8 and 3.9, where ρ is the air density, n represents the revolutions per second, and D is the propeller diameter.

$$C_T = \frac{T}{\rho \cdot n^2 \cdot D^4} \tag{3.8}$$

$$C_P = \frac{P}{\rho \cdot n^3 \cdot D^5} \tag{3.9}$$

For each propeller under analysis, depending on its pitch, diameter and shape of the blades, it is possible to define its own set of C_T and C_P over the range of operational rpm thanks to the previous mentioned theories. Hence, given the thrust requirements in input, the model iteratively sweeps the C_T and rpm combination along a curve fitted over the computed points, until the relative error between the commanded thrust and the value obtained from 3.8 goes under a defined threshold. Once the condition is matched, the rpm is passed to the power coefficient fitted curve and so the values of rpm, C_T and C_P are extrapolated and stored in order to be available for the subsequent model, in which they are used to calculate the torque and power requirements at the crankshaft.

For a conceptual design evaluation study, in which only the rough dimension of each propeller is known, the method defined by Roskam in [62] for propellers with input power of less than 50 HP, is implemented to compute the mass. Equation 3.10 presented below has been converted according to the International System of Units.

$$m_p = 9.771 \cdot 10^{-2} \cdot K \cdot n_b^{0.391} \left(\frac{D_p \cdot P_{max}}{1000} \right)^{0.782} \tag{3.10}$$

In the formula n_b is the number of blades, D_p the propeller diameter and P_{max} the maximum power in input at the propeller shaft. Here, an additional correction factor K is

included to account for different propeller materials available nowadays. After a market research validation, a value of 1.0 is recommended for the usual plastic ones and 0.3 for the new composite technologies.

3.3.3 Electric Motor Model

A brushless direct current (BLDC) electric motor is the basis of the electric motor model in the simulation environment. The reason behind it, is because the use of BLDC motors is rapidly spreading in the unmanned aerial vehicles field, especially for small scale, due to their inherent high efficiency and reliability by removing the necessity of commutation brushes. As common practice, a simplified Kirchhoff's Law equivalent circuit is used to model brushless DC motors performance. Its characterization relies on the three main parameters: motor constants K_V, which describes the proportionality between the motor revolution per minute and its voltage [rpm/V], the no-load current I_0 in amps [A] and the internal resistance R_m measured in ohms [Ω], as displayed in figure 3.5. These are loaded in the circuit to determine the key performance parameters for the electrical side of the tool, such as the current drawn from the battery, the voltage level of the battery and the throttle setting. To solve the circuit, several relations need to be defined.
The starting point is the back-electric-motor-force (EMF) equation:

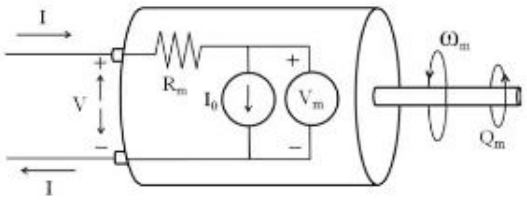

Figure 3.5. Simplified diagram of a BLDC motor equivalent circuit. [43]

$$V_{emf} = V_m - I_m \cdot R_m \tag{3.11}$$

This voltage is given by the difference of the supplied voltage V_m and the voltage drop across the internal resistance. It is directly connected to the rotational speed of the shaft ω_{shaft} through the rotational proportionality constant K_V, according to equation:

$$\omega_{shaft} = K_V \cdot (V_m - I_m \cdot R_m) \tag{3.12}$$

The torque output of the motor τ_{EM} can then be computed as a function of the applied current flowing through the motor:

$$\tau_{EM} = \frac{I_m - I_0}{K_V} \tag{3.13}$$

In order to integrate the throttle variable, power conservation laws between the battery and the EM have been applied. Since the Electronic Speed Controller (ESC), between the

battery and the EM, controls the rotational speed of the EM by reducing the voltage level according to the throttle setting, a decrease in voltage must be related to an increase of current by the same factor:

$$I_M = \frac{I_{batt}}{Throttle} \cdot \eta_{EM} \qquad (3.14) \qquad V_m = V_{batt} \cdot Throttle \qquad (3.15)$$

where V_{batt} and I_{batt} are the voltage and current supplied by the battery, while η_{EM} is the EM efficiency, which depends on the supplied voltage and the torque request. Unless datasheets of the manufacturer are available, the literature suggests an efficiency value of 90% as conservative in view of the rapid development of these technologies. [44] After, equations 3.14 and 3.15 can be now substituted into 3.12 and 3.13 to determine the power in input to the EM and in output at the shaft:

$$P_{EM} = \frac{I_{batt}}{V_{batt}} \cdot \eta_{EM} \qquad (3.16)$$

$$P_{shaft} = K_V \cdot \left(V_{batt} \cdot Throttle - \frac{I_{batt}}{Throttle} \cdot \eta_{EM} \cdot R_m \right) \qquad (3.17)$$

The determination of the throttle, current, voltage and consequent SOC of the battery is now possible by solving a system of equations. More information about this iterative process can be found in [54].
It is possible to model the electronic speed controller considering the efficiency aspect about the energy dissipation inside the ESC, but in this module it has been simplified for a set 90% efficiency for all voltages and load capacities.

Finally, the model requires also the maximum power output of the EM in order to compute its mass. Many linear extrapolation laws of available COTS BLDC have been found in the literature, [41], but generally the assumption of a power density equal to $5kW/kg$ is deemed accurate enough for the state of the art. [44] While for permanent magnet generator, which is the major type applied in the UAV field, the mass is calculated by equation 3.18 based on the data from several generator manufacturers.[39]

$$m_{gen} = 0.385 \cdot \left(\frac{P_{gen,max}}{1000} + 0.44 \right) \qquad (3.18)$$

3.3.4 Internal Combustion Engine Model

The Willans line model introduced in section 2.2.1, is here developed with more detail to create numerical models of internal combustion engines of virtually any desired size, thanks to its scaling approach.
The normalized formulation of the method relies on only two engine parameters: displacement V_d $[m^3]$ and piston stroke S $[m]$. These are used to express the torque and rotational speed of the engines in terms of mean effective pressure p_{me} $[Pa]$, which describes the engine's ability to produce mechanical work, and mean piston speed ν_m $[m/s]$, according to their definition presented in 3.19.

$$\begin{cases} p_{me} = \tau_e \cdot \left(\frac{2\pi}{V_d} \right) \\ p_{ma} = H_{LHV} \cdot \left(\frac{2\pi}{V_d} \right) \frac{\dot{m}_f}{\omega} \\ \nu_m = \frac{S}{\pi} \cdot \omega \end{cases} \qquad (3.19)$$

Here, p_{ma} is the available mean effective pressure in $[Pa]$, representing the chemical energy granted by the fuel, which in this case is assumed to be gasoline, is characterized by an average lower heating value H_{LHV} of 44 $[MJ/kg]$.[38]
With these definitions, equation 2.7 can be rewritten as:

$$p_{me} = e \cdot p_{ma} - p_{mloss} \tag{3.20}$$

where p_{mloss} is:

$$p_{mloss} = \frac{2\pi}{V_d} \cdot \tau_{loss} \tag{3.21}$$

The literature [37] suggests to use the following parametrization to define the Willans line coefficients:

$$\begin{cases} p_{me} = [e_0(\nu_m) - e_1(\nu_m) \cdot p_{ma}] \cdot p_{ma} - p_{mloss}(\nu_m) \\ e_0(\nu_m) = e_{00} + e_{01} \cdot \nu_m + e_{02} \cdot \nu_m^2 \\ e_1(\nu_m) = e_{10} + e_{11} \cdot \nu_m \\ p_{mloss}(\nu_m) = p_{mloss0} + p_{mloss2} \cdot \nu_m^2 \end{cases} \tag{3.22}$$

Where e_{00}, e_{01}, e_{02}, e_{10}, e_{11}, p_{mloss0}, p_{mloss2} are engine characteristic parameters usually obtained by multiple linear regression from benchmark engine test data.
Since for small UAVs usually the size of ICEs ranges from 10cc to 70cc, and since a lot of work and experience has been previously gained on the Desert Aircraft DA35 by Pfurtscheller [54], its size is deemed to be a good reference trade-off. Its datasheets is presented in appendix B.1, and thus the performance data are used as main reference to extrapolate the efficiency-coefficients of equation 3.22 by mean of a least-square fit method, presented in the equation below.

$$\min_{e_{00},e_{01},e_{02},e_{10},e_{11},p_{mloss0},p_{mloss2}} \sum_{i=1}^{n} \left([e_0(\nu_{m,i}) - e_1(\nu_{m,i}) \cdot p_{ma,i}] \cdot p_{ma,i} - p_{mloss}(\nu_{m,i}) - p_{me,i}\right)^2 \tag{3.23}$$

The minimum is found by setting the partial derivatives with respect to e_{00}, e_{01}, e_{02}, e_{10}, e_{11}, p_{mloss0}, p_{mloss2} equal to zero. In appendix A.1 the seven equations obtained from this process are presented. The system is then solved in terms of the efficiency-coefficients, which have been computed and are shown in table 3.1 below.

Once these parameters are defined, the scaling procedure can be implemented by following the listed steps:

- The stroke S_{scaled} and displacement $V_{d,scaled}$ of the scaled engine need to be given as input.
- The mean piston speed and available mean effective pressure are scaled according to:

$$\nu_{m,scaled} = \nu_{m,model} \cdot \frac{S_{scaled}}{S_{model}} \tag{3.24}$$

$$p_{ma,scaled} = p_{ma,scaled} \cdot \frac{V_{d,scaled}}{V_{d,model}} \tag{3.25}$$

Willans Coefficients		
e_{00}	0.0478	/
e_{01}	0.0459	$\frac{s}{m}$
e_{02}	-0.00125	$\frac{s^2}{m^2}$
e_{10}	-2.17 $\cdot 10^{-9}$	$\frac{1}{Pa}$
e_{11}	-2.82 $\cdot 10^{-9}$	$\frac{s}{Pa \cdot m}$
p_{mloss0}	-533.68	Pa
p_{mloss2}	5.32 $\cdot 10^{3}$	$\frac{Pa \cdot s^2}{m^2}$

Table 3.1. Willans multi-linear regression fitted coefficients from DA35.

- The mean effective pressure for the new engine is calculated by using the efficiency-coefficients previously computed:

$$p_{me,scaled} = [e_0(\nu_{m,scaled}) - e_1(\nu_{m,scaled}) \cdot p_{ma,scaled}] \cdot p_{ma,scaled} - p_{mloss}(\nu_{m,scaled}) \tag{3.26}$$

- The torque and speed of the scaled engine can then be determined:

$$\tau_{e,scaled} = p_{me,scaled} \cdot \frac{V_{d,scaled}}{2\pi} \tag{3.27}$$

$$\omega_{scaled} = \nu_{m,model} \frac{\pi}{S_{scaled}} \tag{3.28}$$

- The scaled BSFC map is finally obtained with:

$$\dot{m}_{f,scaled} = p_{ma,scaled} \cdot \omega_{scaled} \cdot \frac{V_{d,scaled}}{2\pi \cdot H_{LHV}} \tag{3.29}$$

These efficiency-related parameters and process are first experimentally validated against the data collected for the DA35, and then a more extensive calibration of the scaling approach is obtained thanks to the database of manufacturers and experimental engine maps for a range of two-stroke combustion engines collected by Matlock [55].

ICE Model Validation

In order to verify the scaling accuracy granted by the method, two identifications procedures relative to ICEs are carried out, analysing first the difference between the reference experimental data and the model, and then the over-sizing of the engine.
In figure 3.6, a comparison between the experimental brake mean effective pressure (BMEP) and the corresponding values resulting from the application of Willans line model for the DA35 is highlighted. On the right, the distribution of the experimental data over the engine operation range is also presented. For both cases the results present a satisfactory

accuracy, with a good fitting as proven by the value of the coefficient of determination, equal to 0.9462.

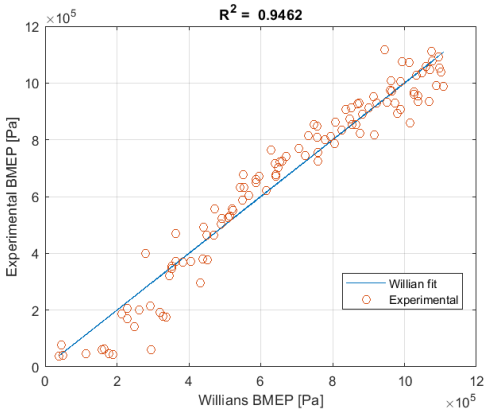

(a) Comparison between measured and simulated MEP for DA35.

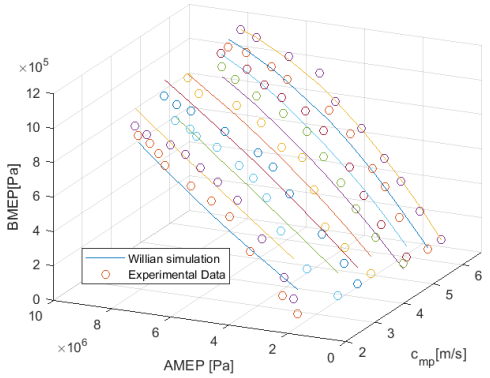

(b) Comparison between Willans line model and experimental data of DA35 grouped by engine speed.

Figure 3.6. Desert Aircraft 35 experimental and simulation data comparison.

In figure 3.7, the fuel consumption data obtained from manufacturer and from the model have been interpolated in MATLAB and the resulting surfaces are displayed. As it is typical with two-stroke engines, the DA35 is most inefficient at low speeds and low torque positions, and is suited more for high RPM and high torque setting applications. It is possible to identify how, despite its apparent simplicity, this representation of the ICE fuel consumption map fairly reproduces the actual engine data for the core region of the operational range, whereas it slightly distorts the boundaries at low rpm and torque.

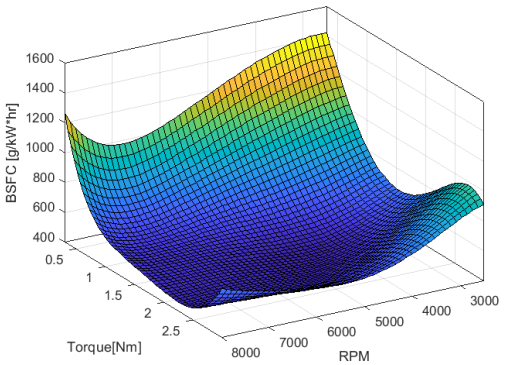

(a) Experimental brake specific fuel consumption map of DA35.

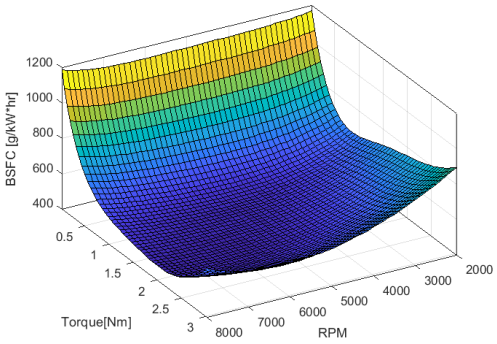

(b) Willans line simulation of the brake specific fuel consumption map for DA35.

Figure 3.7. Experimental and simulated brake specific fuel consumption map of DA35.

The same study was carried out for a Desert Aircraft 50, proving the scaling up applicability of the model. The resulting comparison between the extrapolated surface over the experimental and simulated data 3.8, shows once again how the model is capable of accurately describing a wide region of the fuel map, but lacks at the rpm and torque edges.

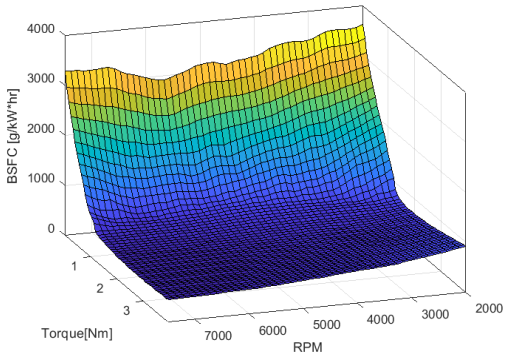

(a) Experimental brake specific fuel consumption map of DA50.

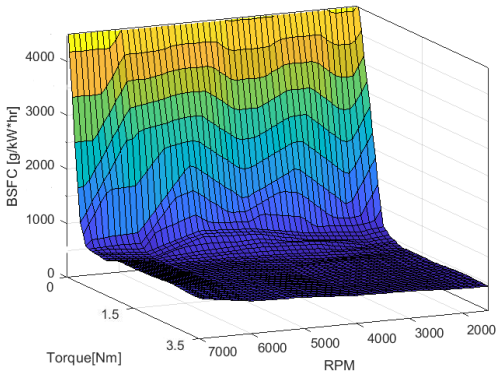

(b) Willans line simulation of the brake specific fuel consumption map for DA50.

Figure 3.8. Experimental and simulated brake specific fuel consumption map of DA35.

This modelling can be repeated on other engines if more steady-state efficiency reference data are available. A denser database of Willans line coefficients for a wide range of engine sizes can bring to higher level of accuracy, since the starting point of the scaling process could be chosen closer to the target point, allowing to better evaluate performance parameters such as the power, BSFC and the fuel flow of a new scaled engine in future analysis. In fact, despite the applicability of the method deemed to be acceptable for this type of preliminary exploration, it is recommended to simulate only engine belonging to the same reference engine's class and only within thirty percent size range, since the accuracy of the predicted data decreases as the size difference between the baseline engine and the required engine increases.

The information extracted from the model allows the simulation framework to return estimates for engine torque, power, BSFC or RPM based on inputs for any scale of engine within the modelling range. Finally, its main advantage lies on the possibility to select the optimal component by sweeping only the engine displacement and piston stroke.

Conceptual design and emissions

In order to support analysis at a conceptual design level, where the user is trying to determine the right ICE for the application, knowing only estimates on the power required or average size, a mass and emission models are also integrated in the tool.

The mass model is taken from [63] and consists of a specific regression function for two strokes engine, through which the ICE mass can be estimated starting from the design variables.

$$m_{ICE} = \left(40.15 \cdot V_d^{0.9046} + 192.5\right) /1000 \tag{3.30}$$

In equation 3.30 the displacement V_d is expressed in $[cm^3]$ and the mass m_{ICE} is in kg. With the Willans method previously explained, the efficiency and performance maps can then be determined.
In case instead of the engine dimensions only the maximum power request from the ICE is known, the process can be reversed through equation 3.31 to determine the ICE size.

$$V_d = \frac{P_{max,ICE} - 454.9}{70.39} \tag{3.31}$$

where the maximum power is expressed in $[W]$. To take into account also the weight for the integration and support of the ICE onboard, a conservative estimate of 25% of the engine weight, as proposed by [27], is assumed. These linear regression laws have been validated inside their studies, proving to match with a small discrepancy the many manufacturer data collected.

Finally, to estimate the CO_2 emission of the aircraft, which mainly comes from the oxidation of gasoline, the emission index defined by ETA, [60], currently set to 0.315 $kgCO_2/kg$ is added into the model.

3.3.5 Electric Propulsion Branch

The main components of the electric propulsion branch are battery, ESC and a EMs, modelled according to what explained in the previous sections. The sequence of functions called inside the system model is presented in figure 3.9. In the first step, the thrust vector computed by the aircraft model along the segment is loaded together with the necessary mission variables as well as individual component data for the motors, propellers, ESCs and the battery system. This information is first used by the propeller model, which for each rotor computes the C_T, C_P and rpm values matching the thrust requirement. Power and torque at the shaft of the EM can then be estimated, and thus an iterative system solver is run to find the converging solution for throttle, voltage and current condition between each EM and the battery that fulfills the demand. The power requirement calculation considers the inherent efficiencies of each of the components to ensure sufficient power remains after losses. In the last step, the SOC of the battery is then updated, together with the emissions and other state variables which are given in output and saved in the FDR at the end of the simulation time-step.

3.3.6 Gasoline Propulsion Branch

The gasoline propulsion branch, although presenting several differences, follows a similar flow of information as the electrical module, as it can be seen in figure 3.10. The iterative loop of each time step starts always from the flight conditions, in terms of equilibrium of forces and environmental factors, loaded into the module together with components data for engine parameters, propeller data, and fuel capacity. Again, regardless of the modelling of the propeller selected, the thrust requirements are translated through a matching algorithm into rpm, torque and power demands that are fed to the ICE model. Here, based on the data available to the user, according to the description given in section 3.3.4, it is possible either to input the power request, which is converted in engine dimensions through equation 3.31, or either input directly the stroke and displacement if the size of the ICE is known,

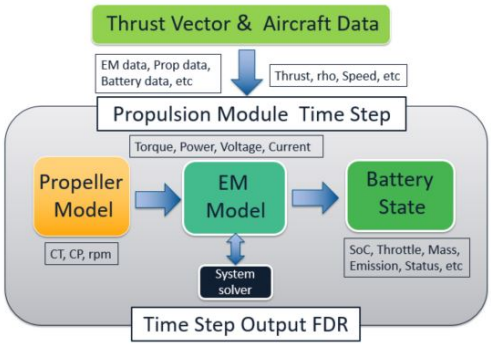

Figure 3.9. System modelling flow for electric propulsion branch.

and thus to generate the engine BSFC, torque, rpm map thanks to the Willans method. Lastly, it is also possible to select between the maps already generated into the database. By means of these maps, the rpm and torque conditions are identified on the interpolated BSFC surface to determine the fuel consumption at that time step. This information is passed to the fuel tank module where the fuel mass is updated and other status variables are given in output and recorded into the FDR. In fact, unlike the electric aircraft, the mass here changes over time as the fuel is burnt. The difference in aircraft mass has an impact on the aircraft's performance, and it is also captured to measure the amount of emissions produced by the aircraft.

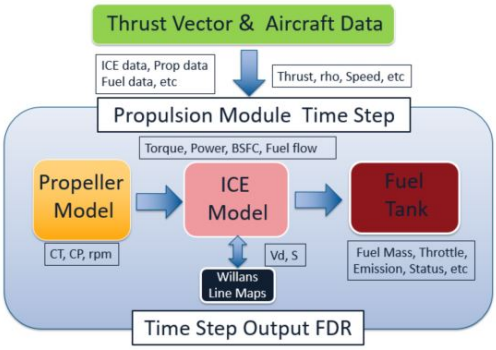

Figure 3.10. System modelling flow for gasoline propulsion branch.

3.3.7 Hybrid Branches

The architecture of both serial and parallel hybrid branches adds some complexity due to the combination and cooperation of the single electric and gasoline modules presented before. The flow of information follows a common structure, portrayed in figure 3.11, with few differences for the specific hybrid case.
As with the other modules, the initial inputs for this branch are the required thrust for the

current flight segment as well as the aircraft characteristics and components data defined in the according class. Again, the propeller model is in charge of converting these requirements into power, torque and rpm for the subsequent modules. These are loaded into the hybrid environment, broken into the two main configurations of hybrid propulsion systems, which operate much like both the electric and gasoline modules in line with the description given in chapter 2 for their high-level operating principles and difference in components.

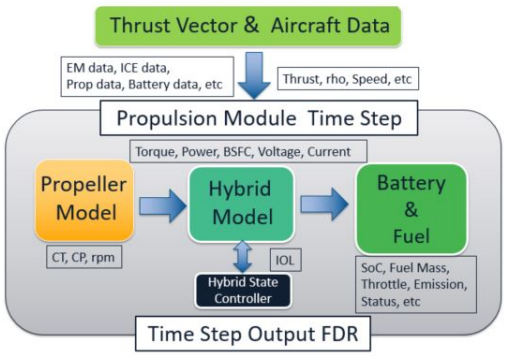

Figure 3.11. System modelling flow for hybrid propulsion branches.

This module is supervised by an energy management system implementing the Ideal Operating Line (IOL) strategy, explained in more detail in the next section, which determines the working mode of the system based on the input power request. The status of the ICE, EM and other components is then determined and the battery charge and fuel mass are updated. At the end of the time step important variables and emissions data just like the electric and gasoline modules, are saved in the FDR.

Ideal Operating Line Strategy

As already discussed in chapter 2, the implementation of the energy management strategy for the hybrid propulsion system is strongly linked to the overall efficiency of the powertrain and it should be optimized in view of the best working synergy between the components for the specific architecture and flight mission. In the design phase of the strategy various considerations need to be taken into account, in order to maximize the performance of the UAV while increasing fuel economy and decreasing the emissions. The main driving parameters to keep in consideration are the optimal operating point of the engine, the minimum engine speed, its turn-on turn-off frequency, recharge strategy of the battery and maximum charge current. The controller used in this work implements a rule-based approach, which was selected as its simplicity, reliability and successful implementation in other projects are well suited for a general application with many initial unknowns [8]. The basic concept behind the hybrid state controller implemented for both the serial and the parallel HEPS in the next section, is the application of the Ideal Operating Line (IOL). The IOL of an engine is defined as the trend smooth line on the fuel consumption map, interpolating the combinations of each torque and rpm points that corresponds to the lowest BSFC. This means that along this line the fuel consumption is minimal for different

power levels and theoretically, it would allow to operate the ICE at its most efficient point. Its generation was embedded inside the ICE model, where thanks to the Willans method the BSFC-Torque-RPM maps of the selected engine can be determined and then, through a minimization algorithm that discretizes the points of lowest possible BSFC for each torque-rpm combination, the IOL is extrapolated by means of a third order fit polynomial regression throughout the engine's operating range. An example of the IOL over constant BSFC contour map of the DA35 and DA50 is displayed in figure 3.12(a) and 3.12(b).

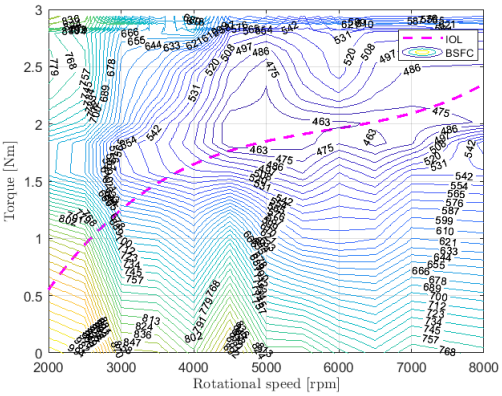

(a) DA35 engine IOL over iso-BSFC contour torque-RPM plot.

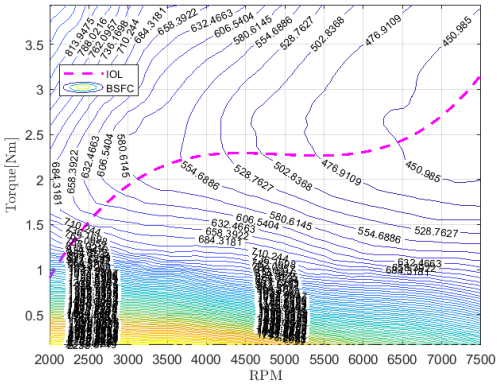

(b) DA50 engine IOL over iso-BSFC contour torque-RPM plot.

Figure 3.12. IOL example curves for reference engines.

In this way, for a standard hybrid mode, the controller determines the engine torque and rpm conditions along the IOL and thus the BSFC value for the operating point. Based on the power request, this result is then used as an input to calculate any remaining power that needs to be covered by the support of the EM. A better explanation of the hybrid operating modes is given in the section below.

Parallel Hybrid State Controller

The parallel hybrid state controller is designed in the most general way, trying to cover all the possible operating conditions for the HEPS and meanwhile allowing the user to set the state variables and control parameters to the best-suited values for the configurations under analysis.
This rule-based controller determines the hybrid mode based on three decision variables: state flags, battery SOC and power request. Since it cannot be known a priori the HF and how the power is allocated on board, the state flags are required to add an extra degree of control to the user, who can always force the hybrid state into charge or stealth modes by activating the *'chargeEnable'* and *'stealthEnable'* variables. However, for VTOL configurations an extra *'vtol'* flag is enabled in order to prevent the system from enabling the recharge mode during axial operations, where all the power is requested in output.
After, the battery SOC together with the power requirement dictate which hybrid state the propulsion system should operate in. In this way, certain hybrid modes may be unavailable during a particular flight segment. The battery charge is compared against *'Min'*

and *'Max'* cut-off values, which can be defined by the user to safely operate the battery inside its limits, which usually range between 15% and 90% [41], or for other safety purposes such as storing enough energy for a full-electric emergency landing in case of engine failure. In this case, the lower limit is computed after the first segment and cannot be exceeded afterwards.

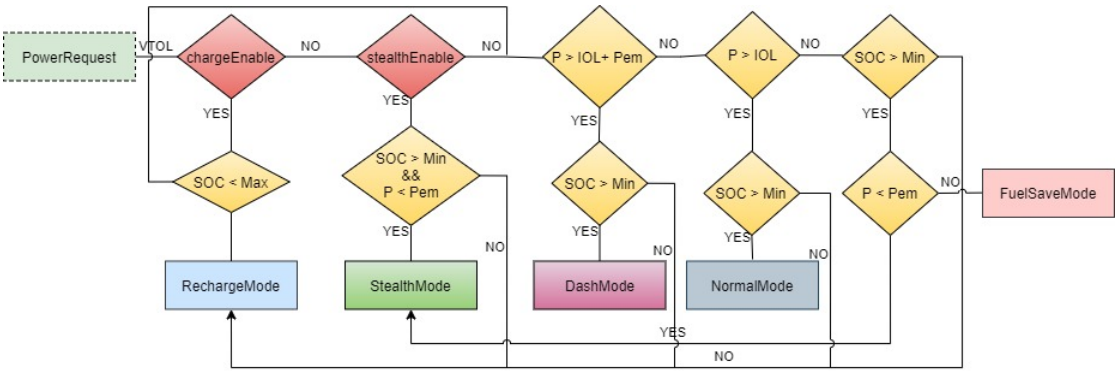

Figure 3.13. Parallel hybrid state controller.

The flowchart represented in figure 3.13 helps to understand the logic behind the controller. It is assumed that for parallel configurations generally the EM is used to support the ICE which represents the main power source. In view of this, the power requirement is split into two main contributions based on IOL 'optimal power' for the ICE to supply, P_{IOL}, and the maximum motor power, $P_{max,EM}$. Using this strategy, the ICE is kept at an ideal operating point whenever possible, and the electric motor will provide the extra power required, or recharge the battery as a generator when the power request is below optimal. The power conditions for the five operating modes of the parallel architecture are summarized in table 3.2: Dash, Normal, Fuel Save, Stealth and Charge.
The Dash mode represents the highest power output and energy consumption of the UAV for segments with extremely high speed, or climb angles up to the vertical operation conditions. Therefore, it needs both the contribution of the EM, which works at its maximum settings, and of the ICE, which covers the remaining request. In the Normal mode the ICE works at the optimal power according to the IOL conditions and the remaining necessary power is supplied by the EM. If the demanded power is lower than the IOL value, based on the SOC of the battery, the recharge mode can be activated, otherwise a second check to compare the power request with the maximum EM power is computed and either the Stealth mode or the Fuel Save mode can be activated. In the Fuel Save mode the engine is decelerated to its idle conditions and only supports the EM. Therefore, this mode relies less on the fuel onboard. The Stealth mode is the most eco-friendly one as it relies only on the EM. All four strategies lead to a decrease of the SOC varying in magnitude according to the mode, as explained by the sign of the current in table 3.2. Lastly, if not forced, the Charge mode is feasible if the ICE operated at the optimal power request exceeds the power requirement and the SOC of the battery is below the maximum charge level. Then the extra supplied power of the engine will be converted by the EM into electric energy to charge the battery with a safety switch protection of 1C maximum recharging current.

One last note for the parallel hybrid electric system should be made regarding the implementation of a clutch or gearing system along the transmission. Classically, small UAV do not implement any kind of decoupling between the propeller and the ICE due to the additional mass penalty and thus it was not included into the controller. However, despite being lighter and less complex, this concept forces the ICE to operate away from its actual most efficient point. In fact, the rpm condition is set by the propeller and, even though the IOL control can partially solve the problem, it does not not always fall inside the engine's optimal region. Instead, a decoupled transmission could bring higher fuel savings, keeping the ICE in its ideal range of torque-rpm and avoiding acceleration and deceleration processes of the engine, just like for the series architecture.

Mode	ICE	EM	Current
Charge	P_{IOL}	P_{req} - P_{IOL}	< 0
Stealth	—	P_{req}	> 0
Dash	P_{req} - $P_{max,EM}$	$P_{max,EM}$	> 0
Fuel Save	P_{idle}	$P_{max,EM}$	> 0
Normal	P_{IOL}	P_{req} - P_{IOL}	> 0

Table 3.2. Operating mode conditions for the parallel hybrid system.

Series Hybrid State Controller

The serial hybrid state controller works much like the parallel one, with few differences regarding the state flags and control parameters. In fact, for this case the power constraints are not related to the EM anymore, since for the serial architecture the EM fulfills the power requirements at every flight condition. Instead, the variables of interest are the power drawn from the battery and the power generated from the ICE-Generator module. Moreover, as explained before, since through the generator the ICE is completely decoupled from the propeller, its operational conditions can be associated to the optimal operational point (OOP), which represents the lowest BSFC region in an engine map. This condition brings an upgrade to the IOL strategy, since now the minimization algorithm can be run for a preselected range of rpm and it does not have to follow the propeller characteristic curves. For example, as shown in figure 3.12, it is preferable to operate two-stroke engines in high torque and high RPM ranges of the engine map to increase the efficiency, otherwise the ICE suffers of substantially lower performance. The serial hybrid configuration, therefore, results to be more fuel-efficient, but part of this advantage is lost in the conversion of the power from mechanical to electrical form inside the generator.
Figure 3.14 shows the serial hybrid controller flowchart. The modes are redefined according to the $P_{max,GEN}$ and P_{opt} which represent the maximum power output of the generator and the ideal optimal power identified for the ICE, as summarized in table 3.3. In the same way as for the parallel, the Dash mode requires the highest amount of power, which is covered by the combination of generator and battery. If the power demand is higher than the optimal condition of the engine, the SOC is evaluated and based on its value the Normal

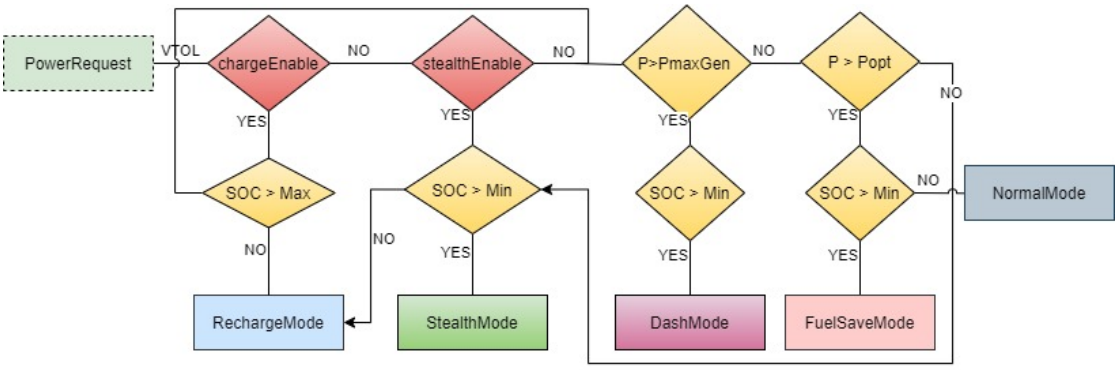

Figure 3.14. Series hybrid controller.

or Fuel Save mode are activated. The first one relies purely on the ICE-Generator system and it does not take advantage of any battery energy. The second one instead, minimizes the fuel consumption by operating the engine at $P_{opt]}$ and drawing the remaining power from the battery. Finally, if they are not forced through the state flags, the last two modes are activated when the power is below the optimal conditions. Then either the Stealth mode or the Recharge mode can be called based on the SOC. Again, a safety switch is integrated to avoid recharging currents higher than 1C.

Mode	ICE/GEN	Battery	Current
Charge	P_{opt}	P_{req} - P_{opt}	< 0
Stealth	—	P_{req}	> 0
Dash	$P_{max,GEN}$	P_{req} - $P_{max,GEN}$	> 0
Fuel Save	P_{opt}	P_{req} - P_{opt}	> 0
Normal	P_{req}	—	> 0

Table 3.3. Operating mode conditions for the serial hybrid system.

3.3.8 Fuel Cell Model

Recently, a mathematical model for Proton-Exchange Membrane Fuel Cells (PEMFC) developed by Phillip Sharikov [64] has been integrated into the simulation framework. The model was built upon 6 inputs: the aircraft power request, its initial temperature, the type of cooling performed, the pressures of the fuel and the oxidizer streams and the fuel cell configuration. The last one is defined by its five most relevant parameters, meaning the number of stacks, the number of cells in each stack, the stack's weight, its volume, and heat capacity. A fuel cell/battery hybrid, which uses a fuel cell electrically coupled with a battery in parallel to drive an electric motor for propulsion, and a fuel cell/gasoline hybrid, which mechanically couples an electric motor powered by a fuel cell to an internal

combustion propulsion have been implemented and the model has been validated using data available from the manufacturer.

3.4 Experimental Validation and Flight Mission Simulation

In this section, the validation of the electric branch of the simulation tool is performed by comparing the results obtained from the framework with the experimental data recorded in both a EM-propeller test bench of the Mini-E components, presented in table 3.2, and with the data recorded from an actual flight test campaign of the same aircraft.

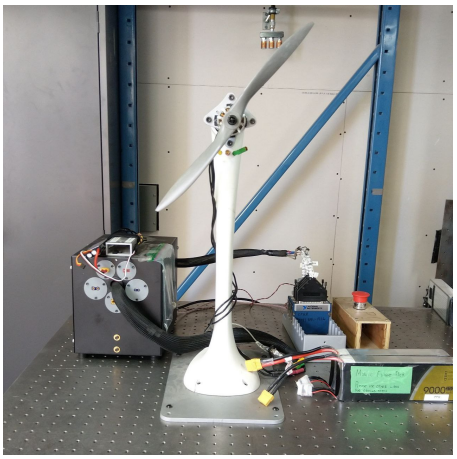

Figure 3.15. Thrust test stand for motor and propeller characterization.

3.4.1 Thrust Test Rig

UVIC CFAR has developed in the past a thrust test rig, shown in figure 3.15, capable to test and characterize inrunner or outrunner brushed or brushless DC motors with propellers up to 24 inches in diameter. The power-electronics inside the main electrical box allow for safe testing with current, voltage and temperature cut-offs for up to 150A and 50V testing for any combination of EM-ESC-battery pairing. All critical variables for DC motor characterization are captured with the NI cDAQ data acquisition system, including current, voltage, RPM, thrust and torque. A FUTEK MBA500 bi-axial sensor measures torque and thrust; the sensor is rated for up to 890N of thrust and 23Nm of torque. A thrust test experiment GUI was developed in LabView in order to interact with the test bench, set safety parameters, monitor test performance and record data.
This platform has been used to cross-check the data recorded in the Pedro's thesis work [22] with the simulation results of all the rotors and electrical components of the Mini-E.

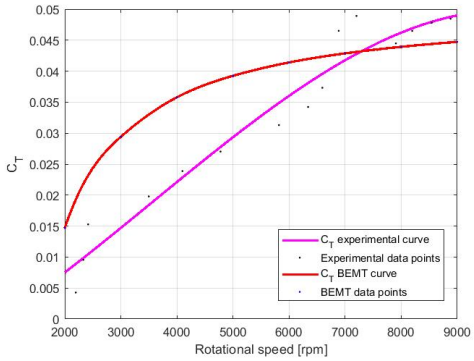

(a) C_T curve for the P14x4.8 T-Motor propeller.

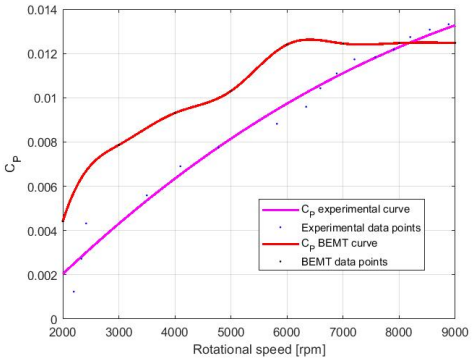

(b) C_P curve for the P14x4.8 T-Motor propeller.

Figure 3.16. Mini-E rotors characteristic curves.

Propeller Model Validation

The first step was to select the right propeller model to match the thrust and power performances to input into the tool. Previously, Pedro [22] had validated the propellers performance, by means of the vortex theory achieving an error inside the 15% boundary of acceptable accuracy for these type of preliminary simulations, taking into account that not all the geometry features of the rotors were known and had to be extrapolated. Therefore, only the comparison between the experimental data and the BEMT simulation model was missing. The results for both the VTOL and pusher propellers are presented in figure 3.16 and 3.17. It is important to mention that the BEMT does not cover the zero stream velocity condition, since the advance ratio J and propeller efficiency η_p go to zero according to their formulation [47]. Therefore the assumption of small relative velocity between the air in front of the propeller and the static test bench was made. Specifically, a value of $2m/s$ was used as input since it represents the real vertical flight condition of the aircraft. By looking at the C_T and C_P curves for the two applications, it is clear that for the rotors of the vertical phase the experimental and simulated values are far apart, with a maximum relative error of -75% (a negative value stands for overprediction), which is clearly unacceptable even for preliminary studies. The reasons behind this deviation might be attributed to the forced assumption of relative speed higher than zero, but especially due to an extremely different geometry between the T-motor and APC propellers at the base of the BEMT model. Thus, for the subsequent studies, the experimental curves were loaded into the tool and used by the propeller model. Instead, the behaviour of the performance curves of the APC propeller closely match the simulation results even with the assumption of low speed, showing a relative error which never exceeds the 10% absolute value. This proves that the parametrization inside the created database works correctly when the propeller geometry is similar to the ones contained in it. The result is of extreme importance since it gives the possibility to set the speed of the aircraft as input to the propeller model according to the flight conditions instead of relying on static curves; this should increase the accuracy for transition and forward flight simulations.

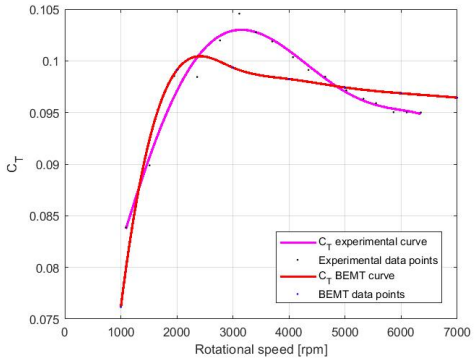

(a) C_T curve for the APC15x13N propeller.

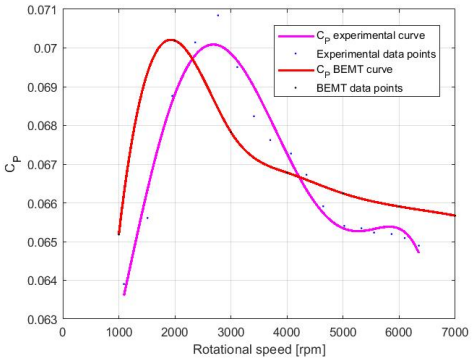

(b) C_P curve for the APC15x13N propeller.

Figure 3.17. Mini-E pusher propeller characteristic curves.

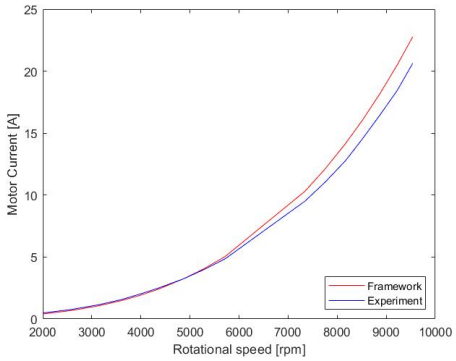

(a) Experimental and simulated torque at the shaft of the EM-Propeller.

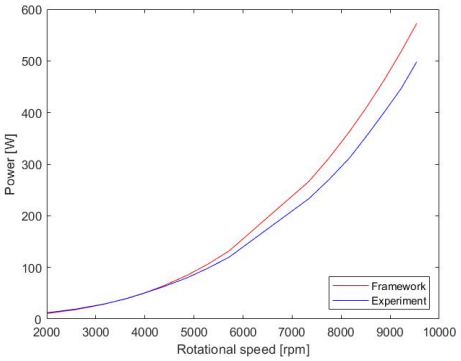

(b) Commanded and simulated throttle at the shaft of the EM-Propeller.

Figure 3.18. Current and Power curve drawn from the battery by the MN4012 over rpm.

Electric Branch Validation

The step after the propeller model selection was the evaluation of the electric performance obtained from the module. It was performed with the data recorded from a series of EM-Propeller tests benches, listed in appendix A.2. As already stated, the evaluation parameters for the electric motor are the battery current, battery voltage and the throttle setting of the EM.
For the rotor used in the vertical segment, since the model is loaded with the experimental curves and receives as input the thrust values, the rpm and the associated torque at the shaft present a minimal error inside the 5% range, as stated in table A.2 and displayed in figure A.1(a). Therefore the relevant variables are the current drawn from the battery, in order to determine its SOC, and the related power, obtained multiplying voltage and current, in order to validate the assumption on the EM efficiency value. Figure 3.18 shows the behaviour of the two parameters, which is relatively close for a large range of rpm

and slightly diverges only at higher settings, probably due to losses not taken into account by the η_{EM}, with an error lower than -15% which is deemed satisfying for the purpose of the tool. The throttle value plotted in figure A.1(b), presents a large deviation at the edges, probably due to a recalibration performed on the ESC which was not available to the author. Nevertheless, since it is only a surveillance parameter, it does not influence the performance of the UAV.

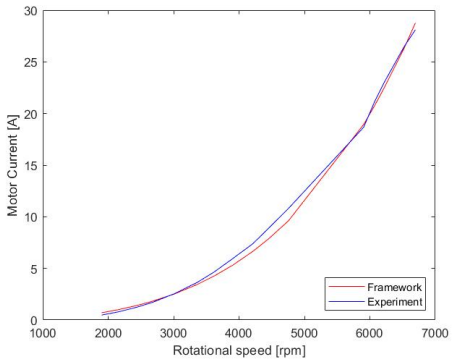

(a) Experimental and simulated torque at the shaft of the pusher EM-Propeller.

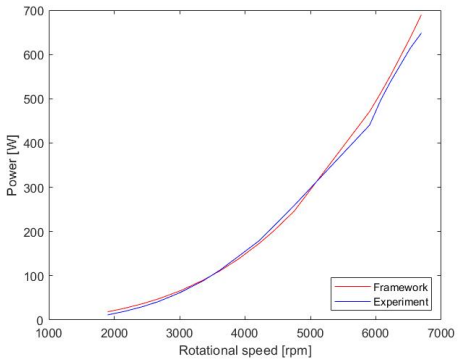

(b) Commanded and simulated throttle at the shaft of the pusher EM-Propeller.

Figure 3.19. Current and Power curve drawn from the battery by the KDE4012 over rpm.

Similar considerations can be made about the EM-Propeller pair for the forward motion. The experimental data and the error of the simulation prediction are listed in table A.3 and A.4. This time, since the propeller curves have been obtained through the BEMT model, the rpm and torque predictions at the shaft present a slightly higher relative error that, with the exception of the edges, results fairly accurate, never exceeding the 15% absolute value over the range of rpm. The electric variables of the battery in terms of current and power, shown in figure 3.19, also in this case, (low throttle settings apart), present a good trend, closely following the experimental values. Thus, it was possible to assess that the electrical branch allows to closely simulate the performances of a battery, ESC, EM and propeller powertrain. This is important because based on the amount of current being drawn from the battery, it will deplete faster and therefore, this influences the SOC of the battery and has a big impact on the operating mode and remaining time of the mission.

Flight Test

Finally, the electric architecture was evaluated against a mission flight test to validate its performance. In this way, rather than a steady-state analysis of the propulsion systems, a wide range of operating points were tested and simulated. In figure 3.20 are shown the mission profile of the flight test and the Mini-E configuration fully instrumented during vertical operations. The test was performed to prove for the first time the airworthiness of the Mini-E in transition and forward motion, and to improve the tuning of the autopilot for certain maneuvers. A better look over the mission profile is given at the end of appendix A, where figures A.3(b) and A.3(a) present in detail the speed and altitude kept by the

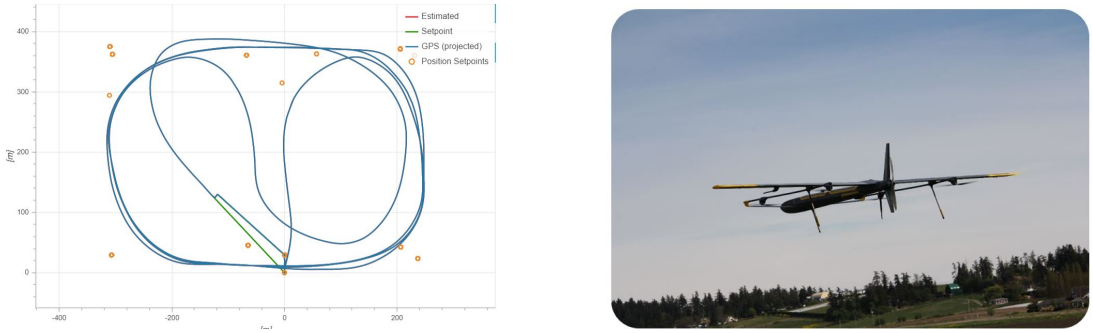

(a) Fligth Mission Profile

(b) Mini-E during vertical take-off

Figure 3.20. Experimental Flight Test Campaign.

aircraft. This real flight mission profile was loaded inside the tool, together with structural and aerodynamic characteristics of the Mini-E. It is composed by a vertical climb up to 60m, a hover time of about 10 seconds to change its attitude according to the subsequent forward transition, cruise for roughly 5 minutes and then transition back, hover to move over the landing location and return to the ground. From the campaign only data about the battery status and throttle commanded to the motor were recorded. Therefore, after post-processing and filtering of those, they have been compared with the predictions of the simulation tool to assess the consistency of the electric branch in real applications. The

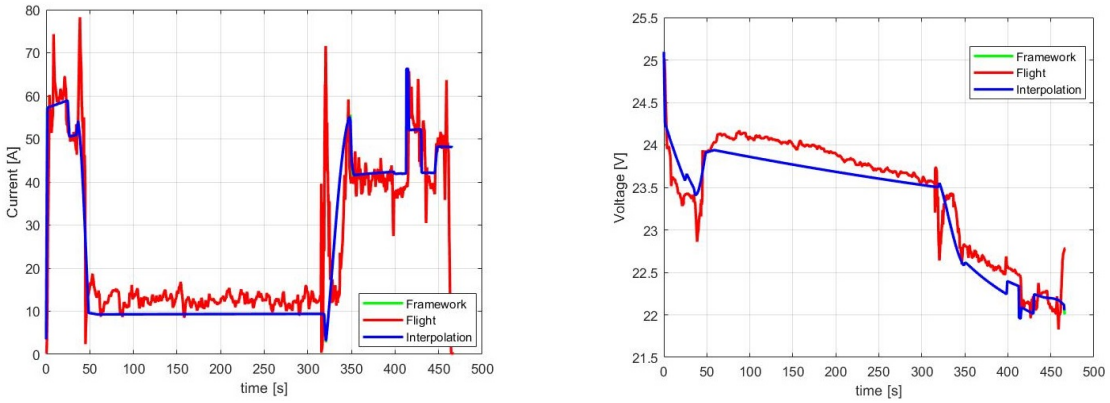

(a) Experimental and simulated current profile over the flight time.

(b) Experimental and simulated voltage profile over the flight time.

Figure 3.21. Battery characteristic of the Mini-E during flight test.

results obtained from this comparison analysis were extremely promising. In fact, as it can be seen in figure 3.21(a) and 3.21(b), respectively, the current and voltage of the battery almost overlap the flight condition, apart for isolated spikes due to sudden maneuvers and external environmental factors to counteract, which are not taken into account in the steady-state model of the UAV embedded in the framework. The greatest error is during

the cruise segment, but can be attributed to the extra current drawn by the avionic which was not taken into account in this study.

The main contribution of this assessment has been the validation of the discharge profile of the battery. In fact, as shown in figure 3.22, the trend of the charge is consistent with a higher discharge rate for the VTOL segments and a lower one during cruise. Moreover, at the end of the flight mission the battery reaches a SOC equal to 70%, which compared to the real SOC value of the battery, obtained by integrating the current over time, gives only a 4% overprediction which can be associated to the neglected current absorbed from the avionics and other auxiliary components. Therefore, the implementation of the electric branch into the Framework is considered to be valid and feasibly acceptable to give predictions of the flight time capacity of the configuration.
To conclude, in spite of these issues in the modelling of transitory behaviours of the aircraft, the model shows a good correlation for the parameters of interest and its level of fidelity is deemed acceptable for a first estimation of the performance of the propulsion system.

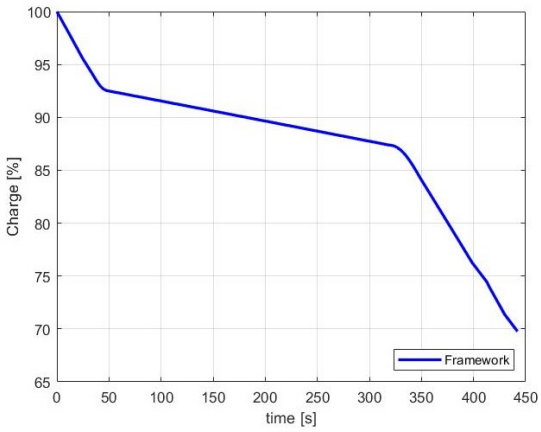

Figure 3.22. Thrust test stand for motor and propeller characterization.

Chapter 4

HEPS Sizing Analysis

This chapter explores the steps followed to size the propulsion system for the given configuration. Four architectures are taken into consideration: electric, gasoline, serial hybrid, and parallel hybrid. First, a purely computational simulation script used to estimate the total mass of the systems is described. Secondly, the methodology to convert these simulation results in actual components available on the market is assessed. Finally, a validation and analysis of the COTS selected is performed.

Figure 4.1. Eushyra tri-rotor CAD model.

Airframe		
Wingspan	3	m
Wing area	0.511	m^2
Canard span	1.447	m
Fuselage length	2.532	m
Fuselage diameter	0.22	m
Mass airframe	3.386	kg
Maximum Take-Off Mass	25	kg
Configuration	80-20	—

Table 4.1. Airframe characteristics.

4.1 Aircraft Configuration

In order to carry out an evaluation analysis of the propulsion system, the employed aircraft needs to be defined. As stated in chapter 1, the aim of this work is to design the propulsion system of a FW-VTOL UAV, named 'Eusphyra', featuring a canard and tilt-rotor configuration shown in figure 4.1, which was developed at CFAR in collaboration with DRDC. The implementation of a tilting rear rotor mechanism was done to reduce the power installed on board, to optimize the usage of the components and thus to reduce the overall weight, as explained in [20]. Moreover, the '80-20' configuration, as stated before, refers to

the relative position of the rotors compared to the centre of gravity, which directly affects the thrust distribution, prioritizing an excess of thrust in the rear propeller in order to maximize the top speed and cruise performance. The main structural characteristics are described in table 4.1 and have been recently updated by [65] to achieve higher endurance. The Maximum Take-Off Mass (MTOM) is set to 25kg due to current Canadian legislation on non-recreational UAV system operations. This constraint strongly affects the design of the propulsion system, but it is necessary to exempt the aircraft from the requirement to obtain a Special Flight Operations Certificate (SFOC) [66]. Together with the geometrical and mass properties, also the aerodynamic characteristics, in terms of L/D, stall speed and aerodynamic coefficients during flight were given and presented in appendix A.4.

4.2 Top Level Aircraft Requirements

The first necessary step to formulate the sizing problem is to identify and establish the Top-Level-Aircraft-Requirements (TLARs), their level of importance and priority. This is essential in order to obtain the main drivers of the sizing methodology. In fact, besides the minimum propulsion mass for the inboard components, the design of the HEPS must also be compliant with the requirements established for its mission, aiming for maximum endurance time and range distances.

Figure 4.2. Baseline mission profile.

Mission Parameters	
Cruise speed	35 m/s
Cruise time	4 h
Cruise altitude	60 m
Dash speed	60 m/s
Dash range	25 km
Hover/Transition	30 s

Table 4.2. Mission data.

The mission profile depicted in figure 4.2, together with the main characteristics of each segment which are summarized in table 4.2, were taken from the first design study performed by [20]. The requirements over the characteristic speeds were set in view of the operational scenario, meaning the top speed of a submarine and the arctic wind gusts velocity during storms [66]. The idea is to simulate what would be an actual Intelligence, Surveillance and Reconnaissance (ISR) mission, which is usually employed in the military sectors for small unmanned aerial vehicles. This type of mission assumes: a vertical take-off from the ship's helipad up to the cruise altitude; a hold in hover to maneuver the UAV toward the region of interest; forward transition, whose time was estimated from the flight test of the scaled version previously discussed; dash out to overcome strong arctic winds; cruise leg where information is gathered with the magnetic sensor and eventually enemies or intruders are identified; finally a return back to base following the same segments. It

is easy to understand that the requirement of long cruise flight time has the central priority on the design since the aircraft holds this condition for more than 80% of the overall mission time. The performance and sizing analysis of the propulsion system architecture is completed referring to this mission from here on.

4.3 Power Based Approach

It is clear that the sizing process for the propulsion system, in this case, could not be merged with the definition of the overall aircraft design. On the contrary, the majority of the methods and tools for the sizing and optimization of hybrid propulsion systems available in the literature [67, 63], focus on both aspects at the same time, by carrying them on together to reach a higher level of optimization and integration. Nevertheless, since this project is still at its conceptual design phase and iterations need to be performed in the future, it is acceptable to first evaluate the single parts and then combine them for a last comprehensive optimization before the final design definition.
Therefore a new sizing process needs to be considered. Similar studies in the literature for electric VTOL configurations [68], propose a power-based sizing approach. Starting from the computation of the power requirements at the rotors and propellers, these are used to size the pairing electric motors. However, the inclusion of hybrid systems makes the study a multi-variable problem since there is a more complex powerchain with different possible combinations of the components that need to be taken into account. The main drivers of the computational analysis, presented afterwards, are in the forms of power requirements to overcome mechanical, electrical and propeller efficiencies of the aircraft. Through this method, a first evaluation of the size and mass of the components can be assessed.

4.3.1 Axial and Hover Flight Analysis

The first segment to evaluate along the mission is the axial operation. It is important to mention that in the previous phases of the concept design of the Eusphyra, the location of the rotors and VTOL architecture have already been defined, leaving the rotor dimensions and type of propulsion system to be stipulated in this study. [22, 20] However, in addition to the mission profile, other specific requirements related to this phase need to be explicated. They are summarized in table 4.3.

VTOL Requirements	
Minimum T/W_{max}	>1.3
T/W_{climb}	1.05
$T/W_{descent}$	0.95
$D_{prop,max}$	<1 m
$D_{rotor,max}$	<0.5 0m

Table 4.3. VTOL propulsion system requirements.

These requirements, defined by the team, are mainly focused on front rotors size, since it is planned in the future to add the feature of retracting the booms; rear tilt-propeller size due to ground clearance and interference with the structural components, other than the Mach value at the tip and performance during cruise; maximum thrust to weight ratio for maneuverability and control purposes; T/W for climb and descent, where the value is given by approximating the drag to 5% of the weight [22].
These values are used as input to compute the power request of the segment by mean of the propeller momentum theory, [48], according to equation 4.1:

$$P_i = T_i \cdot V_c - \frac{k_i \cdot T_i}{2}\sqrt{V_c^2 + \frac{2 \cdot T_i}{\rho \cdot \pi R_i^2}} + \frac{\sigma \cdot C_{d0}}{8}\rho \cdot \pi R_i^2 \cdot (\omega_i R_i)^3 \tag{4.1}$$

Where T_i and πR_i^2 are the thrust and area of each rotor, V_c is the axial climb speed and the third order term $\Omega_i R_i$ states for the blade speed velocity. The remaining parameters were defined according to typical values found in the literature: the rotor blade solidity $\sigma \in [0.07,\ 0.12]$, using 0.1 in all calculations [69]; the blade drag coefficient C_{d0} can be assumed to 0.01 [69]; the induced power correction factor k_i has a value of 1.15 for axial flight [68]; the blade tip speed is variable with the radius R_i and rotational speed ω_i of the propeller.

4.3.2 Transition and Forward Flight Analysis

The computation of the power request during the transition mode is based on a modification of the equation presented in 3.1 for translational flight, to which power terms relative to the fixed-wing mode are added. The evolution of the forces is then followed to compute the peak of power request in order to size the aircraft components correctly for this phase. [68] The power of VTOL motors is given by equation 4.2, and the power of the pusher propeller is given by equation 4.3.

$$P_i = k_i \cdot T_i \cdot \sqrt{-\frac{V^2}{2} + \sqrt{\frac{V^4}{4} + \frac{T_i^2}{4 \cdot \rho \cdot \pi^2 R_i^4}}} + \frac{\sigma \cdot C_{d0} + (1 + 4.6 \cdot \mu^2)}{8}\rho \cdot \pi R_i^2 \cdot (\omega_i R_i)^3 \tag{4.2}$$

$$P_p = \frac{T_p \cdot V}{\eta_p} = \frac{W \cdot V}{\frac{L}{D}\eta_p} \tag{4.3}$$

Where $\frac{L}{D}$ is the thrust to drag ratio, defined by the polar curve of the aircraft; η_P is the propeller efficiency, and $\mu = V/(\omega_i \cdot R_i)$ is the advance ratio.
The total power used by the aircraft in transition is finally given by the sum of all the contributions.

4.3.3 Thrust and Power Calculations

The first parameters needed as input to the power equations, stated before, are the thrusts values of each rotor. By means of the aircraft mechanic model presented in section 3.2, it is possible to compute the required forces for each segment by loading the aerodynamic curves and geometric data of the configuration. In this study, since the literature suggests

a minimum T/W of 1.5 [27] as a reference value to guarantee control and maneuverability in vertical operations, the computations are performed with a T/W_{max} of 1.4 as an average value between the recommended and the requirement of the team; higher values would strongly increase the power request and for a preliminary design analysis, where many conservative assumptions are already taken into account, it appears to be acceptable.

Thrust [N] 80-20		
T/W	Front rotor	Front rotor
1.05	25.75	206.01
1.4	34.35	274.68

Table 4.4. Required thrust in axial operations.

Segment	**Thrust [N]**	**L/D**
Cruise	13.82	17.77
Dash	34.31	7.11

Table 4.5. Required thrust in fixed-wing operations.

The results reported in table 4.4 and 4.5 summarize only the operational conditions and the maximum T/W, since these values are actually the ones adopted as driving parameters of the sizing process. The thrust during transition is not reported since the value evolves with time but is always inside the boundaries defined by the VTOL and fixed-wing (FW) conditions, thus it does not represent a sizing requirement.
It is clear that vertical operations are critical in terms of thrust and thus power demand. Minimizing the power consumption during VTOL stages implies smaller and lighter components, and a reduction of the energy stored onboard, which is beneficial in terms of aircraft weight reduction. Therefore, a minimization process is performed: to estimate the minimum required power at the rotors, the derivative of the power with radius is computed, obtaining the radius that minimizes the power consumption for a given propeller rotation. The results obtained are a trade-off between rotors radius, power request and operational rpm, in order to fulfill all the constraints and to not exceed a Mach value at the tip higher than 0.85 in cruise and dash operations. Table 4.6 summarizes the condition of minimum power for VTOL with a total area of $\sum A_i = 1\ m^2$ at a climb speed V_c of 2 m/s, and for FW, where a constant propeller efficiency value η_p of 0.85 is assumed as a conservative estimation [70].

	T/W	P_{front} **[W]**	P_{rear} **[W]**	R_{rear} **[m]**	R_{rear} **[m]**
VTOL	1.05	303.253	3950.844		
	1.4	432.332	5640.237		
FW	Cruise	568.293	/	0.259	0.438
($\eta_p = 0.85$)	Dash	2434.844	/		

Table 4.6. Required power and area distribution.

Overall, the trade-off between the size of the rotors and minimum theoretical total power consumption leads to a diameter of the front rotors close to the $0.5m$ maximum value prescribed and a rear rotor with a size way smaller the $1m$ limit. Clearly, further reductions

of the propellers sizes could be possible, but at the cost of higher power request which will then affect all the components connected along the powerchain and thus also increase the weight of the aircraft.

4.4 Propulsion System Mass Evaluation

From the computation of the maximum power requirements of the aircraft, the sizing process of the propulsion system could start.
To find the best-suited propulsion system for the configuration, four architectures are defined and compared through the evaluation of their performance, mass and energy consumption along the baseline mission selected. The first architecture implements a purely electric system, with a pack of battery supplying the power requested from the rear EM-propeller pair and the two EM-rotors in the front along all the phases. The second architecture installs an internal combustion engine powering the rear tilting propeller, while for feasibility and mounting reasons, the front rotors are still coupled with EMs and battery. The third configuration is a series hybrid electric system featuring an ICE-generator unit, which, together with the battery, delivers the electric current requested from the EM-propeller mounted on the tilting mechanism. A power unit is also considered in order to control the current flow from the battery and the generator and eventually operate a recharge mode. The front system is the same as for the previous configurations. The last configuration is a parallel hybrid electric system, mounting the same units as the serial one, with the exception of the power unit that is substituted with a VESC (Vedder-ESC) and a mechanical coupling between the EM and ICE shafts which power the tilting shaft connected to the propeller. Also in this case the front structure remains the same.

4.4.1 Sizing Process

In order to size each propulsion system in terms of dimensions, masses and power output, a sizing script based on the models presented in chapter 3 has been implemented in the *MathWorks MATLAB®* environment. Some of the adopted assumptions need to be defined before going through the process. Specifically, as previously stated, the front part of the propulsion system is kept constant through all the architectures, since EMs and rotors are used only in the VTOL and transition part where the configurations share the same requirements. In view of this, in order to simplify the comparison for the hybrid architectures, a common definition of the hybridization factor (HF) is given as:

$$HF = \frac{P_{max,EM,tilt}}{P_{max,EM,tilt} + P_{max,ICE}} \tag{4.4}$$

Where $P_{max,EM,tilt}$ is the maximum power request computed in table 4.6 for the rear rotor, and $P_{max,ICE}$ is the maximum power of the ICE mounted onboard. It is important to mention that both hybrid systems share the same maximum power request at the rear EM due to the constraint for VTOL operations to eventually switch in EM only mode and above all, to be capable of performing an emergency landing in case of ICE failure. Thus, the EM of the parallel system could not be downsized as usually happens for standard configurations. During the sizing analysis, the HF value ranges from 0.5 to 0.8, which

are assumed as boundaries to evaluate the best synergetic combination of the components for the hybrid architectures. The reason behind these values lies on the fact that for the lowest the hybrid mounts two units capable of fulfilling the top requirements alone, and in the highest the power of the ICE is slightly above the request in cruise, taking also into account an extra power margin in order to recharge the battery. Finally, due to many unknown on the supports, mass of the tilting mechanism and losses along the different drivechains, several conservative considerations were taken into account for efficiencies values and additional weight factors according to [27].

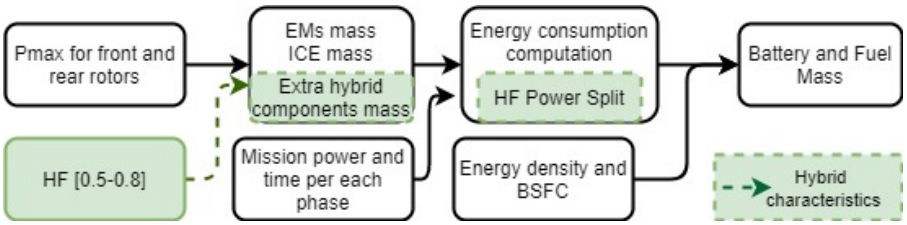

Figure 4.3. Propulsion system sizing process.

The flow of information, presented in figure 4.3, can now be explored. The starting point for each configuration are the maximum power requirements computed in table 4.6, defined by the VTOL segment. Through the mass models equations in section 3.3.3 and 3.3.2, these requirements can be used to compute the masses of the EMs and propellers. For the gasoline architecture, the definition of the ICE size and mass is computed according to equation 3.31 and consequently 3.30. In this way through the Willans method the maps for the engine are constructed and the BSFC for different operating conditions is evaluated. The hybrid architectures have the HF as extra input in order to define the power split between the ICE/generator and EM/battery. From this value, equation 4.4 is inverted to compute the maximum power of the ICE and then the process follows the same steps as for the gasoline.
After having defined the components, the baseline mission profile is loaded into the script with the definition of the aerodynamic and geometric characteristics of the UAV in order to compute the power request for each phase. Knowing the duration and the power, it is possible to obtain the energy required from the sources onboard. Finally, thanks to the BSFC maps and electric energy density specified in chapter 3, the mass of the fuel [1] and battery necessary to perform the mission are computed.

4.4.2 Sizing Results

The results obtained from the sizing process of the different propulsion systems, over the baseline mission profile, are discussed and compared below.
In figures 4.4(a) and 4.4(b) the effect of different degrees of hybridization over the serial and parallel architectures is presented. It is intuitive to understand from the graphs that

[1] In order to take into account the influence of the mass reduction for the gas and hybrid systems, the Bréguet equation adapted for hybrid applications was implemented. [71]

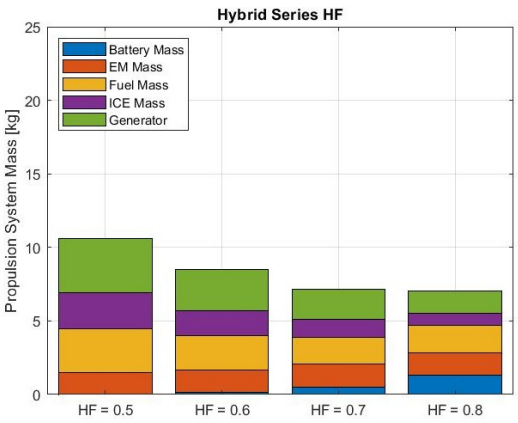

(a) Mass breakdown of the series hybrid propulsion system components for different HF.

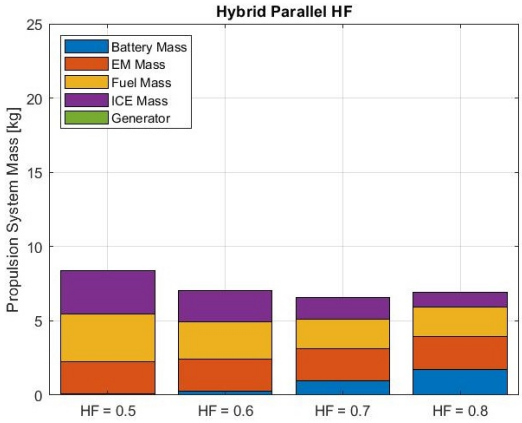

(b) Mass breakdown of the parallel hybrid propulsion system components for different HF.

Figure 4.4. Mass estimation for different HF of the Series and Parallel hybrid systems.

lower HFs imply more powerful ICEs and thus the mass onboard critically increases due to the low power density of these components. Especially for the series configuration, in which a generator is coupled with the ICE, this increase in the power allocated in the combustion side strongly penalizes the total mass of the propulsion system. In fact, the peak of power request lasts just few minutes for the take-off and transition flight. After, the power halves for the dash and steeply drops in cruise. This means carrying onboard a huge excess of power installed that is used for less than 20% of the time in flight. Moreover, even though an oversized engine can sustain all the flight conditions without the need of battery support, and thus saving weight, its operating conditions in dash and cruise are far apart from the optimal. This leads to higher BSFC for a longer time and thus more fuel burnt which needs to be carried onboard.

The propulsion mass has a decreasing trend with the HF until a value of 0.7, clearly visible for the parallel case, where a minimum of overall propulsion mass is reached. This HF breakpoint can be attributed to the best balancing of three main factors: battery mass, ICE size and fuel consumption. As a matter of fact, since the electric part of all the configurations is the same, the best trade-off between these factors leads to a minimum of the propulsion mass. Their values are strictly connected to each other. In fact, as previously explained, the battery mass depends on the power needed to support the ICE in the most demanding phases. At the same time, a smaller engine reduces the excess of power installed during cruise and can work closer to its optimal conditions, which for two-stroke engines, as largely discussed in section 3.3.4, can be found at high torque and rpm settings.

After this point, the propulsion mass tends to increase due to the higher battery mass, related to the fact that the engine reaches a size where even during the dash mode, the battery needs to deliver a big amount of power to support it, and therefore due to the low energy density of this unit the overall mass rapidly increases. Also, the fuel consumption reaches a saturation point after which it is not possible to further reduce the BSFC.

A closer look at the contribution of each component in the propulsion system is given in table 4.7. The mass of the electric motors and propellers is not represented since it is

	HF	P_{ICE}[kW]	$V_d[cm^3]$	m_{ICE}[kg]	m_{el}[kg]	m_{bat}[kg]	m_{fuel}[kg]	m_{tot}[kg]
Series	0.5	5.65	85.33	2.43	3.32	0	2.99	10.82
	0.6	3.76	56.27	1.73	2.82	0.12	2.32	8.67
	0.7	2.42	35.52	1.20	2.39	0.51	1.82	7.34
	0.8	1.41	19.96	0.79	2.01	1.29	1.87	7.23
Parallel	0.5	5.65	85.33	2.92	0.64	0.07	3.23	8.61
	0.6	3.76	56.27	2.07	0.64	0.25	2.51	7.23
	0.7	2.42	35.52	1.44	0.64	0.95	1.97	6.76
	0.8	1.41	19.95	0.95	0.64	1.73	2.02	7.10

Table 4.7. Series and Parallel hybrid propulsion system components mass evaluation.

the same for both cases and it does not represent a factor to operate on. The majority of the terms summarized in the table have been defined before, while the new values are: the mass of the electric components m_{el} which includes generator, VESC and power unit; the emission m_{CO_2} of carbon dioxide and the total mass of the propulsion system m_{tot}. The differences between the values of battery and fuel mass of the two systems are related to the different control logic assumed. As explained in sections 3.3.7 and 3.3.7, through the decoupling of the ICE to the propeller, the series architecture can operate the engine/generator unit at the ideal condition for each power request, without any constraint on rpm or torque. Instead, the parallel one, even though follows the IOL that fits the optimal conditions, without a clutch mechanism it is forced to reproduce the rpm of the propeller, falling in operational points not as well suited as the lowest BSFC region. The IOL also limits the power extracted from the ICE and thus the battery weight slightly increases. Moreover, the classical lower efficiency of the series configuration, related to the multiple power conversions, in this case is partially compensated by the higher transmission efficiency. In fact, no shaft connects the ICE/generator unit to the EM/propeller one, and thus the tilting mechanism can be much simpler and lighter, by being subjected to less vibration and lower loads. On the contrary, for the parallel case two options are now under analysis at CFAR: either tilting the entire drivetrain ICE-EM-clutch-propeller, which would make the damping of vibrations and mounting connections extremely complex; or designing a gearbox to interface the shaft coming from the clutch and the one going to the propeller, adding weight and again high complexity to the system. From a first test bench experiment, the second mechanism showed an efficiency between 50% and 75%, therefore an optimistic value of 85% was taken into account, which is still lower than the usual 90% efficiency of generators [41]. The extra weight of the connections and gearings was considered with a 1.2 safety factor added to the ICE mass. Finally, it is important to mention that the mass of battery is sized assuming that during the cruise segment the system has enough time to recharge the battery for the way back. Furthermore, both battery and fuel also consider a safety reserve of 15% and 6% of charge and gasoline remaining at the end of the mission, respectively.

Similar considerations can be made for the electric and gasoline architectures, whose components mass is represented in figure 4.5 and table 4.8. The values of the engine and EM masses are not reported since are the same as the ones for the parallel system with a HF of 0.5. Although they both take advantage of the lower number of components which allows them to have a lower dry weight compare to the hybrid concepts, their energy usage is strongly inefficient in terms of mass stored onboard. In fact, with more than 20kg of battery required to complete the mission, out of the 25kg for TOW, the electric solution results unfeasible for this application; in spite of the extremely low emissions produced and the lower complexity of the mechanism and mounting, which would be close to the series configuration featuring even less vibrations thanks to the missing engine.
In the same way, as for the parallel hybrid system with 0.5 HF, the gasoline can sustain all the flight phases without needing to carry battery onboard, except for powering the front EM-rotors pair during VTOL and transition. But this oversizing leads to a higher fuel consumption during the cruise flight, which inevitably makes the total mass of the system comparable to the hybrid solutions, taking also into account the same tilting issues as the parallel architecture. With all these considerations in mind, a series hybrid electric architecture featuring an HF of 0.7 is selected as the best trade-off between all the possible solutions and it is taken as a reference system for the market components selection performed afterwards. Although, the parallel configuration is generally preferred to the series one due to its higher efficiency and lower weight thanks to the absence of the generator, in this case these advantages only partially apply due to the VTOL architecture. Therefore, despite it results 8% lighter than the series case, considerations regarding the complexity, efficiency and weight of the tilting mechanism, together with the ease of control and rapid-response during vertical operations, allowed by the EM directly connected to the propeller, led the team to move forward with this architecture for the propulsion system. Nevertheless, the components presented in the next section can easily be adapted also for the other systems.

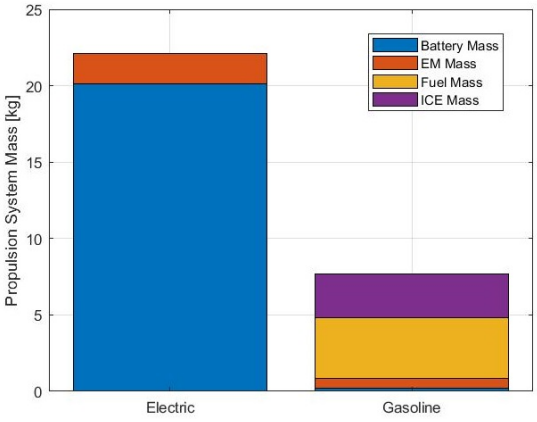

Figure 4.5. Mass breakdown of the Electric and Gasoline propulsion system components.

Aircraft	**Electric**	**Gasoline**
P_{ICE} [kW]	5.65	5.65
m_{el} [kg]	1.03	0.5436
m_{bat} [kg]	20.12	0.23
m_{fuel} [kg]	3.70	0.00
m_{CO_2} [kg]	2.43	11.66
m_{tot} [kg]	22.43	7.89

Table 4.8. Electric and Gasoline aircraft components mass evaluation.

4.5 Components Selection

A survey of the available options in the market was performed in order to obtain a first components selection for the propulsion system of the Eusphyra. The research was conducted by seeking for units that would closely match the results of the previous analysis in size and performances, while respecting the project requirements. The main driver, due to timeline and budget restrictions, was also to reevaluate components already purchase in previous projects at CFAR. Therefore, not all of the findings made by the author were able to be implemented, but are outlined in the recommendation section of this report for possible future improvements on the concept.

	Front EM	**Front rotors**	**ESCs front**	**Battery**	**ICE**
Component	P60 KV173	P22x6.9	Flame 60A	Li-Po 12S-44.4V	DA35
Mass	345g	45g	73.5g	1350g	1170g
Settings	1800W	112.82N	60A	5.45Ah	2344W
	PMU	**Generator**	**Rear rotor**	**Rear EM**	**ICE only**
Component	SGENS-100A-01	S676-500U-21	G32x11	U13-II KV130	DA85
Mass	1250g	930g	107g	990g	2150g
Settings	6000W	2600W	343.35N	5659W	6247W

Table 4.9. COTS selected for the series propulsion system.

The major brands considered for electric motors were KDE motors, T-Motors and AXI motors, which have a long time experience in the aviation field and usually make available datasheets of the components, other than recommending the proper propellers to couple with. In the electronic field, Sullivan Unmanned Vehicle is one of the worldwide suppliers of generator, alternator and voltage regulators or power units and ensures a high reliability of its product. Finally, in the internal combustion engine area, Desert Aircraft, Power4Flight and Currawong Engineering have produced ICE for this size of applications with success for years.
Since no purchase could be done, brands with experimental test data for the components, efficiency curves, thrust over rpm, power request and other mappings and performance curves were privileged, as it added an extra security factor to the previous estimations while providing data for comparison with the performed simulations. Another important factor, of course, was the possibility to fit the components inside the fuselage, in order not to add drag penalties and thus increase the power request.
For the battery pack, the selection of LI-Po type was due to their extremely high coulomb ratings, up to 120C for discharging and 5C charging. In view of the high power output, a 12S-44.4V unit was required in order to reduce the maximum current in the wires. The capacity was selected for safety purposes equal to the energy necessary for a fully electric vertical take-off and landing operations, plus one dash segment sustained in conjunction with the ICE. This led to a 5Ah requirement, which was matched with the Max Amps 5.45Ah

[72] unit presented in table 4.9. Between the many suppliers such as Tattu/GensAce, this one was selected due to the higher value of energy density, equal to 180 Wh/kg.
For the EM-propeller pairs for front and rear propellers, T-motors was chosen as many static thrust test data are available and past projects at CFAR have proven their consistency. The criteria behind the selection of the P60 KV170 [73] and U13-II KV130 [74] was due to current and voltage compatibility with the battery pack, together with the recommended coupled propellers, which size was taken similar to the prescribed one; but even more relevance had their matching with power and thrust requirements computed for the maximum T/W and to limit the RPM-Voltage coefficients. Their main characteristics are listed in table 4.9. Particularly, the P60 unit has already been purchased and tested by [22]. The Flame 60A for the front EMs was chosen taking into consideration manufacturers advices.
According to the modelling, the ICE size and power specifications for the 0.7 HF case perfectly matched the performance and dimension of the single cylinder two-stroke engine by Desert Aircraft DA35 [75], which has been largely studied and tested at UVIC CFAR. Therefore, also in view of its good fitting inside the fuselage, it was selected. The S676-500U-21 produced by Sullivan [76] was chosen owing to its good specifications of minimum amount of space and mass, together with the availability of power and efficiency curves from the manufacturer, presented in appendix B.1. Most importantly it was recommended for engines in the size range of the DA35. Finally, the Power Management Unit (PMU) from Sullivan was selected in order to control and merge the current coming from the generator and battery sides in such a way as to give the power for propulsion to the tilting rear EM-propeller and, eventually, to charge the battery. This device also permits the reverse operation of the generator at the engine starting. The authors opted for the SGENS-100A-01 [77] for its power settings and weight.
These components were arranged together to build the series hybrid configuration, as shown in figure 5.1(b) of the next chapter. The same components can be adapted to the electric and parallel architectures, allowing in this way to run further comparison and analysis with the HEPS simulation framework, as presented in 5. For the gasoline architecture, a Desert Aircraft DA85 appeared to fulfill the power requirements of the rear propeller, taking into account that its dimensions would not fit into the fuselage and thus more drag penalties should be accounted for it.
Finally, one last advantage of the series system designed is its great flexibility and geometric design freedom. Each component can be installed independently of the location of the others, allowing to define the most suitable position according to the magnetic interference constraints for the onboard payload.

4.6 Components Mass Validation

In this last section the sizing script created is used to validate the designed propulsion systems. The previous results obtained through the models, in term of power, masses, energy consumption and emissions are now compared with the one coming from the use of manufacturer data for the selected COTS. The fuel and battery mass are let as free variables in order to estimate the energy consumption of the units installed. In this way, the accuracy of the sizing process and components selection can be assessed. Lastly, a

trend of the propulsion mass as a function of the flight time is explored.

4.6.1 Designed Propulsion Mass Evaluation

The same study, iterated before with the support of the mass and power models for the components, is now repeated with the data coming from the market selection. Therefore, the baseline mission profile, shown in figure 4.2, is again simulated for the four propulsion system architectures, but now with the defined characteristics of the components from table 4.9. Still, conservative factors are kept in order to account for the mountings, inefficiencies and extra mass of the tilting mechanism.

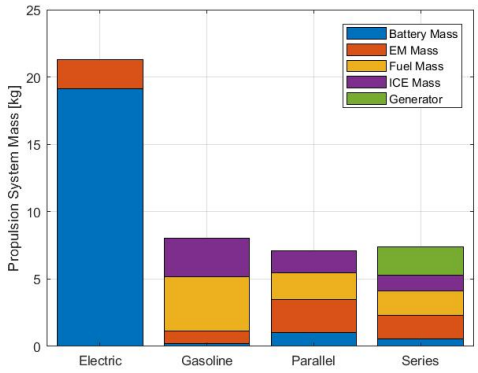

Figure 4.6. Mass breakdown of the four designed propulsion systems.

Aircraft	Electric	Gasoline	Parallel	Series
m_{bat} [kg]	19.11	0.20	1.04	0.58
m_{fuel} [kg]	0.00	3.78	1.79	1.61
m_{CO_2} [kg]	2.43	11.90	5.76	5.14
m_{tot} [kg]	21.58	8.19	7.30	7.61
m_{tot}[%]	-3.93	3.68	7.43	3.47

Table 4.10. Total mass of the four designed propulsion systems.

The results for the mass budget distribution portrayed in figure 4.6 resemble the ones obtained in the fully computational simulation analysis. For all the cases, a small underprediction below 10% over the total mass of the propulsion systems is obtained from the tool, with the exception of the electric case that results slightly lighter thanks to the higher energy density of the battery pack selected. This overprediction can mainly be associated with an oversizing of the front motors, due to voltage compatibility and propeller size matching issues.
Other than this, the sizing script appears to be able of giving an accurate prediction of the propulsion system components mass. Therefore, the configuration warrants further researches and a deeper trade-off analysis through the HEPS simulation environment presented in chapter 3.

Performance over cruise flight time

To conclude, one last analysis is performed on the designed propulsion systems. In this case, instead of changing the mass of the components or power parameters such as HF, the mission profile is the main variable. The goal is to evaluate the trend of the total propulsion mass with increasing cruise time. Specifically, the cruise conditions are swept from 0 to 6 hours of flight time, while the vertical take-off, transition and dash, both forward and backward, are kept as defined at the beginning of the chapter. Therefore, the results should

give an idea of the intrinsic efficiency of the different propulsion systems. In fact, since the mass of the components is now kept constant, what really affects the propulsion weight at take-off is the mass of the energy sources stored on board to cover that flight leg. The most efficiently the propulsion system can take advantage of them and the lightest it is going to be over time. It is important to mention that in the figure below the starting mass of 0h of cruise already takes into account the battery and fuel mass to perform the other segments of the mission.

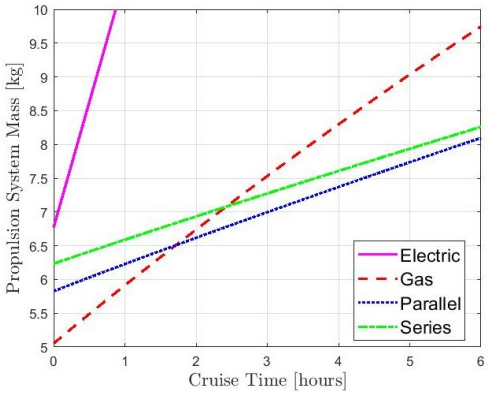

Figure 4.7. Mass of the propulsion system as function of the flight time.

The results presented in figure 4.7 confirm what stated before. The electric configuration, even just after taking-off, dashing for 50 km and landing, overpasses all the other concepts and at 1h of cruise flight it is already over 10kg, which according to [44] corresponds to the upper limit of the mass of the propulsion system for VTOL architectures (which should not be higher than 30% the MTOM). The gasoline, as discussed before, results lighter at the beginning, but due to the higher fuel consumption related to the engine oversizing, after 2h of cruise the mass trend steeply reaches an intersection point from which this solution is not preferable anymore, compared to the hybrid configurations. Finally, the series and parallel architectures show a similar behaviour; although the series presents an initial mass penalty due to the additional generator mounted on board, it slowly reduces this gap thanks to the smarter control logic considered. Moreover, with increasing cruise time, also the recharge strategy of the battery becomes a relevant aspect, which is not taken into account here, and this is why a detailed simulation framework is needed.

To conclude, from this basic sizing analysis is already possible to understand that for an optimal design and correct sizing of the hybrid configuration, not only the UAV features play an important role, but also the mission performed and the strategy adopted to maximize the performance of interest, all together lead to the best component integration on the aircraft. Moreover, the novelty of accurately predict the mass of fuel burnt for an aircraft through an entire mission, results extremely advantageous when designing a UAV. Having the ability to precisely predict the required amount of fuel allows for correct engineering design decisions in the comparison study. Further, this also means that the additional payload capacity of the UAV can be exactly calculated, and the fuel reserves minimized. This would allow for the maximum amount of payload on board or equipment.

Chapter 5

Mission Performance Evaluation

In this chapter, by feeding the Eusphyra aerodynamic and structural characteristics into the aircraft simulation environment, described in chapter 3, the series hybrid propulsion system previously designed is critically assessed against the other architectures. Additional features are integrated in the tool to better control the behaviour of the selected components.

First, a verification of the results obtained from the sizing process over the same mission profile is provided. Then, following a baseline weight analysis of the aircraft empty mass imported from [65], the available propulsion mass is redefined and the mass of the energy sources on board is adjusted in order to achieve the best flight capabilities. Finally, a study focused on the influence of the main mission parameters over the aircraft performance is presented. In the last step, a cost-effective analysis of the aircraft is conducted by estimating the flight time for different payload requirements. The results outline the advantages and disadvantages of each propulsion configuration and the optimal redistribution of the available weight on board to reach the top goals.

5.1 Baseline Mission Study

Although the design of the Eusphyra has not reached its final version yet, in order to ease the visualization of the onboard integration of the series hybrid propulsion system developed, a possible allocation of the concept is presented in 5.1(b). The components are placed according to the magnetic signature directives presented in [65], while trying to maintain the correct scaling and distances from the centre of gravity. As can be seen, the components for the HEPS tightly fit inside the fuselage of the aircraft, proving the optimized sizing without requiring additional modifications to the structure. Their backward allocation due to the interference with the MAD-X sensor, installed in the nose, leaves a wide area in the front part, highlighted in blue, for the payload. Clearly, many mechanical connections, wirings and supports are missing, but the outfit of the propulsion system should keep an identical structure.

(a) Eusphyra flight mission example over the North-West passage.

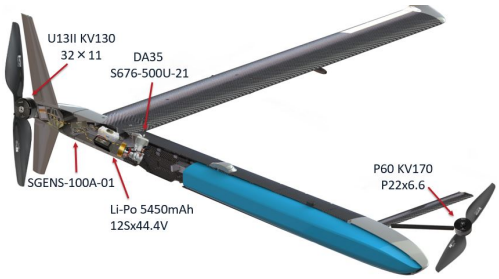

(b) Conceptual integration of the series HEPS components into Eusphyra and payload.

Figure 5.1. Topographic map of Canada and Eusphyra conceptual integration design.

The first set of simulations run had the purpose to demonstrate the results coming from the sizing process. By dropping some of the assumptions made in order to conservatively estimate the power demand, such as on the propeller efficiency or operational rpm, a more realistic behaviour of the propulsion system components is expected along the stated mission profile, which is portrayed in a more figurative way in figure 5.1(a), where a possible application scenario over the North-West passage is displayed.

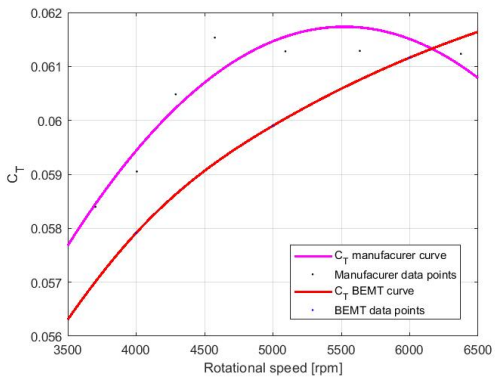

(a) C_T curve for the P22x6.6 T-Motor propeller.

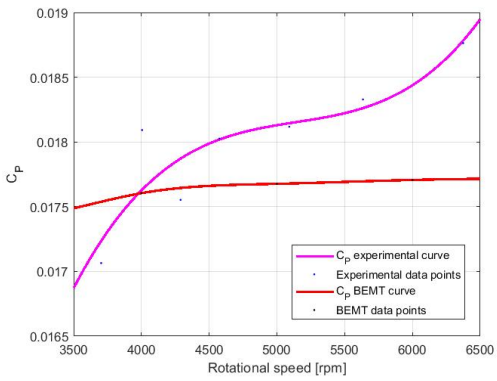

(b) C_P curve for the P22x6.6 T-Motor propeller.

Figure 5.2. Eusphyra front vtol rotors characteristic curves.

5.1.1 Propeller Model Selection

As already discussed in chapter 3, the selection of the best-suited propeller model must be done accordingly to the data available. In this case, only the rough dimensions of the rotors were known, making the vortex model inapplicable. Thus, experimental data from

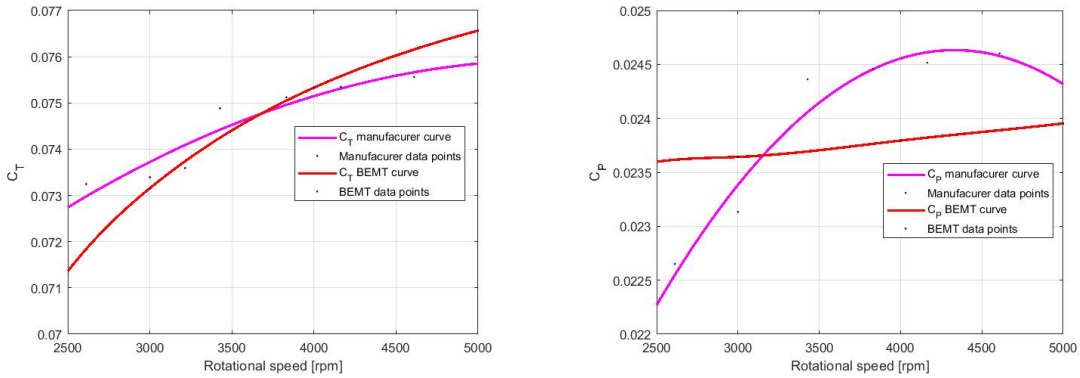

(a) C_T curve for the G32x11 T-Motor propeller.

(b) C_P curve for the G32x11 T-Motor propeller.

Figure 5.3. Eusphyra rear tilting rotor characteristic curves.

the manufacturer were collected and the C_T and C_P characteristic curves were extrapolated. The results, shown in 5.2 and 5.3, are compared against the BEMT model, implemented again by assuming a relative speed of 2 m/s in order to reproduce the vertical take-off and landing flight conditions. For the front rotors, the second order polynomial fitting the experimental data shows for both curves a maximum relative error lower than 10% compared to the BEMT interpolated values. The closer matching might be attributed to a similar geometry between the propeller selected and the one collected in the database. However, since for these rotors test bench data were also recorded and validated by [22], the experimental curves are kept as reference, even though this implies a lower accuracy during the transition phase. The same considerations can be made for the tilt rear rotor, for which the general behaviour of the coefficients do not largely deviate in terms of magnitude from the simulation values. Thus, in order to increase the veracity of the simulation during the transition and forward segments, the BEMT is deemed accurate enough for this conceptual study to solve the thrust-power-rpm matching loop of the tool.

5.1.2 Energy Management Strategy

With a highly detailed knowledge of the components modelled in the hybrid-electric simulation framework and of the power request profile during the baseline mission, it was possible to specialize the control logic of the series hybrid configuration in order to achieve the best management of the energy sources carried on board. The general logic was previously presented in section 3.3.7.
Specifically, since the series hybrid propulsion system allows the engine to be mechanically decoupled from the propeller, there are not any additional constraints other than aiming to operate the engine-generator system at a mutual optimal operational condition, reaching the best efficiency overall. The characteristics of the components selected are presented in appendix B, and, as it is easy to understand by looking at figure B.1(b), the best efficiency for the generator is reached for power ratings between 1 kW and 1.5 kW, at operational rpm higher than 4000. This results in an almost matching condition with the optimal

operating region of the DA35 BSFC map, displayed in figure 3.12(a), which was the main driver in the selection of the component for the cruise segment requirements. Thus, instead of forcing the engine to work along the IOL, a smart controller implementing a minimum BSFC-power matching loop is integrated in order to keep the ICE in a fixed range of rpm, varying instead the torque output to fulfill the cruise or recharge power request during standard flight conditions, as shown in figure 5.4. In this way, the global efficiency of the ICE-Generator system is maximized.

On the contrary, the implementation of this smart controller for the parallel hybrid electric

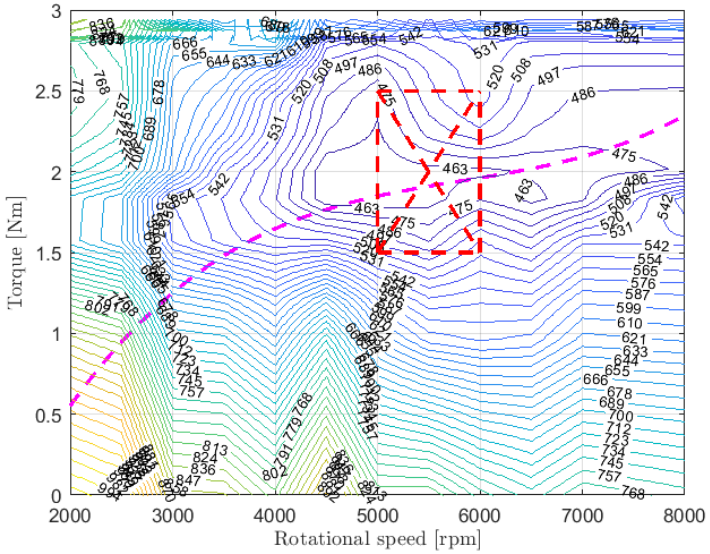

Figure 5.4. BSFC contours map for the DA-35 with the smart controller operating region.

system is not possible, since it would be necessary the integration of a complex gearbox or continuous variable transmission (CVT) in order to decouple the ICE from the rpm imposed by the propeller. This component would add extra weight and inefficiency to the powertrain, making the tilting mechanism even more complicated and heavier. The IOL control strategy of section 3.3.7 is therefore kept for the mission analysis.

5.1.3 Baseline Mission Simulation Results

In this case, the exploration of the theoretical performance of the different propulsion systems is conducted with the goal to achieve the same flight time for all the configurations, with the propulsion weight left as free variable according to the values defined in section 4.6.

To better understand the power requirements computed from the propeller model for the four architectures along the flight path, the electric system power profile for the 4h cruise mission is shown in figure 5.5. In first instance, can be noticed that the power does not fall too far apart from the results of the propeller momentum theory used in the previous chapter, meaning that the BEMT application does not significantly affect the accuracy of the results. Further, this system can be taken as a reference and used as a minimum

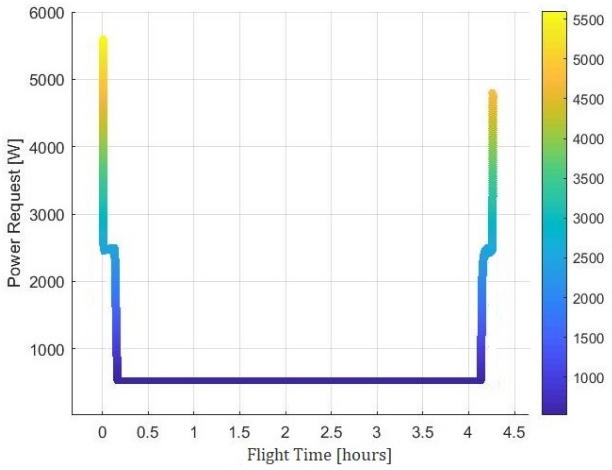

Figure 5.5. Total power demand for the Electric configuration.

requirement since the electric propulsion has the least number of efficiency losses along the powerchain and thus consumes less power.
The main performance factors, evaluated to describe the behaviour of the different architectures in this mission analysis, are the fuel level and battery charge profiles, presented in the following figures, together with the emission and other efficiency indexes analysed in table 5.1.

The battery discharge for the electric system during the mission is presented in figure

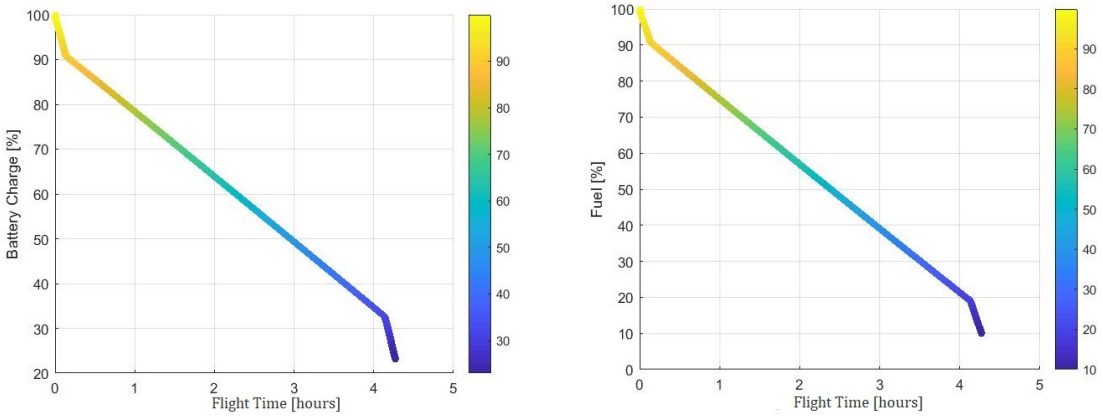

(a) Battery charge curve for the electric simulation.

(b) Fuel level curve for the gasoline simulation.

Figure 5.6. Electric and gasoline simulation results.

5.6(a).
As expected, the take-off and landing, followed by transition and dash phases, deplete the batteries at a faster rate since more power is required and the trend presents a steeper

slope. Whereas, an almost constant discharge can be observed during cruise due to the quasi-steady condition assumed in this segment. The fuel level for the gasoline configuration is shown in figure 5.6(b), which displays an identical behaviour as the battery charge profile, but related to the fuel burnt. For both cases, the amount of fuel and battery capacity defined during the sizing process proved to be accurate enough since at the final stage of the mission, the charge and fuel safety reserve values are not crossed. The SOC has a much higher value than 15% required to protect the batteries and the tank does not drop below 9% of filling.

Figures 5.7 and 5.8 show how the control logic of the hybrid system affects the battery

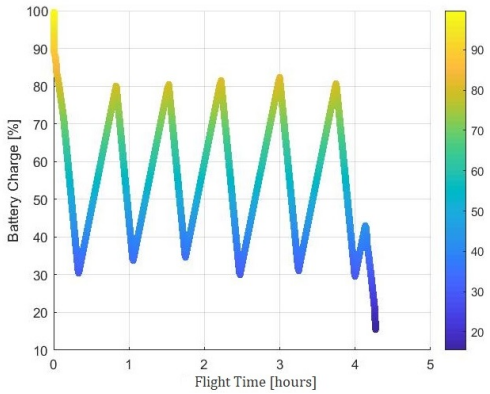

(a) Battery charge curve for the series hybrid simulation.

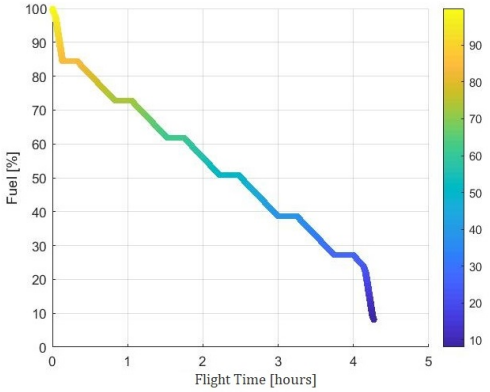

(b) Fuel level curve for the series hybrid simulation.

Figure 5.7. Series hybrid - Charge and Fuel curves.

charge and fuel level profiles of the series and parallel systems, respectively. During the cruise segment, both these configurations present iterative cycles of charge and discharge of the batteries according to the energy management strategy. As it can be seen, the batteries are first almost depleted in order to withstand the take-off, hover, transition and dash segments. Afterwards, when the UAV is in cruise conditions, the recharge mode can be activated, switching to an electric-only mode when the battery reaches the predefined cut-off limit, and going back to recharge mode when the SOC is close to the lower safety value.

Since the operational point of the engine for the parallel system is kept on the IOL, instead of varying accordingly to the OOP as for the smart controller of the series, it relies more on the battery energy and thus presents overall a higher recharging time, which also slightly increase the fuel consumed due to the shorter leg of engine's idle conditions. Despite the simplicity of the rule-based controller implemented to switch between the hybrid operating modes, it allows to reach the mission goals while respecting safety backups of fuel and battery charge percentage. Thus, the sizing results are overall validated proving the accuracy of the tool and assumptions previously made.

A clearer look at the results coming from the mission simulation can be found in table 5.1. As stated before, for all cases the MTOM of the aircraft is kept constant at $25kg$ and each configuration is sized to reach the mission time and associated range set in chapter

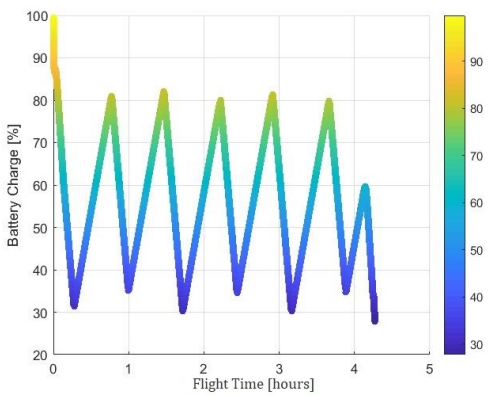

(a) Battery charge curve for the parallel hybrid simulation.

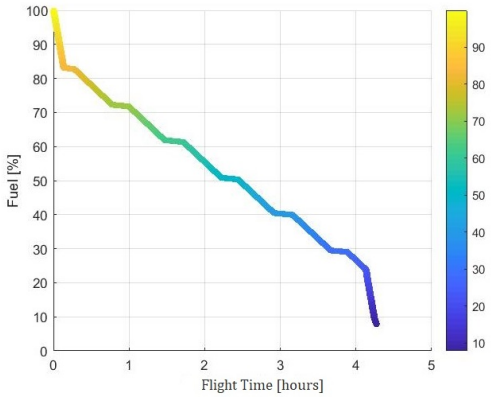

(b) Fuel level curve for the parallel hybrid simulation.

Figure 5.8. Parallel - Charge and Fuel curves.

4, regardless of the weight of the propulsion system and energy sources required to do so, carrying the sensor payload onboard. The '*available empty mass*' defined in the table corresponds to what is left out from the MTOM after the propulsion system is integrated, with fuel and battery, and should be associated to the structural, avionic masses and other auxiliary items. Two efficiency terms to evaluate and compare the configurations are defined: the energy and propulsion efficiencies in $[hr/kg]$. The first one relates the flight time and the weight of the main energy source on board and it shows how efficiently the resource is consumed in order to achieve the prescribed targets. The second one gives an idea of the dry weight of the propulsion system installed to complete the mission.

Parameters	**Electric**	**Gasoline**	**Series Hybrid**	**Parallel Hybrid**
Mission Time [hr]	4.27	4.27	4.27	4.27
Range [km]	549	549	549	549
Available Empty Mass [kg]	0.01	12.87	13.285	13.53
Propulsion Mass [kg]	2.49	4.21	5.26	4.62
Fuel Load [kg]	—	3.7	1.6	1.8
Battery Load [kg]	19	0.72	1.35	1.55
Capacity [Ah]	80	2	5.45	6
Payload [kg]	3.5	3.5	3.5	3.5
Fuel End [%]	—	9.94	7.98	7.93
Charge End [%]	22.9	17.2	15.45	27.8
Energy Efficiency [hr/kg]	0.216	1.154	2.669	2.372
Propulsion Efficiency [hr/kg]	1.715	0.947	0.811	0.886
CO2 Emissions [kg]	1.97	10.5	4.099	4.27

Table 5.1. Baseline mission results summary.

Although the electric aircraft configuration shows the highest propulsion efficiency due to the extremely light weight of the motors and electronic units; it also has the lowest energy efficiency due to the state of the art energy density value of the battery. In this way, completing the mission while carrying the magnetic sensor leaves only $0.1kg$ for the structure and avionic, making this solution unfeasible. Both series and parallel hybrid aircraft configurations are penalized compared to the gasoline concept in terms of propulsion efficiency values because of the additional weight of extra components. However, since the engine of the ICE only configuration results oversized for the majority of the mission, its energy efficiency is less than half of the one from the series and parallel hybrid solutions, which take advantage of the smaller-sized combustion engine that during the low-power requirement cruise segment performs at a lower BSFC, according to the OOP or IOL strategy implemented. This lead to a 56% and 51% of fuel mass savings for the series and parallel hybrid aircraft, respectively. Finally, between the two hybrid configuration, the series shows a 13.8% increase in dry weight due to extra generator mass, but the improved control logic can lead to 11% savings in fuel burnt and 4% reduction in CO_2 emission, thus reducing its operational cost and environmental impact.

5.2 Baseline Mission Optimization for Fixed Propulsion Mass

This section explores the best performance achievable by the four aircraft configurations in the case of a fixed propulsion system mass, settled according to the definition given for the VTOL UAV class in [44] to a third of the TOW , which is roughly equal to the $9kg$. The energy mass was redefined according to the component's weight presented in the previous section. More data on the structural components and avionic mass were collected from [65] and [22], leading to a conservative estimation of $12.5kg$ for the defined 'available empty mass', and leaving $3.5kg$ for the payload. The considerations on the propeller model and control logic are kept as in section 5.1, while the mission profile conserves all the segments, but leaves the flight time as performance parameter to maximize. The results of the cruise optimization simulation analysis are gathered in table 5.2.

Parameters	**Electric**	**Gasoline**	**Series Hybrid**	**Parallel Hybrid**
Mission Time [hr]	1.02	5.01	7.38	7.68
Range [km]	146	608	918	942
Available Empty Mass [kg]	12.5	12.5	12.5	12.5
Fuel Load [kg]	—	3.9	2.4	2.8
Battery Load [kg]	6.6	0.52	1.35	1.55
Capacity [Ah]	26.6	2	5.45	6
Payload [kg]	3.5	3.5	3.5	3.5
Energy Efficiency [hr/kg]	0.155	1.285	3.101	2.743
CO2 Emissions	0.77	11.52	6.42	6.84

Table 5.2. Cruise mission optimization.

The electric aircraft configuration achieves by the far the shortest flight time with $1hr$ due to the constraint on battery weight; moreover, since now the vertical operations represent a bigger portion of the mission, the energy term decreases even more, suggesting that even for short paths the electric is a weak option. In the same way, due to the longer cruise leg, the gasoline energy efficiency shows only a low increase, since the influence of the higher BSFC operating condition of the ICE only during this segment does not give many advantages. On the other hand, in terms of flight time both hybrid configurations strongly outperform the gasoline in about 47% and 53%, respectively. This can be attributed to the downsizing of the engine and the energy management strategy which increases their efficiency during cruise. Specifically, compared to their sizing cases, with an increase of 50% and 55% in fuel, it was possible to achieve 70% and 77% of extra time for the series and parallel, respectively. Finally, even if with a higher dry weight, the smart control logic of the series architecture can bring to a 15% reduction in the fuel burnt, leaving a margin of preference in terms of operational cost and emissions for the series concept.

5.3 Mission Parameters Sweep

This section analyses the influence of the main mission parameters over the aircraft performance. Each segment of the baseline mission is isolated and evaluated in order to determine the behaviour of the UAV for a VTOL only, dash only and cruise only mission. The energy sources onboard are redistributed in order to maximize the range and flight time of the configurations for the specific application.

Cruise only mission

The first study involves a mission simulation mainly focused on the cruise segment for the four architectures. After the vertical take-off, hover and transition phases, a constant cruise condition is maintained as long as the combination of the remaining fuel load and battery SOC is higher than the required energy to transition back and land.
By taking out the dash requirement, it is possible in the hybrid configurations to redistribute the mass available for fuel and battery. Since now the supports of the power drawn from the battery to the ICE or ICE-generator is limited to the vertical phases, the required electrical energy drastically drops and thus the capacity could be halved.

Parameters	Electric	Gasoline	Series Hybrid	Parallel Hybrid
Mission Time [hr]	1.88	5.53	11.2	11.38
Range [km]	238	669	1361	1406
Fuel Load [kg]	—	3.9	3.13	3.58
Battery Load [kg]	6.6	0.52	0.62	0.82
Capacity [Ah]	26.6	2	2.5	3
Energy Efficiency [hr/kg]	0.285	1.418	3.578	3.179

Table 5.3. Mission parameters sweep - cruise.

As can easily be expected, the results collected in table 5.3 show a general increase of

the flight time and range. It is clear that for all the configurations, with the exception of the gasoline aircraft which performs more efficiently at high power demands, the dash requirement has a strong influence on the mission performance since it mainly relies on the electric energy stored onboard for a relatively long leg. Compared to the results of section 5.2, the electric architecture reaches almost 90% extra mission time and 63% of additional range. The lower percentage increment in range can be attributed to the lower speed of the cruise segment compared to the dash. The concept gaining the least advantage in this study is the gasoline one. The increments in time and distance flown are only 10% and 9%, respectively. As already mentioned this is due to the higher BSFC of the oversized engine of the ICE only architecture. Finally, both hybrid concepts reach a significant 52% and 48% increase in flight time with only 30% and 28% of increase in the fuel mass, taken from the reduced battery weight. The more the cruise time increases, the more the influence of the controller logic implemented can be seen; in fact the two configurations are slowly converging in terms of performance thanks to the additional fuel savings, proven also by the higher energy efficiency.

Dash only mission

In this second analysis, the four architectures are simulated on a pure dash mission, besides the necessary phases to take-off and transitioning. The goal is to reach the maximum flight time and range with the aircraft at its top speed conditions. Again, the transition back and land are activated when the combination of the fuel and SOC goes below the safety cut-off values. In order to better operate the hybrid configurations in this high power demand scenario, the mass allocated for fuel and battery has been revised, favouring the latter to reach a balanced configuration, which optimizes how the power is split between the sources and according to their energy density.

The results displayed in 5.4 give an idea of how strongly the dash requirement impacts on

Parameters	**Electric**	**Gasoline**	**Series Hybrid**	**Parallel Hybrid**
Mission Time [hr]	0.45	1.88	0.78	0.85
Range [km]	91	392	159	174
Fuel Load [kg]	—	3.9	1.75	1.9
Battery Load [kg]	6.6	0.52	2	2.25
Capacity [Ah]	26.6	2	8	9
Energy Efficiency [hr/kg]	0.068	0.482	0.445	0.447

Table 5.4. Mission parameters sweep - dash.

the sizing and selection of the components for the configuration. The hybrid architectures that were optimized for cruise conditions are the most affected by it. The main constraint, in this case, is given by the use of the battery to support the engine. Because of that, out of the settled $9kg$, a large part of the mass available is taken by the batteries leading to 1/10 the values of flight time reached in the standard mission. Both the series and parallel concepts behave much more like the electric solution rather than the gasoline one, which outperforms them with a factor higher than 2 for the time flown. These considerations are

supported by the energy efficiency, which shows a higher value for the gasoline.
Even though a proper application of this mission could not be foreseen, in case the dash segment becomes the main one in the mission profile, instead of an additional feature to overcome the arctic winds, it is recommended to integrate a bigger engine, capable of fulfilling the dash power demand without relying on battery energy. This should bring back the hybrid concept as more efficient and advantageous, without losing good capabilities also in the cruise segment. After a first analysis of the BSFC maps generated with the engine model and the availability on the market, the *Desert Aircraft 50*, whose efficiency map is displayed in 3.8(a) and more information can be found in [78], is suggested as a proper trade-off solution.

Hover only mission

For the last simulation case, the performance of the four systems during axial operations are assessed. The classic vertical take-off is followed by a stationary hover. The condition are hold until the battery and fuel synergetic contributions are almost depleted; afterwards the aircraft returns to ground.
Generally, the mission time achieved for all the configurations is much lower than any other case. This can be attributed to the extremely high power request, as well as to the fact that the multirotor operations were not the main TLAR, and therefore the design itself results inefficient for these phases, as it can be seen in table 5.5. The considerations

Aircraft	Electric	Gasoline	Series Hybrid	Parallel Hybrid
Mission Time [hr]	0.27	0.84	0.223	0.258
Fuel Load [kg]	—	1.42	0.35	0.45
Battery Load [kg]	6.6	3	3.4	3.7
Capacity [Ah]	26.6	12	14	15
Energy Efficiency [hr/kg]	0.04091	0.5915	0.6371	0.5733

Table 5.5. Mission parameters sweep - hover.

previously made for the *dash only mission* can be applied almost in the same way as this case. Because of the high power request and the need to draw a big amount of energy from the battery, the hybrid architectures show even lower performance than the electric one, since additional mass penalties are brought by the extra components and thus less battery capacity can be reallocated. For those, a maximum hover time of $15min$ can be accomplished. The gasoline configuration shows by far the best performance, since only a small part of the power is given by the battery. Thus, it is capable to reach $50min$ in air. Again, it is suggested that in case more hover time or vertical operations are required, a configuration in the form of range-extender, as already implemented in other hybrid multicopter studies, such as [79], should be used. In this way no battery would be needed onboard and an engine would represent the main source of power, which then could be converted in electric form by an alternator in order to supply the distributed EMs. In this way the requirements of controllability would be fulfilled and would not be necessary any shaft in the powertrain.

5.4 Payload analysis

To conclude the mission performance study, in case in the future the Eusphyra might extend its application to a package delivery market, or in general to evaluate its carrying capabilities, a payload versus flight time extrapolation analysis for the standard mission profile is conducted. Trends for each architecture are displayed in figure 5.9; the electric case was left out since it would appear only as a short segment in the bottom-left corner and its unviability has been largely demonstrated before. Clearly, since the structural

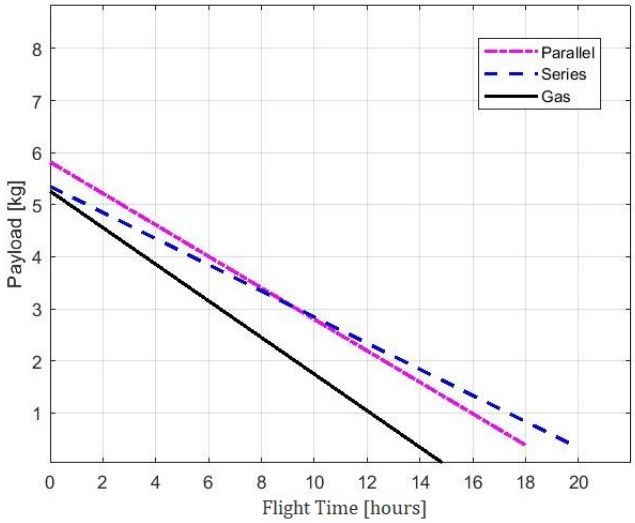

Figure 5.9. Payload versus flight time.

components, avionic, support and propulsion mass are defined, the available mass for payload is related to the fuel and battery mass onboard. In view of that, an increase in payload obviously leads to a reduction in flight time. From the slope of the curves, it is also possible to deduce which system is most efficient in mission time. As largely stated before, the series hybrid configuration is optimized for this phase, thanks to its improved control logic, but the penalties coming from the extra components suggest that, if mechanically feasible, the parallel architecture should be preferred for short flight legs.

Chapter 6

Conclusions

This chapter reviews the work done so far, summarizing the steps followed to achieve the final results and how many challenges encountered during the research were overcome. Finally, the future improvements and advancements which could be done relative to this project are highlighted.

6.1 Achievements

The potential of hybrid-electric propulsion systems, together with stepping stone platforms, such as VTOL UAVs, has been recently emerging as a promising and exciting aspect of research being conducted in various areas of the aerospace industry. Within the scope of this Master's Thesis work, the hybrid-electric propulsion system for a tilt tri-rotor VTOL UAV to be used by DRDC to conduct magnetic reconnaissance operations was designed and evaluated. In order to explore and compare different architectures and the potential benefits that they could bring to the mission envelope expansion, a power-based sizing process and a HEPS simulation framework were used.

First, in the initial stages of the project, a strong effort was made for the improvement of the HEPS simulation platform developed in the MathWorks MATLAB® environment. The scalability and adaptability of the numerical models for the propulsion system was the main driver of the research. To allow the user to compare and investigate a large variety of propulsion architectures and UAV concepts against one another, new basic aircraft mechanic laws were integrated into the tool, together with the expansion from a one-dimensional to a multi-dimensional variable problem in order to cover VTOL and distributed propulsion system configurations as well. In this research, a higher degree of flexibility was given to the tool.
Based on the stage of the design, the user can now rely on multiple options for the definition of the propeller performance, from experimental test data to detailed parametric modeling through the vortex theory, in order to reach the desired accuracy.
The EM was modeled through the simple approach of an equivalent circuit, which gives acceptable quality results with few input parameters; in this way the model can be easily adopted for any intended BLDC size and power. The described models have been validated individually with an EM-propeller test rig and the whole electric branch has been

verified through a flight test campaign comparison, which showed a close match between the simulations and the flight data, with the exception of transitory and sudden behaviors related to the maneuverability and control of the aircraft.
By the implementation of the Willans line method, it was given the possibility to model numerically internal combustion engines of theoretically any size if steady-state efficiency data of a reference engine from the same class are available. Particularly, this scaling model was validated against the manufacturer's experimental maps previously collected, appearing to be generally reliable with some local weaknesses. Nevertheless, the user should use this scaling model diligently, since this method allows to scale only engines belonging to the same reference engine's category and within thirty percent size range of the baseline engine.
The standalone models of the components have then been integrated into the series and parallel hybrid propulsion architectures. An energy management strategy was developed for both systems, trying to keep it general with control state variables, cut-off values and the implementation of the IOL method in order to minimize the fuel consumption, allowing in the meanwhile the user to adapt it to the specific case under analysis. Moreover, a new mathematical model for the fuel cells was also integrated.

After the development and validation of the models, together with the tool architecture, the need to define the input variables, in terms of components characteristics, for the HEPS simulation framework was raised. Thus, the models were taken and adapted into a preliminary sizing code, with the purpose to implement a conceptual design analysis of the different options for the propulsion system of the aircraft under study.
A power-based approach based on the propeller momentum theory was the starting point of the process. Through this method, the power demand of the axial, transition and forward flight was assessed and minimized by matching to optimal operational rpm and radius conditions for the front and rear rotors.
Then, the top-level aircraft requirements were associated to a baseline mission and the components, battery and fuel mass were estimated thanks to the model developed, together with a CO_2 emissions study.
For the hybrid cases, an estimation over the best hybridization factor took place, resulting in the series hybrid electric selection with a HF equal to 0.7 as the best trade-off solution. Knowing the power request, the theoretical size and mass of the components, a market research was conducted in order to identify the COTS that could fulfill the requirements and make up the series hybrid propulsion system to install onboard.
The data of the components selected were then passed to the sizing tool in order to compare the results with a satisfactory matching. Moreover, a trend of the propulsion mass with increasing cruise time was also assessed to estimate the more efficient solution for long flight time missions.

Finally, an overview of the aircraft performance was established from a theoretical point of view by means of the simulation framework. By feeding in the aircraft parameters and the mission profile to be simulated, it was possible to cross-check the results obtained from the sizing process. New features for the control logic and recharge strategy were successfully implemented, together with the definition of efficiency terms to quickly compare the different architectures. A series of trade-off studies was explored by sweeping the mission parameters of interest and observing their influence on system performance in terms of

flight time, range and fuel consumption. Generally, the simulations were done with varying energy (fuel and capacity) levels, but with the same defined take-off weight. The results showed that for any condition, the electric version could achieve the smallest range and endurance, thus it could still be employed for short missions if the requirements of operating totally carbon emission-free and with a substantially lower noise profile would be brought up. The hybrid versions show the biggest advantages in a cruise only condition, with over 11 hours of flight achievable thanks to the possibility of operating the UAV in stealth and recharge mode. Whereas, for dash and axial segments, the gasoline solution could lead to higher endurance. Solutions for overcoming these flight limitations in possible future hybrid electric design versions of the aircraft were presented. Lastly, the UAV capacity of carrying a payload for the longest time was assessed, with the parallel hybrid solution being advantageous for shorter times and the series hybrid best suited for endurance over 10 hours.

6.2 Recommendations for Future Work

UVIC CFAR has long term plans to continue to research and develop HEP technologies for use in a variety of UAV applications. Thus, the author identified and recommends four areas for further research and advancements. Specifically:

- Improvements on the simulation tool;
- Advanced powertrain exploration for HEPS design;
- Test bench implementation;
- Aircraft integration;

Considering this, future studies must aim to optimize the configurations by developing more information on modelling and increase the confidence in the design by testing them. An assessment of the risks and benefits coming from the integration of these systems on board should also be done.

Improvements on the simulation tool

Although the author strongly believes that the aircraft simulation framework can provide an insightful analysis of the trade-offs and comparisons between propulsion architectures, many improvements could be done in this area. Going down on the different levels of the tool, the first biggest disadvantage is the lack of an user-friendly interface. At the moment the user is required to access the mission and aircraft scripts in order to set the parameters and select the state flags for the activation of the proper models. A big contribution to the simulation tool would be building this interface, potentially through the use of MATLAB GUI. This would make the tool easily used by any person that understands the topic under study but does not have programming knowledge, leading to a possible open-source distribution of the tool. It would also allow an easier way to access the databases or the data of previously tested configurations, as well as insert new data and therefore make the extrapolations more accurate and less error-prone. Another solid improvement would be adding

more features to the models, giving different level of abstraction based on the purpose of the study, from conceptual design where only few data are available to the detailed design where all the components can be accurately described. A partial generalization of the model through scaling and mass method approaches was given by the author and should be pursued in the next steps. In the same way, improvements in the energy management system would probably lead to major benefits and an increase in performance as suggested by the literature. [80] The developed IOL, as well as battery depletion recharge strategies, guarantees reliability and ease of implementation, but many publications refer to the more sophisticated fuzzy control [81], or even more complex neural network controllers as recommended strategies to reach higher efficiency gains.[10, 50] Although not directly related with the simulation tool structure, it is also suggested that more simulations are run, analyzing more advanced and complex mission profiles to completely cover the behavior and performance of the aircraft and propulsion systems over multiple scenarios. Finally, a deeper tuning and validation of the model should also be implemented if additional test bench or flight campaigns are performed in the future.

Advanced powertrain exploration for HEPS design

The work developed in this thesis was purely theoretical, being only validated through the use of computational tools. Thus, even if an actual design combining COTS was presented, more research and testings should be done about the challenges of integrating the different sources selected and their compatibility before proceeding with the purchase. In this exercise, the same scale components were assembled into the aircraft for feasibility with conservative estimates for many unknown masses and losses in the supports, transmission and especially in the tilting mechanism. A higher detailed design should be given to the tilt concept, so that actual vibration, cooling and noise studies could be assessed to reach the necessary confidence and certainty in the control and safe installation of the HEPS on actual flying architectures. The fast development of new technologies must also be taken into account in order to improve the design. It is recommended to carefully follow the leap in technologies brought especially in the engine and battery fields [45]. For the first one, an example is the work presented by LiquidPiston, which has recently developed Small Tactical Power Generators in the range of 2-5 kW which claims to be able to provide more than an 80% reduction in weight and an almost 70% decrease in size when compared to the generators currently in use. This concept has been joined with a hybrid approach to the X-Engine solution, presented in appendix B.1. The technology has already been ground and flight tested, thus if in the future it is available for purchase, many of the challenges identified in terms of size, vibrations, noise and heat management would be solved with incredible advantages.

Test bench simulations

To support the integration studies previously mentioned, the natural conversion of the present parallel hybrid electric test bench to a series configuration must be performed. Recently, the test bench has been upgraded with a 10kW dynamometer segment to assist in system characterization, presented in appendix B.1. Through this mean, a wide range of mission profiles can be simulated to test the UAV propulsion system in a range of applications. These mission profiles are critical to the complete characterization of the system,

as steady-state measurements do not fully encapsulate a UAV system's performance. The experimental setup of the series HEPS in the test bench should open the door for many improvements to the design.

Aircraft integration

Future work recommended by the author would include the detailed design and optimization of the HEPS for implementing into the Eusphyra. The end goal of this hybrid-electric propulsion system research must be the integration of the concept into the tilt tri-rotor VTOL UAV that is being developed at UVIC CFAR. The purpose would be to test the propulsion architecture in a real-world scenario and collect helpful test data along the flight tests. It must be noticed that there are several major differences between the ground testing of the HEPS designed and the configuration that would be integrated on the airframe, such as a more compact design, more complex mounting features and auxiliary components. Thus, the author also pursued a market research to identify series hybrid propulsion systems already available on the market for purchase, so that in the future if the design of the full-scale aircraft would suddenly need a baseline hybrid propulsion system, the team will not be unprepared. The range extender Gas-Electric 35cc (GE35) [82] from Pegasus Aeronautics® perfectly suits the design requirements. Its performance data are collected in appendix B.1. In any case, the design would still need improvements and optimization according to the techniques and methods presented in this work, attesting its contribution to this area of research.

Bibliography

[1] ICAO. Future of Aviation. https://www.icao.int/Meetings/FutureOfAviation/Pages/default.aspx. Accessed: 11 October 2021.

[2] Airbus. Global Market Forecast. https://www.airbus.com/en/products-services/commercial-aircraft/market/global-market-forecast, . Accessed: 11 October 2021.

[3] K. Suder. Overview of the NASA Environmentally Responsible Aviation Project's Propulsion Technology Portfolio. In *48th AIAA/ASME/SAE/ASEE Joint Propulsion Conference and Exhibit*, 2012. doi: 10.2514/6.2012-4038.

[4] S. Sahoo, X. Zhao, and K. Kyprianidis. A review of concepts, benefits, and challenges for future electrical propulsion-based aircraft. *Aerospace*, 7(4):44, 2020. doi: 10.3390/aerospace7040044.

[5] M. Hepperle. Electric Flight - Potential and Limitations. In *Energy Efficient Technologies and Concepts of Operation*, 2012.

[6] B. Saha, E. Koshimoto, C. C. Quach, E. F. Hogge, T. H. Strom, B. L. Hill, S. L. Vazquez, and K. Goebel. Battery Health Management System for Electric UAVs. In *2011 Aerospace Conference*, pages 1–9, 2011. doi: 10.1109/AERO.2011.5747587.

[7] J. Ausserer and F. Harmon. Integration, Validation, and Testing of a Hybrid-Electric Propulsion System for a Small Remotely Piloted Aircraft. In *10th Annual International Energy Conversion Engineering Conference, IECEC 2012*. American Institute of Aeronautics and Astronautics, 2012. doi: 10.2514/6.2012-4239.

[8] R. Glassock, J. Hung, L. Gonzalez, and R. Walker. Design, modelling and measurement of a hybrid powerplant for unmanned aerial systems. *Australian Journal of Mechanical Engineering*, 6:69–78, 2008. doi: 10.1080/14484846.2008.11464559.

[9] F. Harmon, A. Frank, and J. Chattot. Conceptual Design and Simulation of a Small Hybrid-Electric Unmanned Aerial Vehicle. *Journal of Aircraft*, 43:1490–1498, 2006. doi: 10.2514/1.15816.

[10] F. Harmon, A. Frank, and S. Joshi. Application of a CMAC neural network to the control of a parallel hybrid-electric propulsion system for a small unmanned aerial vehicle. In *Proceedings. 2005 IEEE International Joint Conference on Neural Networks*, volume 1, pages 355–360, 2005. doi: 10.1109/IJCNN.2005.1555856.

[11] R. M. Hiserote. Analysis of Hybrid-Electric Propulsion System Designs for Small Unmanned Aircraft Systems. Master's thesis, AFIT Scholar, 2010. https://scholar.afit.edu/etd/2044.

[12] M. D. Rippl. Sizing analysis for aircraft utilizing hybrid-electronic propulsion systems recommended citation, 2011. URL https://scholar.afit.edu/etd/1349.

[13] C. Friedrich and P. Robertson. Hybrid-electric propulsion for aircraft. *Journal of Aircraft*, 52(1):176–189, 2015. doi: 10.2514/1.C032660.

[14] Quaternium. HYBRIX.20 the first petrol-electric multicopter. https://www.quaternium.com/range-extender/. Accessed: 27 September 2021.

[15] Top Flight Technologies. Airborg H8 10K with Top Flight Hybrid-Power System. https://www.topflighttech.com/products/airborg-h8-10k-with-top-flight-hybrid-power-system.html, . Accessed: 27 September 2021.

[16] Yeair. Table of specs: yeair! https://yeair.de/specs/. Accessed: 27 September 2021.

[17] A. Yezeguelian and A. Isikveren. Methods to Improve UAV Performance Using Hybrid-Electric Architectures. *Aircraft Engineering and Aerospace Technology*, 92(5):685–700, 2020. doi: 10.1108/AEAT-11-2019-0227.

[18] N. D. Ranasinghe and W. A. Don Lakitha Gunawardana. Development of Gasoline-Electric Hybrid Propulsion Surveillance and Reconnaissance VTOL UAV. In *2021 IEEE International Conference on Robotics, Automation and Artificial Intelligence (RAAI)*, pages 63–68. Institute of Electrical and Electronics Engineers (IEEE), 2021. doi: 10.1109/raai52226.2021.9508033.

[19] Plymouth Rock Technologies. XV: Fixed-Wing, Vertical Take-off and Landing Unmanned Aircraft System. https://www.plyrotech.com/products/xv/. Accessed: 27 September 2021.

[20] B. Luís. Design and Development of a Magnetic Anomaly Detection Unmanned Aerial Vehicle. Master's thesis, Instituto Superior Técnico, 2019.

[21] Defence Cae. Magnetic Anomaly Detection Extended Role (MAD-XR). https://www.cae.com/media/media-center/documents/datasheet.MAD-XR.pdf. Accessed: 21 April 2021.

[22] S. Pedro. Sizing and Integration of an Electric Propulsion System for a VTOL UAV. Master's thesis, Instituto Superior Técnico, 2020.

[23] W. Lu, D. Zhang, J. Zhang, T. Li, and T. Hu. Design and implementation of a gasoline-electric hybrid propulsion system for a micro triple tilt-rotor VTOL UAV. In *2017 6th Data Driven Control and Learning Systems (DDCLS)*, volume 10, pages 433–438. IEEE, 2017. doi: 10.1109/DDCLS.2017.8068112.

[24] D. F. Finger, C. Braun, and C. Bil. A Review of Configuration Design for Distributed Propulsion Transitioning VTOL Aircraft. In *Proceedings of the 2017 Asia-Pacific International Symposium on Aerospace Technology*, pages 1782–1796, 2017.

[25] K. V. Singh, H. O. Bansal, and D. Singh. A comprehensive review on hybrid electric vehicles: architectures and components. *Journal of Modern Transportation*, 27(2): 77–107, 2019. doi: 10.1007/s40534-019-0184-3.

[26] C. Pornet and A. Isikveren. Conceptual design of hybrid-electric transport aircraft. *Progress in Aerospace Sciences*, 79:114–135, 2015. doi: 10.1016/j.paerosci.2015.09.002.

[27] D. Finger. *Methodology for Multidisciplinary Aircraft Design under Consideration of Hybrid-Electric Propulsion Technology*. PhD thesis, RMIT University, dec 2020.

[28] J. Lieh, E. Spahr, A. Behbahani, and J. Hoying. Design of Hybrid Propulsion Systems for Unmanned Aerial Vehicles. In *47th AIAA/ASME/SAE/ASEE Joint Propulsion Conference and Exhibit*. American Institute of Aeronautics and Astronautics, 2011. doi: 10.2514/6.2011-6146.

[29] Z. Wang, X. Pan, W. Zhang, Y. Zhao, H. Li, and P. Liu. The Development Trend of Internal Combustion Engine. *Journal of Physics: Conference Series*, 1626:012139, 2020. doi: 10.1088/1742-6596/1626/1/012139.

[30] Y. Wang, Y. Shi, M. Cai, W. Xu, J. Zhang, W. Zhong, and N. Wang. Optimization of Fuel Injection Control System of Two-Stroke Aeroengine of UAV. *Complexity*, 2020: 1–12, 2020. doi: 10.1155/2020/8921320.

[31] LiquidPiston. Power Reimagined-Rotary Engines. `www.liquidpiston.com`, 2020. Accessed: 11 october 2021.

[32] E. Mattarelli, G. Cantore, and C. Alberto. Advances in The Design of Two-Stroke, High Speed, Compression Ignition Engines. In *Advances in Internal Combustion Engines and Fuel Technologies*. InTech, 2013. doi: 10.5772/54204.

[33] Currawong Engineering. Corvid-29 Engine Maps. `www.currawongeng.com`. Accessed: 27 september 2021.

[34] M. Turesson. Modelling and simulation of a two-stroke engine. Master's thesis, University of Gothenburg, 2009.

[35] D. Buttsworth. Multizone internal combustion engine modelling: Initial assessme of a simulation tool developed in matlab. In *2009 3rd International Conference on Energy and Environment (ICEE)*, pages 343–347. IEEE, 2009. doi: 10.1109/ICEENVIRON.2009.5398624.

[36] A. J. Chaudhari, N. Sahoo, and V. Kulkarni. Simulation models for spark ignition engine: A comparative performance study. volume 54, pages 330–341. Elsevier Ltd, 2014. doi: 10.1016/j.egypro.2014.07.276.

[37] G. Rizzoni, L. Guzzella, and B. Baumann. Unified modeling of hybrid electric vehicle drivetrains. *IEEE/ASME Transactions on Mechatronics*, 4(3):246–257, 1999. doi: 10.1109/3516.789683.

[38] M. Sorrentino, F. Mauramati, I. Arsie, A. Cricchio, C. Pianese, and W. Nesci. Application of Willans Line Method for Internal Combustion Engines Scalability towards the Design and Optimization of Eco-Innovation Solutions. 2015-24-2397 2015. doi: 10.4271/2015-24-2397.

[39] C. He, Y. Jia, and D. Ma. Optimization and Analysis of Hybrid Electric System for Distributed Propulsion Tilt-Wing UAV. *IEEE Access*, 8:224654–224667, 2020. doi: 10.1109/ACCESS.2020.3044449.

[40] T. Donateo and A. Ficarella. Designing a Hybrid Electric Powertrain for an Unmanned Aircraft with a Commercial Optimization Software. *SAE International Journal of Aerospace*, 10, aug 2017. doi: 10.4271/2017-01-9000.

[41] V. Alulema, E. Valencia, E. Cando, V. Hidalgo, and D. Rodriguez. Propulsion Sizing Correlations for Electrical and Fuel Powered Unmanned Aerial Vehicles. *Aerospace*, 8 (7):171, 2021. doi: 10.3390/aerospace8070171.

[42] X. Wei. *Modeling and Control of a Hybrid Electric Drivetrain for Optimum Fuel Economy*. PhD thesis, The Ohio State University, 2004.

[43] D. Lundström, K. Amadori, and P. Krus. Validation of Models for Small Scale Electric Propulsion Systems. In *48th AIAA Aerospace Sciences Meeting Including the New Horizons Forum and Aerospace Exposition*. American Institute of Aeronautics and Astronautics, jan 2010. doi: 10.2514/6.2010-483.

[44] D. F. Finger, C. Braun, and C. Bil. Impact of Battery Performance on the Initial Sizing of Hybrid-Electric General Aviation Aircraft. *Journal of Aerospace Engineering*, 33 (3):04020007, 2020. doi: 10.1061/(asce)as.1943-5525.0001113.

[45] J. E. Harlow, X. Ma, J. Li, E. Logan, Y. Liu, N. Zhang, L. Ma, S. L. Glazier, M. M. E. Cormier, M. Genovese, S. Buteau, A. Cameron, J. E. Stark, and J. R. Dahn. A Wide Range of Testing Results on an Excellent Lithium-Ion Cell Chemistry to be used as Benchmarks for New Battery Technologies. *Journal of The Electrochemical Society*, 166(13):A3031–A3044, 2019. doi: 10.1149/2.0981913jes.

[46] J. Ledoux, S. Riffo, and J. Salomon. Analysis of the Blade Element Momentum Theory. 2020. doi: hal-02550763.

[47] R. Macneill and D. Verstraete. Blade element momentum theory extended to model low reynolds number propeller performance. *The Aeronautical Journal*, 121:835–857, 2017. doi: 10.1017/aer.2017.32.

[48] G. Kuik. Joukowsky actuator disc momentum theory. *Wind Energy Science Discussions*, pages 1–14, 2017. doi: 10.5194/wes-2016-55.

[49] S. Goldstein and L. Prandtl. On the vortex theory of screw propellers. *Proceedings of the Royal Society of London. Series A, Containing Papers of a Mathematical and Physical Character*, 123:440–465, 4 1929. doi: 10.1098/rspa.1929.0078.

[50] T. Lei, Z. Yang, Z. Lin, and X. Zhang. State of art on energy management strategy for hybrid-powered unmanned aerial vehicle. *Chinese Journal of Aeronautics*, 32: 1488–1503, 6 2019. doi: 10.1016/j.cja.2019.03.013.

[51] Y. Xie, A. Savvaris, A. Tsourdos, D. Zhang, and J. Gu. Review of hybrid electric powered aircraft, its conceptual design and energy management methodologies. *Chinese Journal of Aeronautics*, 34:432–450, 2021. doi: 10.1016/j.cja.2020.07.017.

[52] Y. Xie, A. Savvaris, and A. Tsourdos. Fuzzy logic based equivalent consumption optimization of a hybrid electric propulsion system for unmanned aerial vehicles. *Aerospace Science and Technology*, 85:13–23, 2019. doi: 10.1016/j.ast.2018.12.001.

[53] Q. Xue, X. Zhang, T. Teng, J. Zhang, Z. Feng, and Q. Lv. A Comprehensive Review on Classification, Energy Management Strategy, and Control Algorithm for Hybrid Electric Vehicles. *Energies*, 13(20):5355, 2020. doi: 10.3390/en13205355.

[54] D. Pfurtscheller. Development of a hybrid-electric propulsive system model for Unmanned Aerial Systems. Master's thesis, Instituto Superior Técnico, 2019.

[55] J. Matlock. Evaluation of Hybrid-Electric Propulsion Systems for Unmanned Aerial Vehicles. Master's thesis, University of Victoria, 2016.

[56] L. Machado. Design and Development of a Hybrid Electric Propulsion System for Unmanned Aerial Vehicles. Master's thesis, Instituto Superior Técnico, 2019.

[57] R. D. Blevins. *Applied Fluid Dynamics Handbook*. Van Nostrand Reinhold Company, 1984.

[58] J. Matlock, S. Warwick, P. Sharikov, J. Richards, and A. Suleman. Evaluation of energy efficient propulsion technologies for unmanned aerial vehicles. *Transactions of the Canadian Society for Mechanical Engineering*, 43(4):481–489, 2019. doi: 10.1139/tcsme-2018-0231.

[59] MathWorks. Battery block for implementation of a generic dynamic model. `https://www.mathworks.com/help/physmod/sps/powersys/ref/battery.html`. Accessed: 27 august 2021.

[60] Environmental Protection Agency. Greenhouse Gases Equivalencies Calculator - Calculations and References. `https://www.epa.gov/energy/greenhouse-gases-equivalencies-calculator-calculations-and-references`. Accessed: 21 september 2021.

[61] J.-J. Chattot. Optimization of propellers using a vortex model. In *Numerical Simulations of Incompressible Flows*, pages 375–384. World Scientific, 2003.

[62] J. Roskam and C.-T. Lan. *Airplane Aerodynamics and Performance*. DARcorporation, 2016.

[63] J. Schömann. *Hybrid-Electric Propulsion Systems for Small Unmanned Aircraft*. PhD thesis, Technische Universität München, 2014.

[64] P. Sharikov. Fuel Cell Hybrid-Electric Propulsion for Unmanned Aerial Vehicles. Master's thesis, University of Victoria, 2021.

[65] P. Fernandes. Development, Computational and Experimental Characterization of a Canard Aircraft Configutation. Master's thesis, Instituto Superior Técnico, 2021.

[66] T. Jesus. Surrogate-based Multidisciplinary Design Optimization of a Canard Configuration VTOL UAV. Master's thesis, Instituto Superior Técnico, 2020.

[67] D. Finger, C. Braun, and C. Bil. An Initial Sizing Methodology for Hybrid-Electric Light Aircraft. In *2018 Aviation Technology, Integration, and Operations Conference*, 2018. doi: 10.2514/6.2018-4229.

[68] A. R. Serrano. Design methodology for hybrid (VTOL + Fixed Wing) unmanned aerial vehicles. *Aeronautics and Aerospace Open Access Journal*, 2(3):165–176, 2018. doi: 10.15406/aaoaj.2018.02.00047.

[69] J. G. Leishman. *Principles of helicopter aerodynamics*. Cambridge University Press, 2006.

[70] EPI Inc.. Propeller Performance Factors. `http://www.epi-eng.com/propeller_technology/selecting_a_propeller.htm`. Accessed: 21 september 2021.

[71] R. Ravishankar and S. Chakravarthy. Range Equation For a Series Hybrid Electric Aircraft. In *2018 Aviation Technology, Integration, and Operations Conference*. doi: 10.2514/6.2018-3208.

[72] Max Amps. LiPo 5450 12S 44.4V Battery Pack. `https://www.maxamps.com/lipo-5450-12s-44-4v-battery-pack`. Accessed: 4 october 2021.

[73] T-MOTOR. P60 KV170. `https://store.tmotor.com/goods.php?id=420`. Accessed: 4 october 2021.

[74] T-MOTOR. U13-II KV130. `https://store.tmotor.com/goods.php?id=767`. Accessed: 4 october 2021.

[75] HFE International. DA35 EFI Data Sheet 35cc Single Cylinder, Electronic Fuel Injected Two Stroke Engine. `https://hfeinternational.com/wp-content/uploads/2021/03/DA35-Data-Sheet.pdf`. Accessed: 4 october 2021.

[76] Sullivan Unmanned Vehicle. S676-500U-21-Datasheet-2017. `https://www.sullivanuv.com/wp-content/uploads/2017/12/S676-500U-21-Datasheet-2017.pdf`. Accessed: 5 october 2021.

[77] Sullivan Unmanned Vehicle. SGENS-100A-01-Datasheet-2017. `https://www.sullivanuv.com/wp-content/uploads/2017/12/SGENS-100A-01-Datasheet-2017.pdf`. Accessed: 5 october 2021.

[78] HFE International. DA50 EFI Data Sheet 50cc Single Cylinder, Electronic Fuel Injected Two Stroke Engine. `https://hfeinternational.com/wp-content/uploads/2021/03/DA50-Data-Sheet.pdf`. Accessed: 5 october 2021.

[79] K. E. McKinney. Evaluation of hybrid-electric power system integration challenges for multi-rotor uas. Master's thesis, Oklahoma State University, 2018.

[80] D. A. Dehesa Jr. Study of Control Schemes for Series Hybrid-Electric Powertrain for Unmanned Aerial Systems. Master's thesis, Louisiana State University, 2020.

[81] M. Bai, W. Yang, D. Song, M. Kosuda, S. Szabo, P. Lipovsky, and A. Kasaei. Research on Energy Management of Hybrid Unmanned Aerial Vehicles to Improve Energy-Saving and Emission Reduction Performance. *International Journal of Environmental Research and Public Health*, 17(8), 2020. doi: 10.3390/ijerph17082917.

[82] PEGASUS Aeronautics. Range Extender GE35. `https://www.pegasusaero.ca/ge35`. Accessed: 5 october 2021.

Appendix A

Theoretical Informations and Experimental Tests

A.1 Partial derivatives of the least square fit for the Willans line formulation

$$
\begin{aligned}
0 &= \sum_{i=1}^{n} (R \cdot p_{ma,i}) \\
0 &= \sum_{i=1}^{n} (R \cdot \nu_{m,i} \cdot p_{ma,i}) \\
0 &= \sum_{i=1}^{n} \left(R \cdot \nu_{m,i}^2 \cdot p_{ma,i}\right) \\
0 &= \sum_{i=1}^{n} \left(R \cdot p_{ma,i}^2\right) \\
0 &= \sum_{i=1}^{n} \left(R \cdot \nu_{m,i} \cdot p_{ma,i}^2\right) \\
0 &= \sum_{i=1}^{n} (R) \\
0 &= \sum_{i=1}^{n} \left(R \cdot \nu_{m,i}^2\right)
\end{aligned}
$$

with R as shorthand notation for:

$$R = 2 \cdot ([e_0(\nu_{m,i}) - e_1(\nu_{m,i}) \cdot p_{ma,i}] \cdot p_{ma,i} - p_{mloss}(\nu_{m,i}) - p_{me,i})$$

A.2 EM-Propeller Test Rig Results

Table A.1. Experimental results of 14x4.8 rotor test rig with MN4012.

Throttle [%]	Power [W]	Current [A]	Voltage [V]	Torque [Nm]	Thrust [N]	RPM
10	11.98206604	0.483271857	24.79372413	0.017234737	1.042160517	2196.14
15	19.28833916	0.778163083	24.78713845	0.030569688	1.892532116	2232.24
20	28.83967571	1.16394901	24.7775886	0.046574961	2.910209273	2415.80
25	38.88155469	1.569914778	24.76689281	0.061903967	3.874187427	3498.21
30	50.47126347	2.038915538	24.75418023	0.079058617	4.831133574	4098.04
35	61.87722965	2.501239667	24.74139533	0.09400465	5.796574852	4777.65
40	80.65573091	3.262988067	24.71858230	0.117250918	7.34961023	5819.04
45	99.00145588	4.008792312	24.69646842	0.138212172	8.71257061	6340.24
50	120.0526222	4.866225056	24.67114635	0.161611708	10.21882892	6593.80
55	144.1263359	5.849577959	24.63983474	0.186360509	13.80173122	6885.24
60	172.8661989	7.02687332	24.60225819	0.214336995	15.78865763	7201.88
65	201.0000165	8.183163629	24.56460296	0.237731746	15.39700943	7573.98
70	233.3446073	9.516847088	24.52219806	0.265134661	17.09859594	7904.53
75	270.310056	11.04638771	24.47321343	0.296802637	19.13763597	8196.95
80	311.9728565	12.77872637	24.41476699	0.3293923	21.28401134	8544.42
85	354.636344	14.56299626	24.35314772	0.360997475	23.20729192	8881.11
90	400.2837443	16.4813503	24.28798319	0.393766787	25.26418422	9207.58
95	446.8178978	18.44945845	24.21931954	0.424491905	27.31849968	9551.64
100	498.1939604	20.63635363	24.14231995	0.457339036	29.25803672	9902.51

Table A.2. Prediction errors of the simulation for the EM-rotor of the VTOL propulsion components.

Throttle	Voltage	Current	Torque	Power	RPM
-72%	-1%	11%	-4%	11%	0%
-49%	-1%	9%	-3%	5%	0%
-36%	-1%	7%	-1%	9%	-1%
-24%	-1%	5%	-2%	-1%	1%
-15%	-1%	5%	-3%	-7%	2%
-8%	-1%	3%	0%	-3%	1%
-7%	0%	0%	1%	-6%	1%
-3%	0%	-2%	-1%	-8%	2%
-1%	0%	-4%	-2%	-10%	0%
-7%	0%	-14%	-3%	-13%	1%
-6%	1%	-3%	1%	-15%	1%
3%	1%	-9%	0%	-14%	1%
5%	1%	-10%	-2%	-14%	2%
5%	2%	-11%	-1%	-15%	0%
6%	2%	-13%	-1%	-16%	1%
7%	3%	-12%	1%	-16%	0%
7%	3%	-13%	-2%	-16%	1%
7%	4%	-14%	0%	-16%	2%

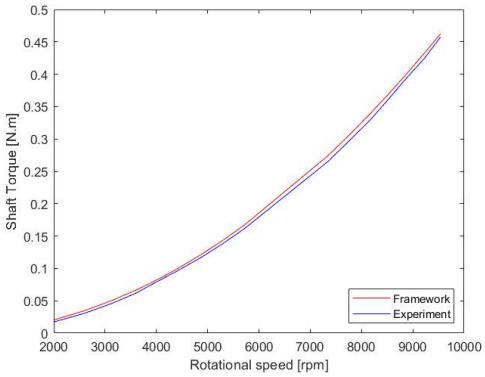

(a) Experimental and simulated torque at the shaft of the EM-Propeller.

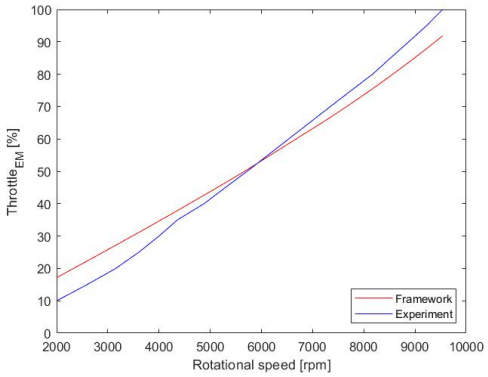

(b) Commanded and simulated throttle at the shaft of the EM-Propeller.

Figure A.1. Torque and Throttle values of the MN4012 over rpm.

Table A.3. Experimental results of 15x13N propeller test rig with KDE4012.

Throttle [%]	Current [A]	Voltage [V]	Torque [Nm]	Thrust [N]	RPM	Power [W]
10	0.4883	24.3871	0.0374	1.920131583	1595.9980	11.90881865
15	0.8119	24.3798	0.0631	2.568448555	2222.1335	19.79258167
20	1.2776	24.3660	0.0952	3.359997768	2735.2455	31.12826296
25	1.7267	24.3505	0.1229	4.101465108	3071.5069	42.04372738
30	2.6127	24.3199	0.1729	5.205353037	3511.0707	63.53316204
35	3.6671	24.2800	0.2229	6.443584909	3814.1751	89.03037581
40	4.7297	24.2374	0.2680	7.475443579	4085.8439	114.6271664
45	6.1009	24.1800	0.3164	8.672804767	4452.5081	147.5066672
50	7.3671	24.1170	0.3577	10.05145257	4743.5170	177.6551676
55	8.9822	24.0433	0.4093	11.19173488	5037.3219	215.9281092
60	10.8318	23.9553	0.4578	12.744576239	5211.5546	259.4443788
65	12.7003	23.8646	0.5021	15.57353257	5562.5082	303.0373785
70	14.1536	23.7825	0.5424	18.31752807	5625.3761	336.5636445
75	16.2724	23.6696	0.5883	19.23052256	5851.0876	385.0972966
80	18.5388	23.5434	0.6321	19.45924445	6092.4911	436.3951397
85	21.2665	23.4052	0.6849	20.56	6238.5755	497.6461149
90	23.0191	23.2797	0.7121	21.54139987	6384.6582	535.78926
95	26.6320	23.1014	0.7747	23.67328786	6582.4636	615.1210746
100	28.1128	22.9929	0.7929	24.89117611	7481.3965	646.2902987

Table A.4. Prediction errors of the simulation for the EM-rotor of the forward propulsion components.

Throttle	Current	Voltage	Torque	RPM	Power
50%	12%	3%	32%	-18%	16%
35%	11%	3%	22%	-12%	14%
24%	10%	3%	19%	-9%	13%
13%	5%	3%	12%	-6%	12%
8%	-4%	2%	0%	-2%	4%
5%	-7%	2%	-6%	4%	1%
0%	-9%	2%	-9%	8%	-3%
-4%	-11%	2%	-11%	5%	-7%
-6%	-9%	2%	-8%	3%	-3%
-9%	-6%	2%	-11%	8%	-7%
-10%	-4%	2%	-7%	2%	-5%
-6%	4%	1%	-12%	8%	10%
-3%	7%	1%	-7%	5%	11%
-6%	9%	0%	-8%	2%	9%
-12%	2%	0%	-5%	3%	7%
-14%	-2%	0%	-7%	1%	3%
-17%	-2%	0%	-6%	5%	3%
-16%	-1%	0%	-9%	8%	4%
-17%	2%	-1%	8%	12%	6%

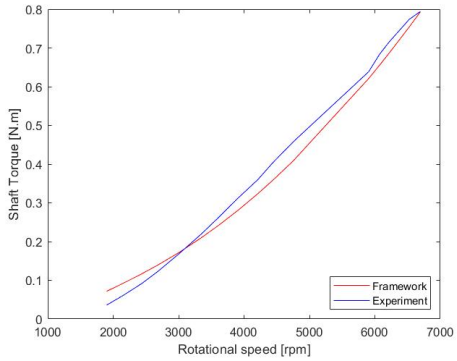

(a) Experimental and simulated torque at the shaft of the pusher EM-Propeller.

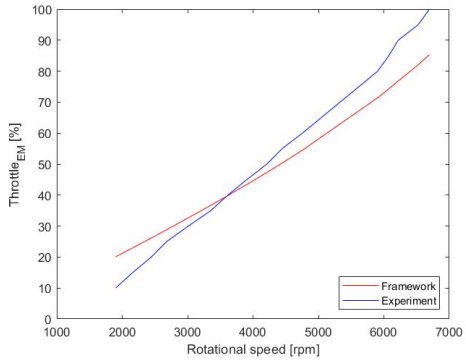

(b) Commanded and simulated throttle at the shaft of the pusher EM-Propeller.

Figure A.2. Torque and Throttle values of the KDE4012 over rpm.

A.3 Flight Test Simulation Results

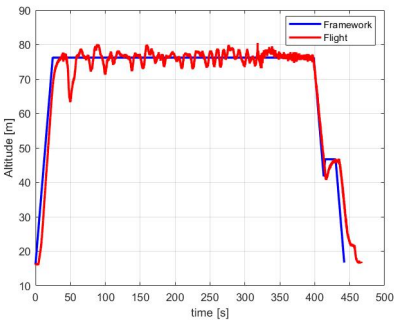

(a) Mini-E speed profile along the flight mission.

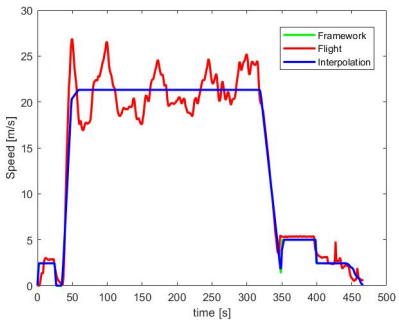

(b) Mini-E speed profile along the flight mission.

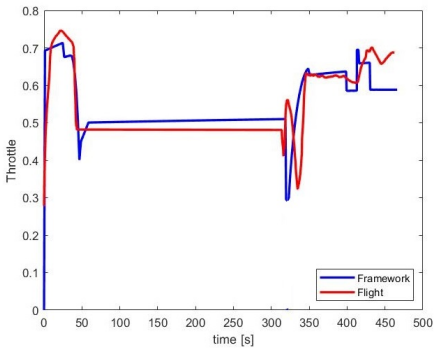

(c) EMini-E throttle command along the flight mission.

Figure A.3. Mini-E flight mission data.

A.4 Eusphyra Aerodynamic Characteristics

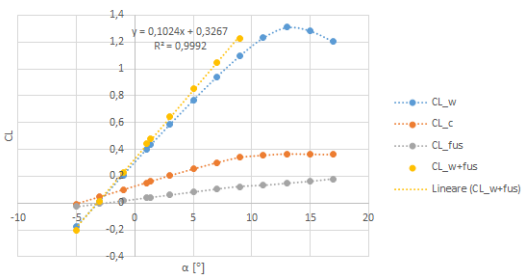

(a) C_L curve versus angle of attack.

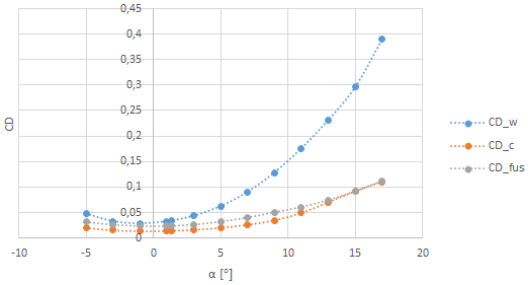

(b) C_D curve versus angle of attack.

Figure A.4. Eusphyra aerodynamic characteristics.

Appendix B

Technical Data-sheets

B.1 Manufacturer Data

Desert Aircraft 35 Performance Map

J1349 Power[W]

Throttle\RPM	1000	2000	2500	3000	3500	4000	4500	5000	5500	6000	6500	7000	8000
0	#N/A	#N/A	#N/A	#N/A	#N/A	#N/A	#N/A	#N/A	#N/A	#N/A	#N/A	#N/A	#N/A
4.7	#N/A	#N/A	#N/A	#N/A	#N/A	#N/A	#N/A	#N/A	#N/A	#N/A	#N/A	#N/A	#N/A
9.8	#N/A	-8	#N/A	#N/A	#N/A	#N/A	#N/A	#N/A	#N/A	#N/A	#N/A	#N/A	#N/A
14.9	#N/A	#N/A	31	-20	47	68	81	87	74	69	71	0	#N/A
20	#N/A	#N/A	100	173	158	192	245	292	333	344	341	#N/A	#N/A
24.9	#N/A	#N/A	261	320	375	363	424	504	579	632	638	#N/A	#N/A
29.8	#N/A	#N/A	394	486	552	602	652	751	815	792	856	859	904
34.9	#N/A	#N/A	449	561	656	761	889	999	1116	1104	1142	1236	1193
40	#N/A	#N/A	473	606	717	840	1014	1136	1271	1307	1393	1475	1526
49.8	#N/A	#N/A	516	664	801	947	1179	1313	1476	1552	1671	1777	1934
59.6	#N/A	#N/A	535	690	834	1013	1258	1424	1564	1652	1798	1938	2112
80	#N/A	#N/A	546	696	858	1041	1332	1512	1658	1765	1952	2075	2302
100	#N/A	#N/A	547	699	861	1048	1336	1521	1682	1791	1947	2099	2344

BSFC[g/kW-hr]

Throttle\RPM	1000	2000	2500	3000	3500	4000	4500	5000	5500	6000	6500	7000	8000
0	#N/A	#N/A	#N/A	#N/A	#N/A	#N/A	#N/A	#N/A	#N/A	#N/A	#N/A	#N/A	#N/A
4.7	#N/A	#N/A	#N/A	#N/A	#N/A	#N/A	#N/A	#N/A	#N/A	#N/A	#N/A	#N/A	#N/A
9.8	#N/A	#N/A	#N/A	#N/A	#N/A	#N/A	#N/A	#N/A	#N/A	#N/A	#N/A	#N/A	#N/A
14.9	#N/A	#N/A	#N/A	#N/A	#N/A	2351	2208	1907	2677	2664	2933	#N/A	#N/A
20	#N/A	#N/A	1606	1138	1287	1109	1022	830	835	800	767	#N/A	#N/A
24.9	#N/A	#N/A	843	703	696	648	735	633	595	586	592	#N/A	#N/A
29.8	#N/A	#N/A	667	564	536	523	523	504	486	521	501	540	539
34.9	#N/A	#N/A	669	552	530	498	453	452	457	474	453	472	563
40	#N/A	#N/A	717	626	544	504	452	453	459	460	465	468	476
49.8	#N/A	#N/A	762	639	607	540	485	465	503	525	494	483	481
59.6	#N/A	#N/A	749	662	656	676	524	509	522	534	514	515	517
80	#N/A	#N/A	834	705	655	704	598	578	540	571	565	563	576
100	#N/A	#N/A	815	805	702	649	625	607	597	635	620	619	634

Raw Power[W]

Throttle\RPM	1000	2000	2500	3000	3500	4000	4500	5000	5500	6000	6500	7000	8000
0	#N/A	#N/A	#N/A	#N/A	#N/A	#N/A	#N/A	#N/A	#N/A	#N/A	#N/A	#N/A	#N/A
4.7	#N/A	#N/A	#N/A	#N/A	#N/A	#N/A	#N/A	#N/A	#N/A	#N/A	#N/A	#N/A	#N/A
9.8	#N/A	-8	#N/A	#N/A	#N/A	#N/A	#N/A	#N/A	#N/A	#N/A	#N/A	#N/A	#N/A
14.9	#N/A	#N/A	32	-20	48	69	83	90	76	71	73	0	#N/A
20	#N/A	#N/A	102	178	162	196	251	300	341	352	350	#N/A	#N/A
24.9	#N/A	#N/A	268	328	384	372	435	517	593	648	654	#N/A	#N/A
29.8	#N/A	#N/A	404	499	566	617	669	770	836	812	878	881	928
34.9	#N/A	#N/A	460	575	673	780	912	1025	1145	1132	1172	1267	1224
40	#N/A	#N/A	485	622	736	862	1040	1166	1304	1341	1429	1513	1565
49.8	#N/A	#N/A	529	681	821	972	1209	1347	1514	1592	1714	1823	1984
59.6	#N/A	#N/A	549	708	855	1039	1291	1461	1604	1695	1844	1988	2166

Sullivan S676-500U-21 Performance

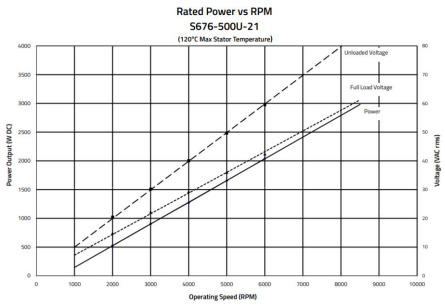

(a) Output Power vs RPM of the S6776-500U-21.

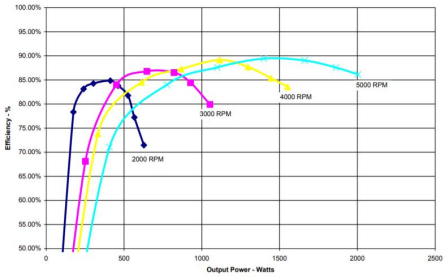

(b) Efficiency vs Output Power of the S6776-500U-21.

Figure B.1. Sullivan alternator.

LiquidPiston

Specifications			
Model	X Mini Alpha Prototype	X Mini Beta Prototype	Mature Design
Type	70cc SI-HEHC cycle air-cooled rotary engine		
Fuel	Port injected, multi-fuel (Gasoline, JP8, Kerosene, etc.)		
Compression Ratio	9:1		
Power (hp) / RPM	3.0 hp / 10 k	3.6 hp / 9 k	5 hp / 14 k
Dimensions	6.6"x6.2"x5.4"= 221 in³	6.6"x6.2"x5.4"= 221 in³	6"x6"x5"= 180 in³
Dry Weight ++	5 lb.	4.5 lb.	4 lb.
Peak Efficiency SFC (g/kW-hr)	18% 460 g/kWh	22% 378 g/kWh	25% 333 g/kWh
Specific Power	.6 hp/lb.	.8 hp/lb.	1.2 hp / lb.
Time between overhaul	30+ hours	150 hours	1000 hours

++Engine core, excluding fuel / ignition / cooling systems

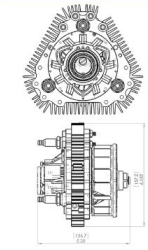

(a) LiquidPiston's X Engine specification.

(b) ParallelHEPS UAV concepts from LiquidPiston.

Figure B.2. LiquidPiston concepts.

CfAR Parallel Hybrid Electric Test Bench

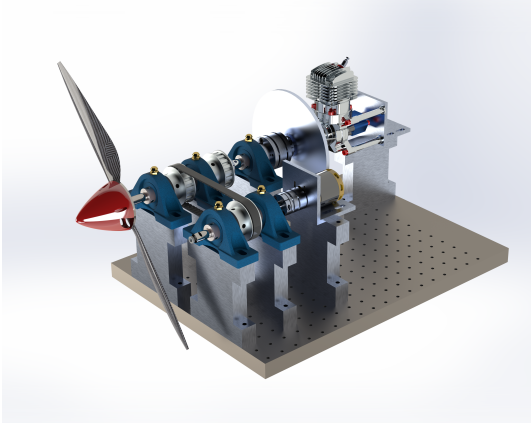

(a) CAD render of the parallel hybrid-electric test bench at UVIC CFAR. [55]

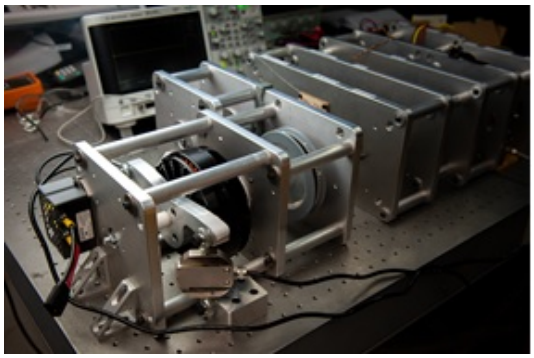

(b) Experimental setup of the dynamometer test bench at UVIC CFAR.

Figure B.3. CFAR hybrid test bench.

Pegasus Aeronautics

(a) GE35 Range Extender.

GE35 Range Extender - Technical Specifications	
Base Weight, Dry	2.60kg (5.73lb)
Engine Type	35cc two-stroke, liquid-cooled cylinder
Max. Cont. Electrical Power Output	2,000W [1]
Operational Voltage	24V through 50V
Interface Protocol	CAN, Serial, and redundant PWM signals
Starting Method	Self-starting via mapped PWM function, CAN, or Serial [2]
Throttle Control	Automatic, responds to applied electrical load
Fuel Delivery	Fuel-injected, ECU-controlled
Initial Time Between Overhaul	200 hours
Airworthiness Standard	STANAG 4703
Ingress Protection Rating	Up to IP67 available
Software	Pegasus Advanced Diagnostic Suite

[1] Electrical power output can vary depending on platform integration
[2] Can be mapped to all three interfaces simultaneously for redundancy

(b) GE35 Range Extender - Technical Specifications.

Figure B.4. GE35